JPL NO. 9950-304

PHASE 2 OF THE ARRAY AUTOMATED ASSEMBLY TASK FOR THE LOW COST SOLAR ARRAY PROJECT

DOE/JPL 954873-79/08

R.B Campbell, J.R. Davis, J.W. Ostroski,
P. Mai-Choudhury, A. Rohatgi,
E. J. Seman, R.E. Stapleton

Final Report

October 1, 1978 - October 30, 1979

Contract No. 954873

This work was performed for the Jet Propulsion Laboratory, California Institute of Technology, under NASA Contract NAS7-100 for the U. S. Department of Energy, Division of Solar Energy.

The JPL Low Cost Solar Array Project is funded by DOE and forms part of the DOE Photovoltaic Conversion Program to initiate a major effort towards the development of low cost solar arrays.

Westinghouse R&D Center
1310 Beulah Road
Pittsburgh, Pennsylvania 15235

PHASE 2 OF THE ARRAY AUTOMATED ASSEMBLY TASK

FOR THE LOW COST SOLAR ARRAY PROJECT

R.B. Campbell, J.R. Davis, J.W. Ostroski,
P. Rai-Choudhury, A. Rohatgi,
E. J. Seman, R.E. Stapleton

Final Report

October 1, 1978 - October 30, 1979

Contract No. 954873

This work was performed for the Jet Propulsion Laboratory, California Institute of Technology, under NASA Contract NAS7-100 for the U. S. Department of Energy, Division of Solar Energy.

The JPL Low Cost Solar Array Project is funded by DOE and forms part of the DOE Photovoltaic Conversion Program to initiate a major effort towards the development of low cost solar arrays.

Westinghouse R&D Center
1310 Beulah Road
Pittsburgh, Pennsylvania 15235

TECHNICAL CONTENT STATEMENT

This report was prepared as an account of work sponsored by the United States Government. Neither the United States nor the United States Department of Energy, nor any of their employes, nor any of their contractors, sub-contractors, or their employes, makes any warranties, express or implied, or assumes any legal liability or responsibility for the accuracy, completeness or usefulness of any information, apparatus, product or process disclosed, or represents that its use would not infringe privately owned rights.

FOREWORD

The work reported here was carried out in the Semiconductor Research Department under the management of Dr. D. J. Page. The Technical Director was Dr. P. Rai-Choudhury and the Principal Investigator was Dr. R. B. Campbell.

Others who contributed to the program and the report are as follows:

J. R. Davis	-	Cost Analysis and Device Modeling
J. Ostroski	-	Plating and Antireflection Coating
A. Rohatgi	-	Device Modeling
E. J. Seman	-	Cell and Module Fabrication
R. E. Stapleton	-	Ultrasonic Bonding

Silicon dendritic web was supplied by the Crystal Sciences Department, Dr. R. Mazelsky, Manager. The report was prepared by Dr. R. B. Campbell with final editing by Dr. S. Farukhi. The technical assistance of H. Abt, W. Cifone, J. McNally, L. Rohall, D. Schmidt and S. Youngk is acknowledged. Typing was done by M. C. Santoro and K. B. Haun.

TABLE OF CONTENTS

TABLE OF CONTENTS (Cont'd.)

LIST OF TABLES

LIST OF TABLES (Cont'd.)

LIST OF FIGURES

LIST OF FIGURES (Cont'd.)

1. SUMMARY

The process sequence for the fabrication of dendritic web silicon into solar panels has been modified to include aluminum back surface field formation. Sputtering is the preferred method for depositing the aluminum. Plasma etching has been shown to be a feasible technique for pre-diffusion cleaning of the web. This would replace wet chemical cleaning. Several contacting systems have been studied. The total plated Pd-Ni system (Motorola Process) is not compatible with our process sequence; however, the evaporated TiPd-electroplated Cu system has been shown stable under life testing. Ultrasonic bonding parameters have been determined for various interconnect and contact metals but the yield of the process is not sufficiently high to use for module fabrication at this time. Over 400 solar cells, about 11 cm^2 in area have been fabricated according to the modified sequence. No sub-process incompatibility was seen. These cells have been used to fabricate four demonstration modules. A cost analysis (SAMICS) of the modified process sequence resulted in a selling price of $0.75/peak watt (1980$ in 1986).

2. INTRODUCTION

The objective of this program is to specify a process sequence and to further develop process steps specifically for the low cost manufacturing of solar arrays from single crystal dendritic web silicon. All costs, including silicon web at $0.23/peak watt (1980$) are to be considered with the aim of producing encapsulated modules with 10% efficiency for a selling price of $0.70/peak watt in 1980 dollars.

The processes selected for development during the second phase of this program were the feasibility of using plasma etching as a substitute for wet chemical cleaning, the aluminum back surface field process, various metallization systems which may be more cost effective than evaporated TiPdAg, spraying methods for antireflection coating deposition, and ultrasonic interconnection techniques.

Wet chemical cleaning is not considered cost effective due to the materials expense and the added cost of disposing of toxic liquids. Plasma etching, where an rf glow discharge is used to break down various gas compositions into highly reactive species, is a possible substitute. These gas species then react with the silicon surface and thus clean by etching. We have studied this method as a substitute for the pre-diffusion (wet chemical) cleaning of the dendritic web silicon. As presently produced, the web silicon has surface oxides which must be removed before diffusion. Our experiments have shown that once the loose oxides are removed, plasma etching is as effective a method for pre-diffusion cleaning as wet chemical methods.* When the plasma cleaning is attempted with the oxides on the

*It is anticipated that with further development the web can be grown without these oxides, and can be diffused without pre-diffusion cleaning.

surface, the surface becomes irregular and patchy. Cells subsequently produced on this surface show inferior properties.

The process sequence we developed during the first part of this program used boron diffusion to prepare a back surface field. This procedure does produce operational back surface fields with maximum V_{oc} of about 0.585V. Various theoretical considerations suggest that an aluminum back surface field would give a further V_{oc} enhancement of at least 20 mV. In addition, cost studies using a conceptual factory show the aluminum process should be less costly than boron diffusion if the same process yield can be achieved.

During this past year we have studied various methods of applying the Al to the back of the cell and techniques for driving the Al into the silicon. Several methods for applying the Al have been shown feasible (including the Spectralab process specification for silk screening Al paste). However, due to the difficulty in silk screening between the dendrites, a sputtering method for the deposition has been chosen for the process sequence. The Al back surface field cells also show operational back surface fields, but the open circuit voltage enhancement is only marginally better than the boron diffused cells. A number of experiments have been carried out to determine the causes of the relatively low V_{oc}. Although the evidence is not conclusive, the results of these tests suggest that the cell properties (after the Al BSF formation) are controlled by the front junction emitter. Whether this is an intrinsic characteristic of our front junction diffusion, or an interaction with the Al BSF formation process is not known at this time.

Solar cells, deployed in an array must meet stringent requirements for stability and reliability. Perhaps, the most important factor in attaining this stability is a reliable contact system. Evaporated TiPdAg has become the accepted standard for space solar cells, but its use in terrestrial cells may not be cost-effective. Several alternatives to this system have been suggested. Motorola has issued a process specification on a total plated system consisting of Pd and Ni.

Another alternative would be to replace the Ag with a less costly metal and to use a deposition technique that is more area selective than evaporation.

We have tested the Motorola contacting process in our process sequence. It was possible to obtain ohmic contacts, but the cleaning solutions and etches used in the process attacked the antireflection coating. By making certain modifications in the Motorola process, total plated contacts were applied to the web cells without damage to the antireflection coating; however, the cell parameters were inferior to those with the baseline TiPdAg contact system. We concluded that it was not feasible to insert this metallization system into our process sequence without significant modification due to a lack of compatibility.

In another aspect of the metallization study it was shown that electroplated copper could be substituted for evaporated silver with no degradation of cell parameters. Since copper is a very fast diffuser in silicon, a life test was carried out where cells with evaporated TiPd electroplated Cu contacts were heated at 225°C for up to 600 hours. After this time there was no measurable change in the cell parameters. Therefore, the electroplated copper appears to be a suitable substitute for evaporated silver and would be more cost effective.

In our process sequence, the antireflection coating is applied by dipping immediately after the back surface field is formed. It might be an advantage if this coating was applied later in the sequence, perhaps after interconnection so that the coating (glass) would protect the interconnect metals. A small program was carried out in this area to determine cost effectiveness and compatibility with the entire sequence. It was found possible to coat the material using a hand-held sprayer, but for obvious reasons, the uniformity of the film over the cell surface was poor. We are presently working with an outside vendor* on techniques for applying this coating.

*Integrated Technologies, Inc., Acushnet, MA 02743.

The interconnection of the cells into series/parallel circuits to form the module is an important step in that the connection process must be reliable and amenable to automation. In our design, each cell will require a total of 14 interconnections; therefore, a large number of bonds are required for a given unit module. The process, then must also have a nearly 100% yield in terms of good bonds and cell breakage.

The ultrasonic bonding technique has been used for the production of rapid and high strength bonds between various metal foils and has been automated. It has also been shown feasible for bonding interconnect foils to solar cell contacts. This method does not require the use of expensive solder or corrosive fluxes. A further advantage is that there is no metal buildup on the cell (other than the interconnect strap) which leads to a simpler module fabrication.

Samples for most of the tests with ultrasonic bonding have been prepared using the spot welder. This procedure enables the materials to be joined to be contacted by an ultrasonically driven tool in one given area. After the bond is made, the tool is re-positioned and another bond made the same way. A second type of welder-seam-bonder uses an ultrasonically driven tool which rolls along the workpiece. This type of bonder would be of special advantage in solar cells in that a continuous strip of foil is bonded along the cell contacts the length of the cells.

The work during this program has concentrated on determining the bond parameters (force, time, power) for achieving strong reliable bonds between interconnect metals and the contacts on the cell. These parameters have been determined using the spot bonder, but the yield of the process is low. Preliminary tests using a seam bonder do suggest, however, that a higher yield is achievable with this method.

A continuing cost analysis using SAMICS methodology has been carried out on our process sequence. The entire sequence, modified to include the aluminum back surface field formation, results in a selling price of $0.75/peak watt (1980$ in 1986). In addition, the SAMICS

calculation has been used to show the importance of capital equipment costs and panel efficiency to the overall cost. In general, this cost method has been used as a tool to examine modifications in our process sequence and to determine their cost effectiveness.

The specifications and control parameters for the various sub-processes of the sequence are given in Appendix B of this report

3. TECHNICAL RESULTS

3.1 Plasma Etching

The plasma etching process uses gas compositions, generally CF_4 and O_2 which are broken down into a variety of active species by an rf glow discharge. These active species form a low temperature, highly reactive plasma, which can react with surface contaminants on the silicon to form volatile products. These volatiles are then pumped from the system.

The plasma etching process is attractive for solar cell fabrication since it could eliminate wet processing steps and chemicals. Wet processing may not be a cost effective step.

Plasma etching was investigated as a substitute for pre-diffusion cleaning step of the dendritic web. At the present time, the as grown dencritic web comes from the furnace with a lightly adhering, brownish oxide coating. Analysis has shown this coating to be various oxides of silicon. With further development in the growth process, it is anticipated that this oxide layer will not occur. However, at this time a pre-diffusion cleaning is required. This cleaning includes an $HF-H_2O$ swab to remove the oxide together with further wet chemical treatment of $H_2O_2 \cdot HCl$ and $H_2O_2 \cdot NH_4OH$ to remove any impurities on the surface.

In the experiments reported here, some of the web samples were plasma cleaned or etched in the as-grown condition while others were swabbed with an $HF-H_2O$ solution. Previous experience has shown that if samples are diffused in the as grown condition or with the $HF-H_2O$ swab only, the cell efficiency will be several percent lower (absolute) than with properly prepared samples. Thus these two conditions are a fair test for the effectiveness of plasma etching.

Table 1 represents the results of these experiments. All tests were made on a single web crystal (RE 26-5) so that valid intercomparisons could be made. The plasma cleaning/etching was done in an LFE-301A reactor.

In Treatment 1, the as grown web with the oxide coating was plasma cleaned for 3 min. at 200 watts rf with 300 cc/min. of O_2. Treatment #2 was the same as #1 except that PDE-100 (a proprietary etching gas produced by LPE Corporation) was substituted for the oxygen.

Treatments 3 and 4 were the same as 1 and 2 except that the web was lightly swabbed with an $HF:H_2O$ solution to remove the loose oxide film. Treatment #5 is our baseline cleaning process involving:

HF/H_2O swab,
Hot H_2SO_4 soak (2 min.),
$NH_4OH:H_2O_2:H_2O$ chelating cleaning,
$HCl:H_2O_2:H_2O$ cheating cleaning,
DI H_2O rinse.

The data in Table 1 show that Treatments 1 and 2 result in cells that are much poorer than the baseline treatment (#5). The major difference is in the V_{oc}, FF and lifetime. This would indicate that some lifetime killing impurities remained on the surface after the plasma treatment and diffused to the junction during the high temperature processing.

Treatments #3 and #4 result in cells that are as good as the baseline cells. It should be noted that when webs, which have only the HF cleaning procedure, are diffused, the results are always inferior to the baseline cleaning process since these indicate a 2% decrease in the efficiency. Therefore, it can be concluded that the plasma etching or cleaning of HF cleaned web is a suitable substitute for a baseline wet chemical cleaning.

A cost estimate has been made of this process using SAMICS methodology. The inputs are shown in Table 2. The calculation was

TABLE 1

PLASMA CLEAN/ETCH TEST*

	Treatment	J_{sc} (ma/cm^2)	V_{oc} (V)	FF	Eff(%)	τ_{OCD} (μsec)
1.	Web - as grown + 3 min. plasma clean	32.3	.502	.689	11.2	6.2
2.	Web - as grown + 3 min. plasma etch	34.0	.514	.706	12.1	7.3
3.	Web - HF clean + 3 min. plasma clean	33.3	.545	.743	13.3	23.0
4.	Web - HF clean + 3 min. plasma etch	33.3	.541	.723	12.9	20.0
5.	Standard web cleaning process	33.2	.545	.737	13.1	24.7

*Web - RE 26-5; 10 Ω-cm; Boron BSF

AR coated

AM-1 - 100 mW/cm^2

TABLE 2

PLASMA ETCHING SUB-PROCESS
INPUTS INTO SAMICS CALCULATION

Total Output	25 MW/yr
Silicon Throughput	5000 cm^2/min
Floor Space	350 sq. ft.
Labor	1.0 Person years
Capital	$840,000 (1980$)
Commodities	60 tanks of purge gas
	60 tanks of etching gas

carried out by inserting the plasma etch as a sub-process in the process sequence and determining the value added. This value added was $0.018 (in 1986 in 1980$).

The yield for this sub process was taken to be 100%; however later in the calculation an 85% yield of cells and a 95% yield of panels was assumed, which increases the cost of the plasma etching step to $0.023 (in 1986 for 1980 $).

3.2 Back Surface Field Studies (BSF)

3.2.1 General Background

The presence of a high-low junction near the back surface of an n^+p junction structure results in enhanced open circuit voltage and short circuit current. The higher V_{oc} of the BSF cells is due to the reduced back surface recombination velocity and a built-in voltage in the p^+p region. The built-in field in the high-low junction reduces the loss of photogenerated carriers and enhances the quantum efficiency of the base region of the BSF cell and results in higher I_{sc}.*

* A more complete treatment of the factors affecting back surface field performance is given in Appendix A of this report.

The above effects can be summed up in the functional expression for the junction leakage velocity (Spp^+) of minority carriers across the p^+p depletion region given by[1,2,3]:

$$Spp^+ = f\left|\left(\frac{N_A}{N_A^+}\right)\left(\frac{D_{p^+}}{L_{p^+}}\right)\left(\Delta E_G\right)\left(\frac{W_{p^+}}{L_{p^+}}\right)\right|$$

where: D_{p+} = electron diffusion constant in p^+ region

L_{p+} = electron diffusion length in p^+ region

W_{p+} = width of p^+ region

N_A = acceptor concentration in p region

N_A^+ = acceptor concentration in p^+ region

and ΔEg is a band gap narrowing term in the heavily doped p^+ region, which increases with the p^+ doping.

As the value of Spp^+ approaches a minimum, the effective bulk lifetime in the p region increases and the enhancement of the cell parameters discussed above occurs.

Based on this equation, certain material and device parameters which will cause Spp+ to be a minimum can be identified. First, the minority carrier diffusion length in the p^+ region, L_{p+} should be as large as possible. Although no direct measurements have been made on the magnitude of L_{p+}, Hauser and Dunbar[4] suggest that it varies from a few tenths of a micron at $N_A = 10^{21}/cm^3$ to several microns at $N_A^+ = 10^{18}/cm^3$. Second, the functional relationship for W_{p+}/L_{p+} is the hyperbolic cotangent. Since coth θ has a minimum value of 1 for $\theta > 3$, W_{p+}/L_{p+} should be greater than 3. Third, the ratio of N_A/N_A^+ shouldbe small. Since N_A in itself should be near $10^{15}/cm^3$ so that an efficient n^+p junction can be fabricated, the value of N_A^+ should be large. There is an obvious trade off here because as N_A^+ increases L_{p+} decreases and ΔEg increases. Sinha and Chattopadhyarya[(2)] have shown that for a 5 μm p^+ region and

an N_A of $10^{15}/cm^3$, the surface recombination velocity first decreases because of the decrease in the ratio of N_A/N_A+ but beyond $N_A+ \approx 2 \times 10^{19}/cm^3$, Spp^+ begins to increase due to the band gap narrowing effect.

In light of this information and disucssion, we should consider the characteristics of boron doped and Al doped BSF to determine which is preferable for high efficiency solar cells. Table 3 lists some of these parameters.

TABLE 3

COMPARISONS OF B AND A DOPED BACK SURFACE FIELDS

	B-doped	Al-doped
N_A+ (#/cm^3)	10^{21}	5×10^{18}
L_p+ (μm)	.1-.3 μm	2-5 μm
W_p+ (μm) obtainable	1-2	>10

From the above data, it is obvious that $W_p+/L_p+ > 3$ can be satisfied for both B and Al BSF. However Spp^+ should be lower for Al BSF because of band gap narrowing in the B BSF offsetting the benefit of the high N_A/N_A+ ratio.

Considering all these factors, Sinha and Chattopadhyaya[2] suggest that Spp^+ will be a minimum for $10^{19}/cm^3$ to $10^{20}/cm^3$. This indicates that to a first approximation that Al back surface field may be preferable.

During the first part of this present contract, several experiments were carried out with boron doped BSF's.

3.2.2 Boron Diffused Back Surface Fields

Previous experiments had indicated that boron doped back surface fields using either a BBr_3 source or a doped boron CVD oxide were essentially equivalent. To extend and verify this data, a diffusion experiment was carried out with four different web crystals and a float zone Si baseline which were diffused using three different techniques (BBr_3 for a 0.4 μm junction; BBr_3 for a 1 μm junction and B-doped CVD oxide for a 1 μm junction). This experiment was to have determined if boron diffused BSFs could be improved either by deeper junctions or with the doped oxide source. The data are shown in Table 4. In this test, the cells were all processed in the same manner except for the boron diffusion technique.

The data show that V_{oc} and I_{sc} correlate well with the lifetime, rather than with increasing junction depth or doping technique. This suggests that the cell parameters are controlled by variables (bulk lifetime, front surface condition) other than the back surface field.

After this test, all further BSF studies were conducted using Al as the dopant, since the enhanced V_{oc} due to Al has been reported to be above 0.605V.

3.2.3 Aluminum Back Surface Field Studies

The Al BSF studies carried out emphasized the following areas:

1. Effect of back surface condition on Al alloying, i.e., n^+ or p surface.
2. Methods of applying Al evaporation, sputtering, silk screening.
3. Techniques to alloy Al rf or resistance heated furnace, temperature required and ambient gas.
4. Al penetration depth and dopant profile.
5. Protection required for front junction.

Parts 2 and 3 were generally studied together while 4 was used mainly as a diagnostic technique.

Table 4

Boron Diffused - Back Surface Fields

(Measured at AM-1; AR Coated - 1.4 Enhancement)

Crystal #	BBr ($X_j \approx 0.4$ μm)	BBr ($X_j \approx 1.0$ μm)	Boron Oxide ($X_j \approx 1.0$ μm)
	Efficiency		
RE50-1.2	13.0	12.4	--
RE54-1.2	14.1	14.7	14.3
RE54-2.1	12.8	12.3	13.3
J80-5.1	10.9	10.4	9.0
Float Zone Si Baseline	14.7	--	14.8
	I_{sc} (mA)		
RE50-1.2	30.9	30.8	--
RE54-1.2	32.2	32.6	32.6
RE54-2.1	30.9	30.9	31.6
J80-5.1	28.2	30.0	30.9
Float Zone Si Baseline	31.8	--	32.4
	V_{oc} (V)		
RE50-1.2	.547	.533	--
RE54-1.2	.570	.573	.566
RE54-2.1	.538	.526	.551
J80-5.1	.507	.516	.535
Float Zone Si Baseline	.580	--	.570
	τ_{OCD} (μsec)		
RE50-1.2	12	8	--
RE54-1.2	35	34	35
RE54-2.1	12	7	22
J80-5.1	2	3	5
Float Zone Si Baseline	35	--	13

3.2.3.1 Back Surface Condition

There are several choices for the preparation of the back surface prior to application of aluminum.

The simplest is to apply the Al over the back of the cell immediately after the phosphorous diffusion, leaving the phosphorous glass in place on both the front and back of the cell. However, when this was tried (with evaporated, sputtered or silk screened Al) the Al formed small balls during the alloying. These balls, about 1-3 mm in diameter were uniformly distributed over the back surface of the cell. After these Al balls and the glass oxide were etched off, very little reaction between the Al and Si was noted. Based on these results, the phosphorous glass was removed from the back of the cell before the Al was applied in all further tests.

It was next determined if the Al could be alloyed through the n^+ skin after phosphorous diffusion.

In this series of experiments, 9.6 μm of Al was evaporated on the back of the cell structure of both dendritic web and float zone crystals.

These cells used in these preliminary tests had been diffused in phosphorous before the Al deposition to form an n^+p junction structure. During this diffusion, phosphorous also diffused into the back of the wafer leaving an n^+ skin. In one case, this n^+ layer was removed by etching before the Al deposition, while in the other case the Al was evaporated directly on this n^+ layer. The samples were placed on a Si coated carbon susceptor and heated to 820°C in 5 minutes held for 15 seconds then cooled by turning off power. Cells were made from these samples and compared with non-BSF cells, i.e., n^+p structures. These data are shown in Table 5 and are averages of a number of cells.

The p^+p junction profiles of representative cells are shown in Figures 1 and 2. Figure 1 is the concentration profile of a float zone silicon where the Al was evaporated on a n^+ layer, (remaining from a phosphorous diffusion). In this case the Al was alloyed through the n^+ layer to form the p^+p structure.

TABLE 5

Al BSF Cells - 9.6 μm Evaporated Al - RF Heated

(AM1 - AR Coated)

	I_{sc}(mA) (No BSF)	V_{oc}(V)	FF	EFF(%)	τ_{OCD}(μsec)
FZ Cells	30.8	.543	.762	13.45	6
BSF - (Al Evaporated on n^+ layer					
FZ Cells	31.4	.591	.769	15.1	36
WEB Cells	31.5	.576	.750	14.4	43
BSF (Al Evaporated on p-type surface after n^+ layer etched off)					
FZ Cells	30.4	.591	.764	14.5	29
WEB Cells	31.0	.572	.768	14.5	40

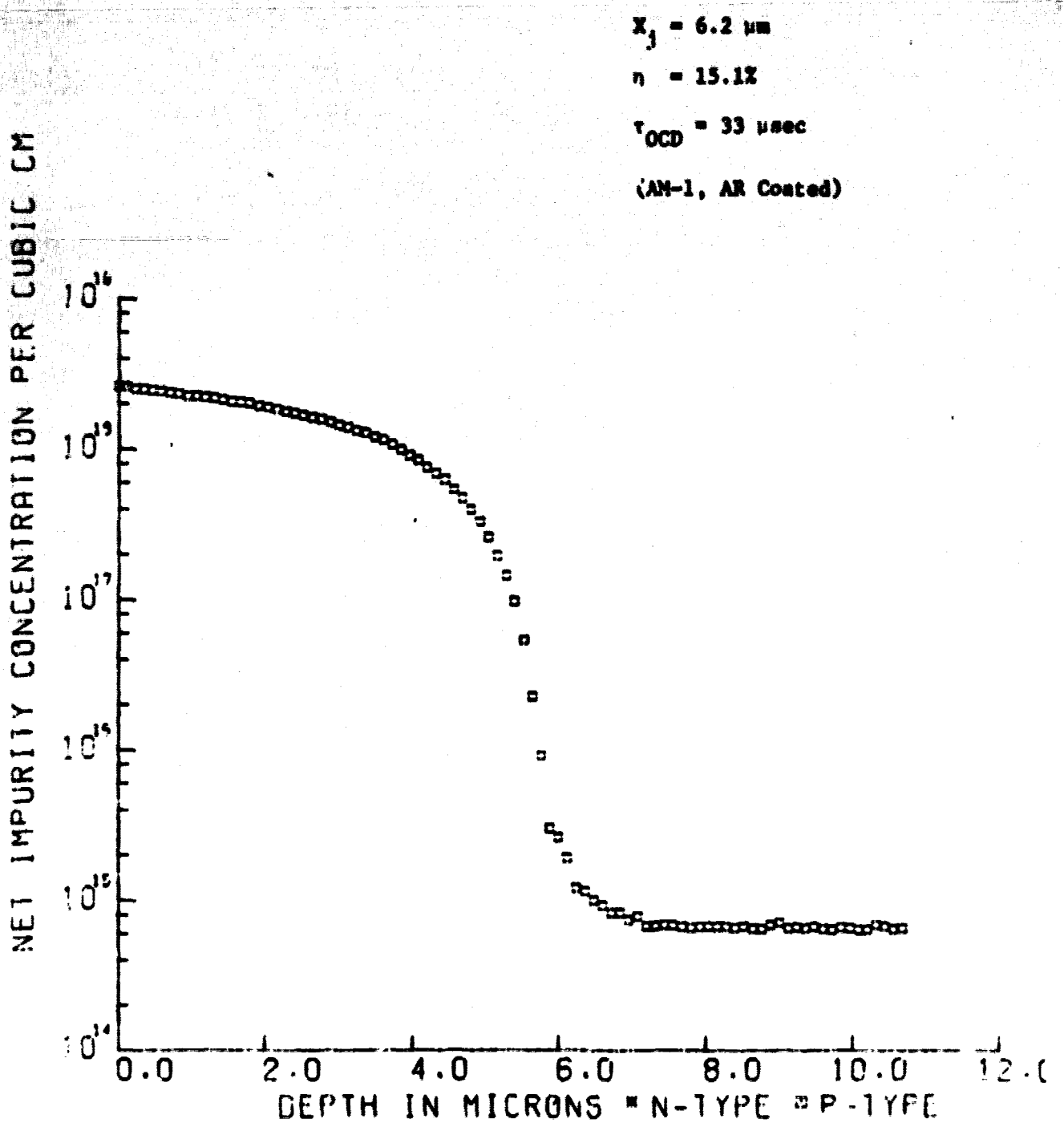

Figure 1. Float zone silicon concentration profile of Al BSF; Al applied on n^+ layer.

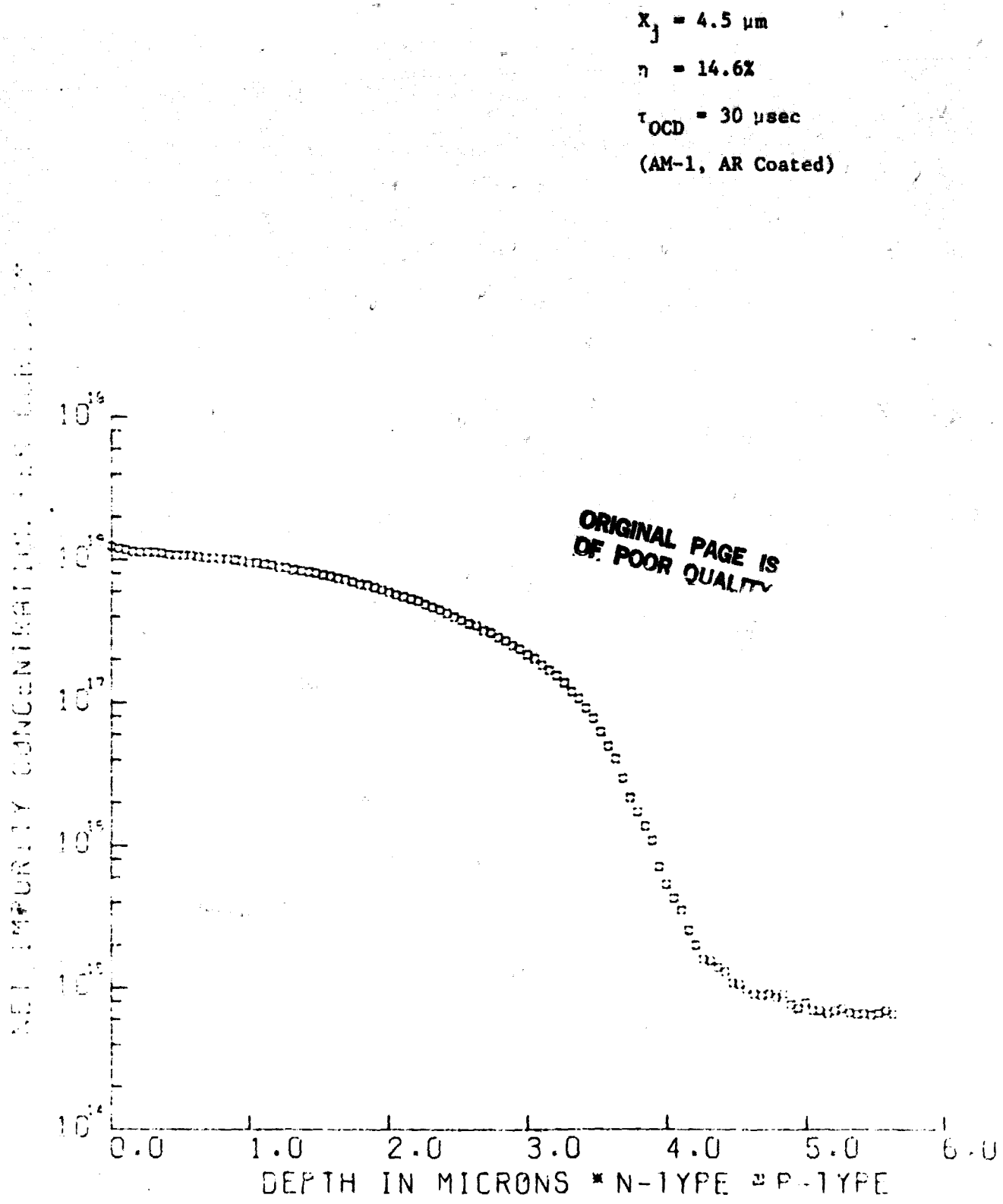

Figure 2. Float zone silicon concentration profile of Al BSF; Al applied after n^+ layer removed.

Figure 2 is the concentration profile of a float zone silicon cell where the Al was evaporated on a p-type surface (n^+ surface etched off).

The p^+ layer obtained when the Al was alloyed through the n^+ skin is about 2 μm thicker than when alloyed into a p material. Although this difference is small, it is a real effect in that the same variation was seen on a number of cells.

The p^+ penetration into the web was generally about 1 μm less than for the float zone material.

Several comments can be made regarding this preliminary data.

- The junction depth in the two samples (4-6 μm) approaches the 10 μm believed to be required for optimum BSF operation.
- There is an enhancement of about 50 mV due to the Al BSF (cf FZ BSF and no BSF).
- There appears to be some advantage in driving the Al through the n^+ skin, but the difference is small. Driving the Al through the n^+ skin is however, a more cost effective process.

During the course of these experiments, it was noted that the Al did not always alloy in smoothly. In these cases, the Al would form balls on the surface and alloy in from these balls, giving a non-uniform penetration.

As mentioned above, this set of samples were prepared using evaporated aluminum. Further tests showed that this method had a very poor yield of good devices in that uniform alloying was not achieved. The Al tended to puddle on the back surface. We were not able to determine the cause of this nonuniformity. Different cleaning methods and evaporation techniques were tested without success.

3.2.3.2 Application of Al and Firing Techniques

The three main methods studied for applying Al to the back of the cell: evaporation, sputtering, and silk screening. The Al used for evaporation and sputtering was high purity (Al > 99.99). For silk screening tests a prepared Al paste was used (Englehard #3484). After we received Spectrolab's Process Specification for Al BSF formation, we used AMPAL Al powder #631 prepared into a paste according to the specification.

The alloying methods used were a resistance heated furnace in an N_2-O_2 ambient and an rf heated furnace (graphite susceptor coated with silicon carbide) in N_2 or H_2 ambient. With the rf heated method several different heating and cooling rates were tested.

- Silk Screening

The samples were silk-screened using a prepared Al paste sold by Englehard Co. (#3484). The paste was applied using a 25 μm screen and the samples were dried at 200-250°C before any alloying procedure was attempted. After drying, the thickness of paste was 20-25 μm and the density was estimated to be about 65% of pure aluminum.

To determine the effect of heating time and temperature on the thickness of the regrown layer and to determine an optimum time/temperature regime for alloying, samples of float zone p-type crystals screened with the Englehard paste were heated at 800°C, 825°C, and 850°C for 30 sec, 60 sec, and 120 sec. In nearly all cells, the screened material appeared to wet the surface uniformly and did not bubble up or lift off the surface. At higher temperatures and longer times, the crystals were warped and the 850°C/120 sec. sample fractured. This warpage was not apparently related to the degree of preparation and when the excess Al was etched off the back surface of the crystal returned to its original flat form.

The depth of the regrown layer was measured by a spreading resistance technique on an angle lapped surface.

An anomaly was noted in this series of tests. In two cases the dopant concentration profile indicated evidence of nonuniform alloying. This effect is shown in Fig. 3. In this figure, the depth into the crystal in μm) vs. the dopant concentration is shown. As seen, there is an abrupt change in concentration at 2.8 μm with the regrown layer penetrating to 6.5 μm where the base dopant concentration is noted. This effect can be compared to a normal dopant concentration trace shown in Fig. 4. The sample showing the anomaly was etched and the area where the spreading resistance was measured was examined microscopically. A thin imperfection line was noted at the resistance discontinuity point. The chemical/crystallographic makeup of this band has not been determined; however, it represents a region of low Al concentration.

The depth of the regrown layer determined from these measurements as a function of time and temperature is shown in Table 6. These data do not show the expected relationship between the thickness of the regrown layer and the time/temperature conditions, probably due to lack of control of important variables. It may be noted that somewhat similar data was reported by W. Taylor et al.[5] These data show V_{oc} and I_{sc} peaking at certain firing times with both V_{oc} and I_{sc} lower at shorter and longer firing times. Our experiments were carried out in a resistance heated furnace in a nitrogen ambient, and it is quite probable that oxygen back-streamed into the furnace, since the oxidation of the Al powder would occur more rapidly than that of the lower temperature samples. Therefore, in certain instances (e.g., high temperature) oxidation could impede the alloying process and reduce the regrown layer thickness. This oxidation process does not completely explain the data in Table 6 but does give some idea of the complexity of the problem.

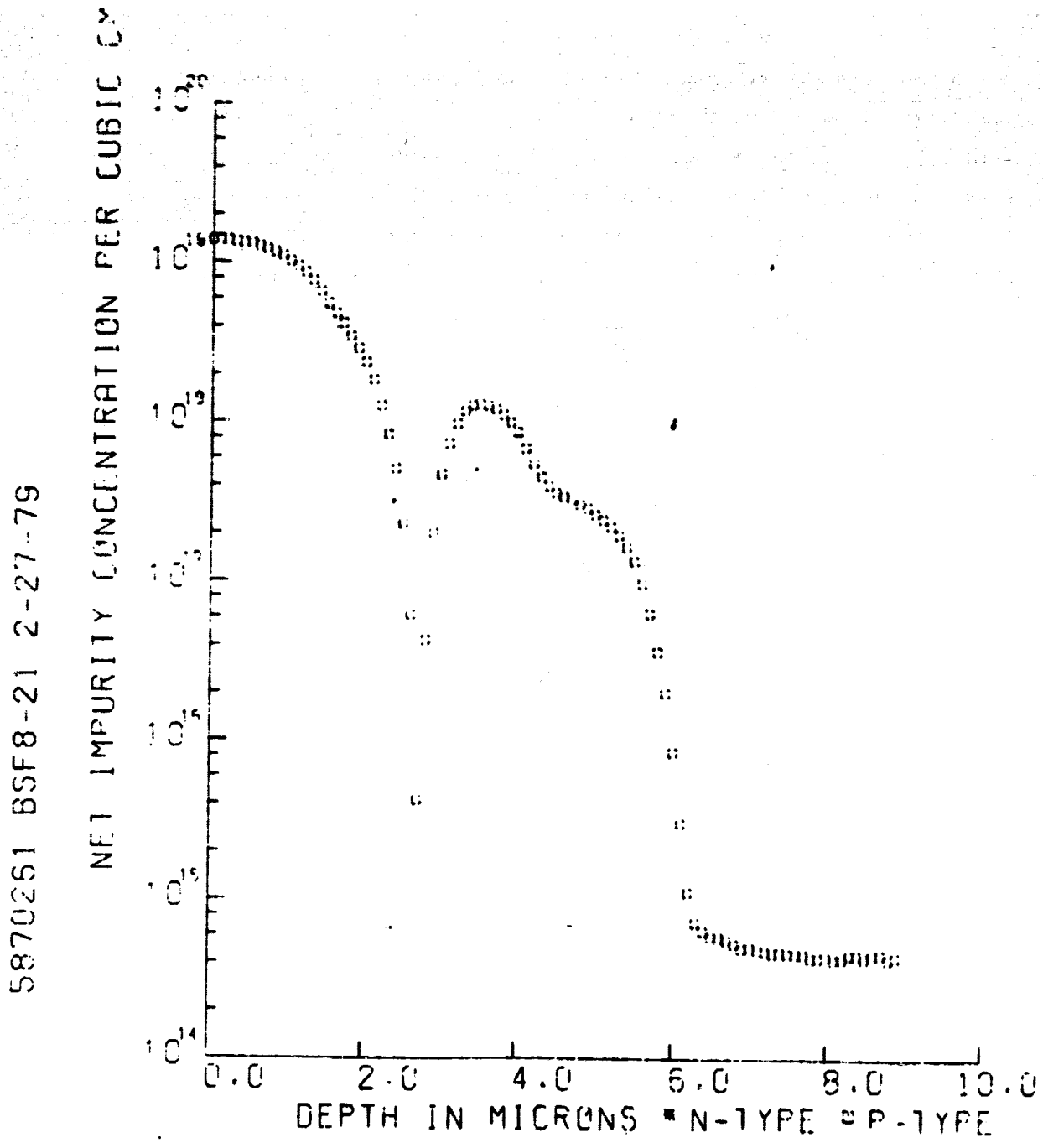

Figure 3. Anomalous concentration profile in silk screened Al BSF.

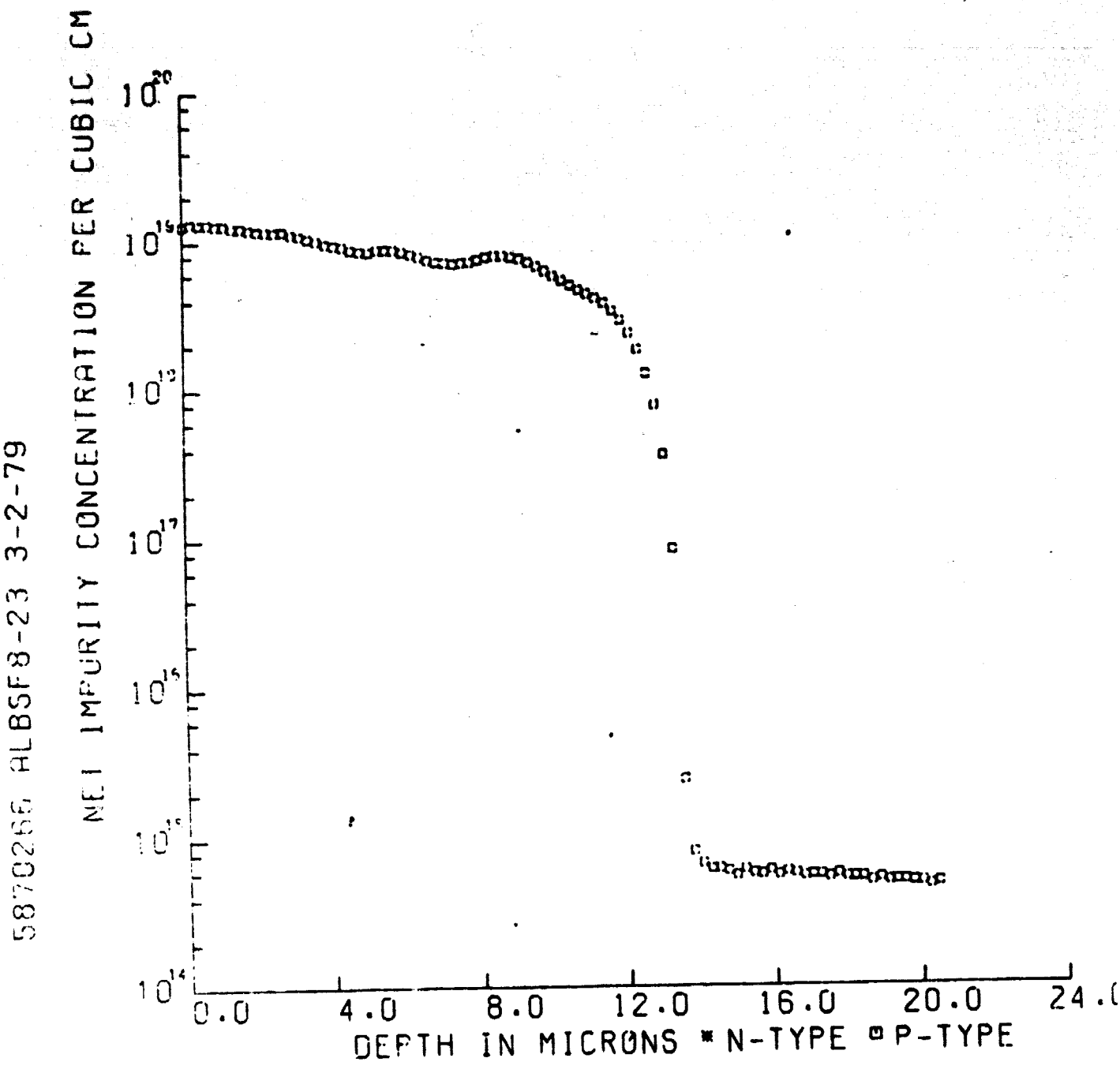

Figure 4. Screened Al, alloyed at 825°C for 60 sec.

TABLE 6

Thickness of Regrown Layer at Various Times and Temperatures - Silk Screened Englehard #3484

Temp. (°C)	Time (sec)	Thickness of Regrown Layer (μm)
800	30	2.1
800	60	6.5
800	120	7.5
825	30	2.5
825	60	13.8
825	120	6.0
850	30	8.0
850	60	3.8
850	120	1.0

At this point a process specification on silk screened Al back surface fields became available from Spectrolab. This process specification detailed the preparation of a screenable paste using "AMPAL"* powder. The next series of tests used this paste and the process outlined by Spectrolab.

The paste was applied with a stainless steel screen having an open grid area 0.004" x 0.004" . After the paste was applied it was dried at 200°C for 15 minutes and then alloyed in an RF heated furnace at 850°C in H_2 or in a resistance heated furnace at 850°C in N_2.

The silk-screened samples did not show any excessive bubbling or lifting of the Al layer during alloying as was noted with the evaporated material and some of the previous samples using other pastes. In both the resistance heated furnace and in the RF furnace, the melted Al on the back surface after alloying was sufficiently unoxidized, so that further metallization was not required to form a back contact. There was, however, some warping of the cell structure after the alloying and the cells were brittle. This warpage, due to the thick Al, meant the metal had to be removed to relieve the stress. In several cases this warpage was sufficiently bad to crack the silicon. This could indicate that large area screen printed devices may be difficult to fabricate by this process due to warpage and breakage.

Table 7 shows the cell data for this experiment. All dendritic web samples were from web crystal W-141-1.4.** The first two processes (1 and 2) compare slow cooled (≈ 2°C/min) and normal cooled (≈ 10°C/min) silk screened web samples alloyed in an RF furnace. The lifetime of the slow cooled material is about about that of the normally cooled, and this effect is mirrored in the short-circuit current. The low efficiency of the fast cooled material is due to both the low I_{sc} and fill factor.

---

*AMPAL #261; Atomized Metal Powders, Inc., Flemington, New Jersey.

**In order to screen the dendritic web samples, the dendrites were removed by scribing.

TABLE 7

CELLS WITH Al BSF PRODUCED BY ALLOYING SILK SCREENED "AMPAL" PASTE

(AM-1; 100 mA/cm^2; AR coated; Web #W-141-1.4)

	Process	V_{oc}(V)	$I_{sc}(\frac{mA}{cm^2})$	FF	η(%)	τ_{OCD}(μsec)	p^+ width (μm)
1.	Web-RF Fce 850°C-Normal Cool	.559	30.8	.69	11.9	2.5	2
2.	Web-RF Fce 850°C-Slow Cool	.558	33.8	.73	13.9	5	4
3.	Web Sputtered Al 850°C-Slow Cool	.565	34.7	.70	13.6	4	4
4.	Web-Boron BSF	.569	32.6	.74	13.8	6	—
5.	FZ Si-RF Fce 850°C-Slow Cool	.540	33.3	.73	13.4	13	5
6.	FZ Si-RF Fce Sputtered Al 850°C-Slow Cool	.572	34.8	.72	14.5	20	6

Process 3 samples are controls and are fabricated on the same web crystal with the Al BSF produced by alloying a sputtered Al layer. Process 4 samples are also controls and are boron BSF cells produced by BBr_3 and $POCl_3$ diffusion followed by the standard photolithographic process (see Figure 18 of reference 8). Process 2 compares favorably with these control samples.

Process 5 samples are fabricated on float zone Si with the BSF produced by alloying in the silk screened AMPAL paste. These results are to be compared with Process 6, which are FZ silicon cells with alloyed in sputtered Al layers. The loss of lifetime in the silk-screened FZ cell (20 μsec to 13 μsec) may be due to some lifetime killing impurity, since all control samples were reacted at the same time as the experimental samples. The effect of the lifetime loss is noted in both I_{sc} and η for the cells in Process 5.

The data indicate that Al BSF cells can be fabricated using silk screened "AMPAL" paste which are essentially equal to the sputtered Al process.

The measured values of the OCD lifetime and the short-circuit current, while not as high as expected for an Al BSF, do indicate an operational back surface field. However, the open-circuit voltage is also affected by the contribution to the reverse saturation current from the front junction, and it is possible that the front junction was degraded due to the fabrication of the Al BSF.

The OCD lifetime of the sputtered Al BSF is generally higher than the cells with a silk screened Al BSF. (See next section.)

- Sputtered Aluminum Layers

Due to the nonuniformity and lack of reproducibility noted with the evaporated Al, and to the difficulty in silk screening web without removing the dendrites, a number of experiments were carried out using sputtered Al on the back surface. In these trials, the phosphorus

diffused web or float zone silicon was back-sputtered for 10 minutes (to clean the surface) before 10 μm of aluminum was sputtered.

The cells were heated in an rf furnace at 800°C, 825°C, 850°C, and 875°C in an H_2 ambient. In this process, the rf generator is preset to a power level so that the sample reaches the required temperature in about 30 sec. When the temperature is reached (as ready by an IR pyrometer) the power is turned off and the sample cooled. With the inevitable slight overshoot in temperature, the sample is probably at the required temperature for 10 to 20 sec.

In general, these sputtered layers behaved well under the drive-in conditions. Over 90% of the samples showed a complete and uniform Al layer on the surface after the drive in. The remaining 10% showed areas where Al did not wet the Si, and puddles of Al were formed. The cells were brittle and extreme care was needed in handling.

Table 8 shows the results of these tests. The thickness of the regrown p^+ layer increased gradually with increasing temperature. The cell lifetime decreased slightly at the highest temperature and limited the V_{oc} enhancement and the efficiency. The maximum V_{oc} occurred at 850°C with 0.588V for the FZ material and with 0.577V for the web.

The p^+ layer is sufficiently thick that higher values of V_{oc} and efficiency would be expected. It appears that some lifetime killing mechanism is operating to reduce the maximum efficiency.

The OCD lifetime for these cells with a sputtered Al BSF was generally higher than that of the cells with a silk screened Al BSF.

Due to the positive results of these experiments and the difficulty in silk screening web material, sputtering was taken as the standard method for depositing Al in our process sequence.

3.2.4 Front Junction Protection

In the aluminum back surface field studies reported in previous sections, we have shown that metallurgically the p^+ region satisfies the

TABLE 8

CELL PARAMETERS - SPUTTERED Al

(12 Ω-cm Si)

Drive Temp. (°C)	p^+ thickness (μm)	Matl.	V_{oc} (V)	Eff. (%)	τ_{OCD}(μsec)
800	2	WEB	.577	14.5	20
825	6-8	FZ	.585	14.4	37
	3	WEB	.569	14.1	22
850	8	FZ	.588	15.2	34
	9	WEB	.577	14.8	26
875	9	FZ	.574	14.1	32
	5-10	WEB	.568	13.9	22

- AM-1; 100 mw/cm^2 -- AR coated
- Values given are averages of 8-10 cells
- Fired in rf heated furnace - H_2

design criteria for the high-low junction. The penetrations achieved are in the 5-15 μm range with the required dopant profile and proper surface concentration of Al ($6 \times 10^{18}/cm^2$).

In spite of these results, the open-circuit voltage has not exceeded 0.59V while many contractors report V_{oc}'s > 0.60V.

The device lifetime, and therefore, the open-circuit voltage are controlled not only by the p^+p junction (BSF) and the bulk, but also by the front n^+ region. Thus, it is possible that the ultimate properties of the solar cells are limited by the front emitter region. The back surface fields discussed above are operating and do produce an enhancement of 30 to 40 MV, but the ultimate properties (i.e., V_{oc} > 0.6V) may be controlled by the front junction.

In an effort to determine if a small amount of aluminum was contaminating the emitter region, either during aluminum application or alloying, several experiments were carried out in which the front surface was protected, and an experiment in which the n^+ layer was diffused in after the p^+ layer was prepared. These results, as well as the experimental conditions are given in Table 9. The data given are the averages of 8 to 16 cells for each treatment. In all cases the p^+ layer was prepared by alloying in a silk-screened layer of AMPAL #631 paste (as described earlier). The penetration of the p^+ layer was 6 to 8 μm.

The samples, in which the phosphorus glass diffusant source was in place during the alloying, gave uniformly superior results. Treatment #3 (n^+ layer formed after p^+ layer) was the poorest and these results may be due to a grading of the p^+ junction during the 850°C diffusion to for the n^+ layer.

Treatment #1 (top surface protected by SiO_2) produced cells which were also considerably poorer than the cells fabricated with the phosphorus glass protection.

Although not conclusive, these data do suggest that there is some effect on the top surface (i.e., top n^+p junction) during the BSF formation.

It should also be noted that even in the best case (Treatment #2) where the cells have a 24 μsec lifetime and a p^+ layer of 5 μm, the maximum V_{oc} is 0.57V.

TABLE 9

Al BACK SURFACE FIELD RESULTS (AVERAGE VALUES)

(Silk Screened AMPAL - #631 - 850°C Drive In)

Treatment	I_{sc} (mA)	V_{oc} (V)	FF	η(%)	τ_{OCD} (μsec)
1. SiO_2 on n^+ side	30.96	.562	.723	13.3	16
2. $Phos_+$ glass on n^+ side	31.67	.572	.746	14.3	24
3. p^+ layer formed before n^+ layer	30.96	.540	.730	12.9	12

Notes

Treatment 1 - Phosphorous glass removed after $POCl_3$ diffusion; SiO_2 applied to one n^+ side to protect surface from Al. Al driven through back n^+ layer.

Treatment 2 - Phosphorous glass removed fron one side; left on one n^+ side to protect surface from Al. Al driven through cleaned back n^+ layer.

Treatment 3 - Al driven into p crystal; excess Al removed and n^+ diffusion carried out. p^+ surface reconstructed with Ti Pd Ag.

Measured at AM-1; 91.6 MW/cm^2 - AR coated

3.2.5 Costs of Back Surface Field Formation

Using SAMICS methodology, studies were carried out to determine the cost differentials between boron doped BSF's, and sputtered and silk screened Al BSF's.

TABLE 10

COSTS OF BACK SURFACE FIELD FORMATION
(Value Added for Given Process — 1980$)

Boron Diffused	0.079$/watt peak
Sputtered Al	0.058$/watt peak
Silk Screened Al	0.039$/watt peak

Table 10 gives the results.

The boron diffused BSF process costs about twice the silk screened Al process. This is mainly due to the added sub-processes required such as etching and masking, and the equipment required to carry out these processes.

A number of tests have indicated that if the cell processing is carried out without the dendrites, the overall yield, due to breakage would be low. Therefore, the screening process would require considerable machine development so that the silk screening could be done between the dendrites.

The major cost factor in the sputtering process is the large capital investment required for sputtering equipment sufficiently large to handle the large throughput. Several vendors have supplied budgetary estimates for such equipment. Although expensive (> 10^6 $) there is no basic problem; but engineering design for scale-up is required.

These cost estimates were made assuming equal cell yield from all three processes. In our processing studies, however, we have found

that the apparently inherent brittleness and warping of the Al BSF cells does reduce the yield and make processing more difficult.

We have also assumed that the unreacted Al on the back of the cell is used as back metallization. Although this appears to be feasible, cell deformation may pose a problem. If it is necessary to remove the Al and remetallize, the cost of the Al BSF would increase significantly.

We have also seen that thinner silicon can be used as a base stock with boron diffused BSF, and this thinner material would decrease the overall cost by reducing the cost of the input material.

Thus a comprehensive trade off study would be required to determine which process is indeed most cost effective.

3.2.6 Summary of BSF Studies

The results reported in this section on back surface field studies can be summarized as follows:

1. A model has been developed which provides optimum design rules for back surface field structure. This model gives insight into the relative importance of surface and bulk recombination on solar cell parameters.

2. Boron diffused back surface cells have shown a maximum V_{oc} of 0.580V. This is probably near the optimum value for a B diffused BSF.

3. Al BSF structures have been prepared using evaporated, sputtered and silk screened Al. All give essentially similar results with maximum V_{oc}'s of 0.58 to 0.59V.

4. The optimum V_{oc} for Al BSF structures has not been attained; possibly because the emitter region is limiting performance.

5. The bulk lifetime, as measured by the open-circuit decay method, is generally lower for silk screened Al BSF cells as compared to sputtered Al BSF cells, and boron BSF cells.

6. Solar cells having Al back surface fields are generally more brittle than boron diffused BSF cells. This condition was still noted when the excess aluminum was etched off the back of the cell. This brittleness causes considerably problems in cell processing and module fabrication. Consideration could be given to removing the Al and re-metallizing, but this would add significantly to the cost of the process.

3.3 Deposition of Antireflection Coating by Spraying

To obtain greater flexibility in our process sequence we investigated a spraying method in which the antireflection (AR) coating could be applied at any of several places in the sequence.

As one example of a possible advantage of this flexibility, if the AR coating could be applied later in the sequence, certain total plated contact systems might be feasible in the sequence. However, any change in the overall cost must also be considered, e.g., a mask may be needed for the plating process.

Initial experiments were carried out using an air brush (Paasche Model VL) with the metal-organic solution of Ti and Si oxides. All substrates were prepared in the same manner as in the solar cell cleaning techniques. Four solution systems were used: ethyl alcohol, butyl alcohol, ethylene glycol and 2 ethyl-1-hexanol.

With the present standard solution (3.5% mixed oxide concentration in ethyl alcohol) all spraying tests resulted in heavy, nonuniform films which cracked and lifted from the silicon after baking.

After diluting the standard solution to a concentration of 1.2% mixed oxides in ethyl alcohol, cracking was less obvious but the film was still not uniform as noted by excessive color variations over the web.

Somewhat improved results were obtained when a 1.8% solution of oxides in ethyl alcohol was diluted with ethylene glycol to a final oxide concentration of 1.2%. The results from this solution showed some slight cracking at the web dendrite interface but the film thickness was more uniform as evidenced by the uniform blue color of the film.

By substituting 2 ethyl-1-hexanol[6] for the ethylene glycol in the above equipment, further improvement was noted in greater color uniformity and less cracking.

It is felt that both ethylene glycol and ethyl-1-hexanol are ideal candidates for solvents to be used in automatic spray equipment.

These tests indicated that spray coating of the AR is a feasible process, however none of the samples prepared using a hand-held spray gun showed the required uniformity over the entire surface as is obtained with the dip coating method.

A sample of the coating solution and a number of web cells and web material were submitted to a vendor of automatic spray equipment. These experiments are not complete.

3.4 Contact Studies

3.4.1 Ti-Pd-Cu System

It was previously reported[7,8] that the Ti Pd electroplated copper system showed promise in that it behaved the same way as the Ti Pd electroplated Ag system, even when sintered at 400°C. This work has been continued by studying the long-term stability of the Ti-Pd-Cu system and the behavior of the evaporated Pd electroplated Cu system. (See Section 3.4.2 for a description of the copper-plating process.)

To test the stability of the Ti-Pd-Cu system, an accelerated test was carried out where samples were heated at 225°C for times up to 600 hours.* Table 11 shows the results of this test. The baseline evaporated Ti Pd electroplated Ag contacted samples were included in the test as a control.

After 600 hours, there was no noticeable change in the cell parameters and the test was terminated.

From these data we conclude that the evaporated Ti Pd electroplated Cu system is as stable as the Ti Pd Ag system under the conditions of the test. Therefore, the Ti (or Ti silicides) do serve as a barrier to the diffusion of the into the silicon.**

3.4.2 Copper Plating Process

The copper plating process used in this work is compatible with our present system. To produce a uniform and adherent layer of copper it is preferable to first flash coat the areas to be plated with a thin film of copper. A proprietary electroless copper plating solution is used and was obtained from Shipley Co., Inc., Newton, MA. This is then followed with an electrolytic copper layer of 5 to 6 μm. See Tables 12 and 13.

The critical part of one copper plating process is after the electroless copper plating is where the PR and excess metals were rejected in acetone. The photoresist must be totally removed for it has a tendency to leave films which interfere with the adherence of the subsequent copper plating. Details are in the process outline, which follows.

---

*The Ti Pd Cu samples were prepared by removing previously electroplated silver and electroplating Cu onto the remaining Ti Pd. The Ti and Pd thicknesses were 120A and 500A respectively. Th electroplated layer was 3 to 4 μm for both Ag and Cu.

**In one earlier test under the same conditions, the Ti Pd Cu contacted samples degraded considerably after 100 hrs. at 230°C. We were not able to repeat this result, and the data in Table 12 are the end result of several further tests, all of which showed no degradation of the Ti Pd Cu system.

TABLE 11

Test for Stability of Ti-Pd-Cu Contact System
(Each Entry is Average of 4 Cells)

Test Cond.	I_{sc} (mA)		V_{oc} (V)		Eff (%)	
	Ti Pd Ag	Ti Pd Cu	Ti Pd Ag	Ti Pd Cu	Ti Pd Ag	Ti Pd Cu
As Fabricated	21.4	21.0	.520	.520	8.1	8.2
75 hrs./225°C in N_2	21.4	21.0	.520	.518	8.2	8.2
23 hrs./225°C in N_2	21.1	20.8	.520	.518	8.1	8.1
375 hrs./225°C in N_2	21.1	20.8	.522	.522	8.1	8.1
600 hrs./225°C in N_2	21.1	20.9	.521	.522	8.1	8.2

Cells not AR coated

Measured at AM-1; 91.6 MW/cm^2

TABLE 12

ELECTROLESS COPPER PLATING SOLUTION

The electroless copper plating solutions have been obtained from Shipley Co. Inc., Newton, MA. The system consists of three solutions CP 70A, CP 70M and Cuposit Z. The proportions used are as follows:

1. Add 1 part CP 70A and 2 parts CP 70M to 16 parts of deionized water.
2. Add 1 part Cuposit Z to the mixture just before plating.
3. Maintain bath temperature at 49°C $\pm$ 2°.
4. Time 20 seconds.
5. Rinse in running deionized water for 10 minutes.
6. Dry with N_2.

TABLE 13

ELECTROLYTIC COPPER PLATING SOLUTION

1. Dissolve 200 grams of Cu SO_4 $5H_2O$ in 1 liter of deionized water.
2. Add carefully, 30 ml of H_2SO_4.
3. Plating temperature 70 - 120°F
4. Current density 20 - 40 mA/cm^2.
5. Ratio of cathode to anode 1:1.
6. Anodes - copper; cathodes - silicon with metal grids.

Process Outline

1. Immerse solar cells with antireflection coating, photoresist and grid area defined with Ti Pd metallization into a electroless copper plating solution for 20 seconds. Rinse in running deionized water for 5 minutes.
2. Place cells into a pyrex baking dish and cover with acetone for five minutes. Swab off loose metal and photoresist with cotton swabs and acetone. Spray cells clean with acetone. Swab again using methanol and cotton swabs. Spray clean with methanol. Dry in N_2.
3. Place cells into a holder that is connected to a power supply and immerse into a electrolytic copper bath.
4. Plate at a current density of 20 to 40 mA/cm^2 with agitation for 30 minutes to give a 5 to 6 μm layer of copper.
5. Rinse in running DI water for 10 minutes and dry with N_2.

3.4.3 Pd-Cu System

In the first Annual Report on this contract,[8] we discussed the evaporated Pd-electroplated Cu system. This system could not withstand sintering above 150°C. Further experiments were carried out to study the effect of (1) thicker Pd layers and (2) sintering the Pd before Cu plating to form Pd silicides.

In these experiments, 800 Å and 3000 Å of Pd were evaporated on the sun side of the cell and 4 μm of Cu was plated on the Pd. The data on these samples is shown in Table 14 in the unsintered column. In this table, η, I_{sc}, V_{oc} and FF have their normal meaning. R_s is the cell

series resistance, R_{SH} the shunt resistance and I_j is the excess junction current measured at 0.3V. From the unsintered data, there is no indication of any difference from a baseline contact system. These samples were then sintered at 300°C for 15 min. in N_2. As seen in Table 14 this process degrades the cells considerably, mainly by a 2 to 3 order of magnitude increase in the excess junction current (R_{SH} is nearly constant). It thus appears that unsintered Pd is unable to form a barrier for Cu diffusion, even at 3000 Å thickness.

In the next experiment, the layers of Pd (again 800 Å and 3000 Å) thick were sintered at 300°C for 15 min. in N_2 to form Pd silicides. After this treatment, 4 μm of Cu was electroplated on the surface. This data is shown in Table 15. Also seen in Table 14 are the results when the Pd Cu system is sintered at 300°C. Again, there is severe degradation due to an increase in the junction excess current. The conclusions that can be drawn from this data is that Pd sintered at 300°C does not form a barrier for Cu diffusion. (The degradation noted is due to Cu and not Pd because the cells with Pd only were measured and showed a very low junction excess current.)

These data show that the Pd Cu system is sensitive to heat treatment, and thus a barrier metal is required.

3.4.4 Total Plated System

Possible methods for lowering the cost of silicon solar cell processing are constantly being examined. To this end, we are investigating the electroless Pd-Ni plating system as described by Motorola. However, we are coating the Pd-Ni plated layers with electroplated Ag instead of dipping it into liquid solder.

We have not investigated the cost factors in this process nor have we run a SAMICS calculation. However, the process does require a significant amount of wet chemical treatment and the use of corrosive and toxic substances which require special handling equipment and disposal techniques. These considerations suggest a careful study is required before the total plated system can be proven cost effective.

TABLE 14

EVAPORATED Pd - PLATED Cu CONTACTS

	800Å Pd + 4 μm Cu		3000Å Pd + 4 μm Cu	
	Unsintered	Sintered	Unsintered	Sintered
$\eta(\%)$	8.96	4.67	9.15	3.0
I_{sc}(mA)	21.5	20.9	21	21
V_{oc}(V)	0.542	0.501	0.552	0.360
FF	0.727	0.426	0.746	0.4
$R_s(\Omega)$	0.8	0.4	0.6	0.3
$R_{sh}\|_{-1V}$ (KΩ)	40	40	33	30
$I_j\|_{.3V}$ (mA)	0.01	5.67	0.082	14

- Sintering was done at 300°C for 15 min. in N_2.
- Sintering degrades the junction response severely.
- It appears that unsintered Pd is unable to form a barrier for Cu diffusion regardless of Pd thickness.

TABLE 15

SINTERED Pd - PLATED Cu CONTACTS

	800Å Pd Sintered at 150°C 4 μm+ Cu		3000Å Pd Sintered at 300°C 4 μm+ Cu	
	Unsintered	Sintered	Unsintered	Sintered
$\eta(\%)$	8.77	4.62	8.71	2.46
I_{sc}(mA)	20.4	20.4	20.9	18.5
V_{oc}(V)	0.538	0.488	0.543	0.298
FF	0.755	0.458	0.725	0.42
$R_s(\Omega)$	1.5	0.46	0.8	0.3
$R_{sh}\|_{-1V}(K\Omega)$	100	60	250	10
$I_j\|_{.3V}$(mA)	0.019	4.5	0.038	11

- Sintering was done at 300°C for 15 min. in N_2.
- Sintering the heat treated Pd-Plated Cu contacts severely degrades the junction response.
- Pd sintered to 300°C does not serve as a barrier for Cu diffusion.
- Degradation is related to Cu and not to Pd because Pd sintered alone at 300°C gives good cells.

In the Motorola process a dilute Pd solution is used to sensitize the silicon cell by a displacement reaction. This is followed by an electroless Pd solution utilizing an autocatalytic reaction for plating the Pd to the sensitized surface. After a heat treatment in nitrogen at 300°C, electroless Ni is plated onto the Pd surface. The final step in the Motorola process however, differs from that used by Westinghouse; in our method silver is electroplated over the Ni, while the Motorola process reflows solder over the Ni. The plating solutions given in Motorola specification are shown in Table 16.

In initial test runs with the standard Motorola process, it was noted that the required etches and rinses attacked the antireflection coating (used as a plating mask), and thus much of the silicon surface was plated as opposed to plating only in the grid areas.

This attack on the AR is not a problem in the complete Motorola process since they use silicon nitride as an AR coating and this is impervious to the etches and rinses.

Due to these results, the Motorola process was modified with the HF and aqua regia rinses being carried out for shorter lengths of time. This modified process is shown in Table 17.

With this modification, a test run of 30 cells (all from the same web crystal) were processed through this modified procedure (including an electroplated Ag top metal replacing the solder dip). Before the initial plating, the cells had an AR coat with the contact grid etched to the Si.

The data on these cells are given in Table 18. Only 15 cells survived to the testing stage. The main loss mechanism was a slight attack of the AR coating by the Pd plating solution with subsequent nucleation of Pd on areas other than the cell grid structure. During the second plating, the nickel plated over much of the cell surface, apparently using the Pd nuclei as starting points.

In Table 18, the cells with very poor properties (31, 32, 52) had high series resistance on the order of 5 to 10Ω. This may be due to

TABLE 16

PLATING SOLUTIONS

(MOTOROLA SPECIFICATION)

Palladium Sensitizing Solution

1. To 1500 ml of 50°C deionized water add 50 ml HCℓ and 0.04g of palladium chloride. Stir until dissolved.

2. Add 10 ml ammonium fluoride-stir.

Palladium Stock Solution

1. Add 10 ml of HCℓ and 1.9g of palladium chloride to 100 ml of 50°C deionized water - Stir.

Electroless Palladium Solution

1. Add 30 ml of palladium stock solution to 165 ml of NH_4OH. Allow to stand 1 hour and filter into 750 ml of deionized water.

2. Add 27g of $NH_4Cℓ$ and 3.75g sodium hypophosphate. Stir.

3. Use solution at 50°C and a pH of 9.7-9.8.

Electroless Nickel Plating Solution

1. Dissolve 15g of nickel chloride in 440 ml of deionized water.

2. Add 25g NHCℓ, stir until dissolved. Add 42g sodium citrate, stir until dissolved. Add 5g sodium hypophosphate and 65 ml of NH_4OH. Stir until dissolved.

3. Use solution at 80°C and a pH of 10.0.

TABLE 17

MODIFIED ELECTROLESS PLATING FOR Pd and Ni

1. Etch cells to open grid in AR coating and rinse in DI H_2O (Use 60/40/100::$NH_4F/HCl/H_2O$).

2. Place cells into a teflon carrier and immerse into a palladium sensitizing solution under a high intensity light for 3 minutes while agitating gently. (Maintain high intensity light within 6 inches of the cells.)

3. Rinse carrier and cells in running deionized water for 5 minutes.

4. Again immerse cells into the palladium sensitizing solution under a high intensity light for 5 minutes while agitating gently.

5. Rinse carrier and cells in running deionized water for 5 minutes.

6. Place carrier and cells into the electroless palladium solution (50°C) for 1 minute while agitating. Ambient light is kept low.

7. Rinse carrier and cells in running deionized water for 5 minutes.

8. Place cells into a quartz boat and insert into a quartz tube furnace at 300°C with a N_2 flow for half hour. Cool.

9. Place cells back into carrier and immerse into a electroless nickel plating solution at 80°C for 5 minutes while agitating.

10. Remove carrier and cells from the nickel solution and rinse in running deionized water for 5 minutes.

11. Plate silver electrolytically.

TABLE 18

Parameters of Cells Fabricated Using Modified Electroless Plating for Contacts[9]

Cell #	I_{SC}(mA)	V_{OC}(V)	FF	EFF(%)	τ_{OCD}(μsec)
11	27.9	.515	.719	10.8	1.7
12	28.1	.510	.721	10.9	1.6
21	26.8	.514	.711	10.4	1.8
22	26.9	.513	.718	10.5	2.1
31	19.3	.483	.365	3.6	.9
32	22.6	.501	.363	4.4	2.0
41	29.2	.502	.697	10.8	1.2
42	28.7	.502	.672	10.2	1.2
52	18.5	.479	.351	3.3	1.8
61	29.0	.508	.721	11.2	1.8
62	28.6	.500	.707	10.7	1.8
71	27.8	.496	.629	9.2	3.1
72	28.6	.508	.704	10.8	2.9
81	26.0	.480	.661	8.7	1.0
82	27.2	.501	.704	10.2	1.0
STD(3)	29.8	.556	.740	13.3	12.0

1) AM-1 Illumination - 91.6 watts/cm^2, AR coated.

2) All cells fabricated from same web crystal.

3) These are the parameters of cells fabricated from the same web crystal but with evaporated Ti-Pd-Ag contacts.

incomplete removal of the AR from the grid areas. Thus, the metal would not be in continuous contact with the silicon. The generally lower fill factor on the other cells is apparently due to a slightly higher series resistance than normally achieved. In general, the efficiency of the best cells was 2.5 to 3% (absolute) lower than the standard processed cells. Some decrease in the I_{SC} may be due to an attack by the solutions on the AR coating which would make it less effective, i.e., lower enhancement. After these measurements, selected cells were sintered for 15 minutes at 425°C. There was no systematic improvement.

From these results and those of earlier tests, we conclude that the Motorola process specification is not immediately transferable to the process sequence we use. It is also concluded that substantial effort would be required to make use of this process specification.

3.5 Interconnection Technology

3.5.1 Interconnection Requirements

Completed solar cells must be interconnected in series and/or parallel arrangements within a module in such a manner that the interconnection process does not interfere with the preceding or subsequent steps.

Interconnect reliability is of major concern. For the interconnections to maintain high bond strength and conductivity the effects of corrosion, formation of intermetallic compounds, mechanical stress and metal fatigue must be minimized.

In addition to these technical requirements, the interconnect process must be low cost and amenable to high throughput and automation.

And, most importantly, the bonding process must have high yield in terms of acceptable bonds and cell breakage. A large number of bonds will be required for each module, and several failed bonds or one broken cell can degrade the entire module.

3.5.2 Ultrasonic Bonding Evaluation

3.5.2.1 Introduction

A number of methods for interconnecting solar cells were discussed in the last annual report[8] on this contract. Such methods include conductive adhesive bonding, parallel gap welding, laser welding, thermo-compression bonding, soldering and solder reflow. However, based on a number of technical and cost factors, early in the program we chose to investigate ultrasonic bonding as a cell interconnection method.

Ultrasonic bonding has a number of advantages for interconnecting solar cells and should be considered a viable alternative to solder bonding. Some of these advantages are listed below:

- most materials can be bonded
- low contact resistances are possible
- strong bonds can be achieved
- corrosive flux removal operations are unnecessary
- total cell thickness is minimized (solder build-up)
- moderate capital cost
- low energy consumption
- amenable to automation with high throughput.

Bonding between two materials can be made to take place when the material surfaces are scrubbed against each other at ultrasonic frequencies. The detailed method by which the bonding takes place is not known in all cases. When thermo-plastic materials are bonded, the scrubbing action appears to generate sufficient heat that local melting of the surfaces occurs. When metals are joined, it is less likely that melting occurs; instead, it is hypothesized that either (1) surface oxides and contaminants are abrasively removed and atomic contact between clean metals is achieved, which in turn leads to chemical bonding or (2) the scrubbing action causes microfractures in the surfaces of the metals and these fractures interlock forming a strong metal-to-metal bond.

Whatever the exact mechanism of ultrasonic bonding between metals, the process is successful in applications ranging from joining large copper busbars onto electric motor alternators to attaching fine wires to thin films on integrated circuits.

Because the exact nature of the bonding process is not known, the achievement of acceptable ultrasonic bonds is largely an empirical process. A large number of parameters determine the quality of an ultrasonic bond. In so far as the materials are concerned, the thickness, temper, surface condition and the materials themselves are important. Among the bonding parameters are the ultrasonic frequency, the vibrational amplitude, the size and shape of the tool, the tool material, the vibrational power input, the clamping force between the tool and the work piece, and the length of the time interval during which power is applied. It has also been shown that the properties of all the materials beneath the work piece have an effect. Although there are a large number of variables, experience has shown that once the materials to be joined have been chosen, that some combination of the force power and time of the welding will result in good ultrasonic bonds.

Ultrasonic bonding machines are of two basic types. The simplest type — the spot bonder, is one in which the ultrasonically-driven tool contacts the materials to be joined in a single area. After a bond is made, the tool is lifted and repositioned in preparation for the next bond. An analysis of this operation shows that the throughput rate of bonds is limited by the time required to reposition the tool between bonding operations. In the second type of machine, commonly called a seam bonder, the ultrasonically-driven tool is in the shape of a wheel which is made to roll across the workpiece, making a continuous linear bond. This type of machine is widely used to splice the ends of metal foils and plastic sheets. The advantages of applying this type of machine to solar cell interconnection are obvious if the interconnect material is in the form of a continuous tape or web to be bonded along one edge of a solar cell. Even if the interconnect is in the form of discrete tabs bonded at points one centimeter apart, the use of a seam welder type of

machine will result in increased bonding speed: a spot bonder can bond and position itself for another bond at a rate of about one bond per second; a seam welder can roll along a solar cell edge (or along a long line of solar cells) at a rate of 15 cm/sec, making 15 bonds per second.

For these reasons given above, Westinghouse has proposed that solar cell interconnection should be accomplished with thin metal foils (e.g., aluminum or copper) ultrasonically bonded to solar cell metallization.

A preliminary experimental survey of materials and ultrasonic bonding parameters was undertaken in 1978 at the Sonobond Development Laboratory by Westinghouse personnel. The machine used was a Sonobond ML-6010 (W1060D) spot bonder with a 0.062" diameter tool having a two-inch tip radius. This machine operates at a frequency of 60 KHz (max power output is 10 watts). The results of this study were reported in the First Annual Report.[8] It was concluded that when proper processing parameters are used, low resistance, strong bonds can be made between a variety of metal foils or ribbon and dendritic web solar cell metallizations.

To further optimize this process and establish the capabilities for using ultrasonic welding in the fabrication of the modules, the same model spot welder discussed above was purchased. With this equipment, tests were made to study the bond parameters and determine yield. Before studying failure mechanism we have to establish a capable bonding process. The bonding parameters were determined for different interconnect metal-contact metal systems, including tests on the metal system used in the modules, i.e., Al-Al and Al-Cu.

During the latter part of the program, some preliminary experiments using an ultrasonic seam welder were carried out. This apparatus bonds using a continuously moving circular weld head.

3.5.2.2 Bonding to Electroplated and Evaporated Silver

The first series of tests were carried out to determine the effect of the bond parameters on various metal foil interconnects and to study the failure mechanism of bonds. The contact metal was evaporated or electroplated silver. Since the metal foil interconnect was not initially specified, the tests were made with copper, aluminum and nickel foils.

These tests were made with the Sonobond (Model W-1060D) welder shown in Figure 5. Metal bonding parameters (force, time, and power) were selected based on previous experience with a similar unit at Sonobond Corporation and on trial runs on the new machine at Westinghouse. Copper, aluminum and nickel ribbons were bonded to plated silver and evaporated silver (Ti/Pd/Ag) metallization. The bonds were pull tested and the interface after ribbon lift-off was examined and photographed at 100Z. The results are summarized in Table 19. Aluminum bonds to evaporated silver were of uniformly high strength. Copper bonded to evaporated silver and nickel to electroplated silver gave somewhat higher strength bonds but with less reproducibility. An examination of the silicon surface (bond interface) after lift-off showed that the highest bond strengths correlated with significant cratering. The crater area was estimated, and the bond strength was calculated based on force per unit area. Values ranging from 1000 to 3000 psi were typical. The investigation revealed that the lack of reproducibility appeared to be the most significant problem which would have been the result of several factors:

- poor metallization adherence due to surface contamination
- movement or resonances in the silicon or metal tab during bonding (variations in energy coupling at the bond interface),
- room and table vibrations.

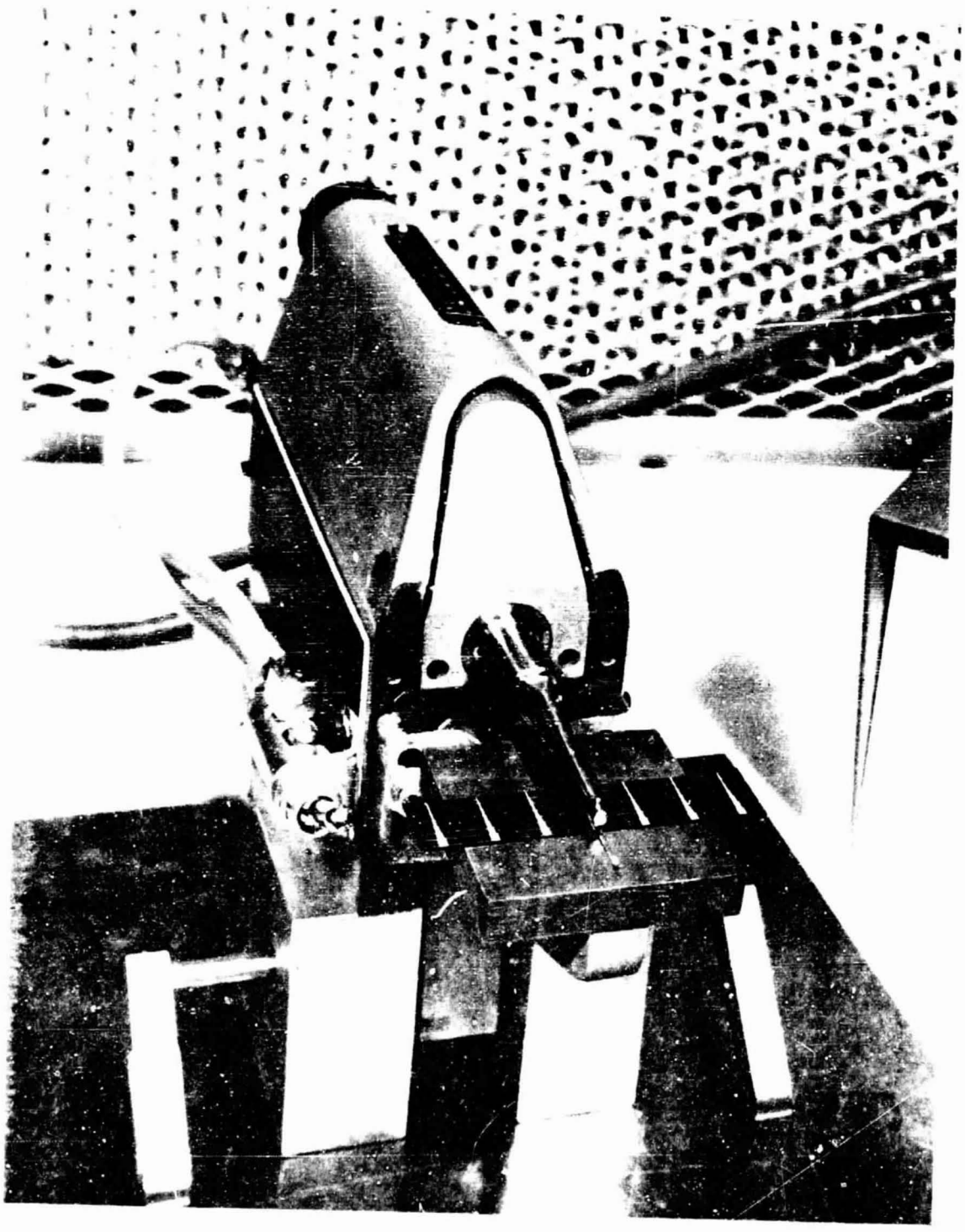

Figure 5 Sonobond ultrasonic weld head (Model W-1060D).

TABLE 19

RESULTS OF BOND TESTS
(SONOBOND W-10600 WELDER)

Ribbon to Metal Surface	90° Peel Test			Bond Parameters			Interface Inspection
	Average (Grams)	Std. Dev.	MAX (MIN)	Power (Watts)	Force (OZ)	Time (Sec.)	
Copper (2 mil) - Plated Ag	32	57	118(0)	26	30	3	Cratering of Silicon (Concoidal fracture = High Str. Bonds)
Copper (2 mil) - Evap. Ag	109	73	181(14)	18	18		Cratering of Silicon (Concoidal Fracture = High Str. Bonds)
Aluminum (1.5 mil) - Plated Ag	36	15	64(16)	18	18	.07	---
Aluminum (1.5 mil) - Evap. Ag	43	18	72(11)	17	21	.07	Cratering of Silicon (Matte Texture in Fracture Area)
Nickel (1.5 mil) - Plated Ag	94	133	188(0)	26	30	3	Cratering of Silicon (Concoidal fracture = High Str. Bonds)

A second and more extensive group of bond tests, with copper and nickel ribbon ultrasonically welded to plated silver, were made. The ribbon was 50 mils wide by 1.5 mils thick. Bonds were made or attempted over a wide range of clamping forces, power, and weld time settings on the Sonobond unit. The objective of these tests was to determine the range of variables over which good bonds could be achieved and to identify those factors which contributed to bond strength variability in the first test series.

The 4 x 4 clamping force-power matrix in Figure 6 shows the shaded area where bonds were observed for 1.5 mil thick copper ribbon to 4 μm thick electroplated Ag with an evaporated Ti/Pd underlayer. The weld time in this matrix was 1.2 seconds. The metallized cells used in these tests did not receive any post-deposition sintering since previous data showed that, on occasion, the sintering step resulted in some loss of cell efficiency. A similar 4 x 4 clamping force-power matrix was evaluated for shorter weld times (0.035, 0.10, and 0.2 seconds). No bonds were made at these time intervals for copper ribbon to plated silver, even at the highest force (38 oz) and power (30 watt) levels. A total of 48 trials were made (5 bond attempts at each power-force setting).

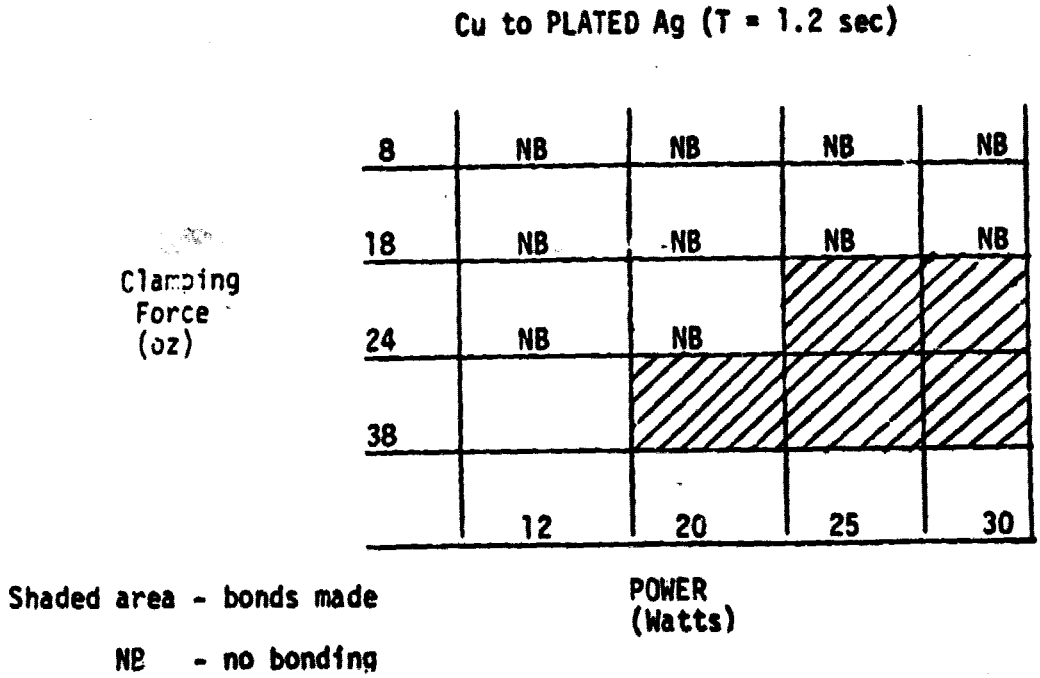

Fig. 6 4 x 4 clamping force - power matrix for copper ribbon ultrasonically welded to plated silver (1.2 second weld time).

A similar series of tests were run for 2 mil thick high purity (> 99.99%) nickel ribbon to plated silver-metallized silicon web cells. Good bonds were observed in the shaded area of the 4 x 4 matrix (1.2 second weld times) shown in Fig. 7. Note that bonds were made at lower clamping forces (8 to 18 ozs.) compared to 24 to 38 oz. for copper ribbon (Fig. 5). The nickel ribbon welded at higher clamping forces adhered to the bonding tool tip rather than the cell.

Table 20 shows the 90° pull-strength data for copper ribbon bonded to plated silver. The strength of 18 bonds was measured at the clamping force-power settings shown in the table. The overall average bond strength was 139 grams. An examination of the bond areas on the substrate and ribbon after the pull-test showed that most failures occurred in the copper ribbon rather than at the metallization-substrate interface. Typically, a small section of the ribbon was pulled-out and section remained attached to the cell. The photomicrographs in Fig. 8 show the effect for two different copper to plated silver test specimens.

The bond strength data for nickel ribbon in Table 21 shows considerably more scatter than the results for copper ribbon, and the overall average strength is lower for 26 bonds (44 grams). Figure 9 shows a photomicrograph of the bond area on the cell for a high strength specimen (181 grams). A small piece of the nickel ribbon is still attached to the substrate. The bond area on the substrate for a lower strength specimen (22.7 grams) is shown in Fig. 10. The photomicrographs show that about one half of one bond area has a mirror-like surface (exposed silicon substrate) where the metallization was pulled away with the ribbon. The other half of the bond area containing a small section of the silicon cell pulled out, indicates that a metallurgical type bond was made in this area. These effects are typical for all of the bonds that were inspected at high magnification.

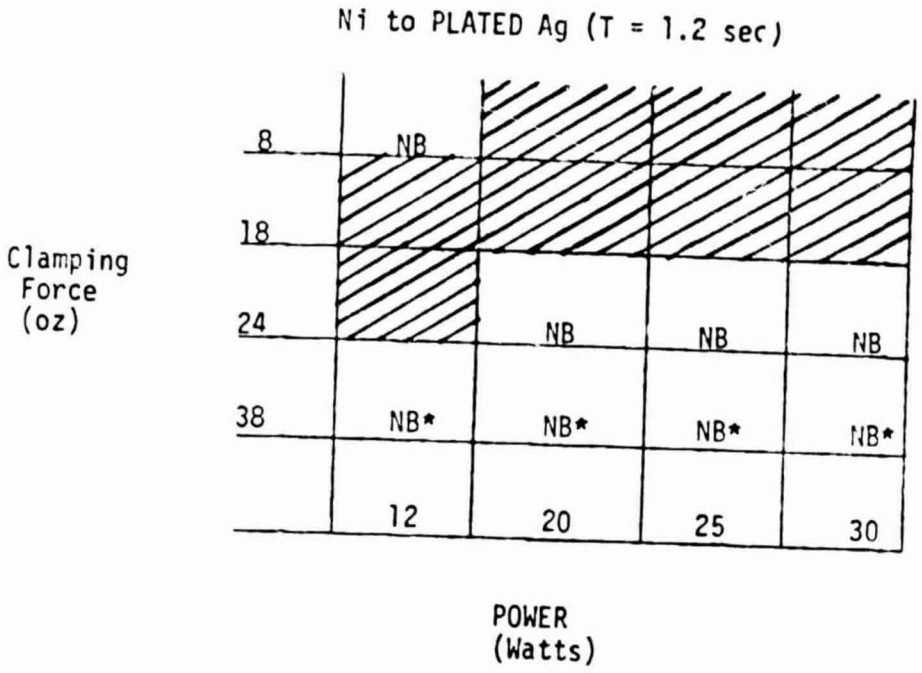

Fig. 7 4 x 4 clamping force - power matrix for nickel ribbon ultrasonically welded to plated silver (1.2 second weld time)

TABLE 20

90° PULL TEST DATA

1.5 MIL COPPER RIBBON BONDED TO PLATED SILVER (4μ)

Power (Watts)	Clamping Force (OZ)	90° Peel Strength Average (Grams)	Std. Dev.	Max.	Min.	Bonds Tested	Failure Mode
12	38	5	2	7.0	2.0	3	All metal ribbon-Metallization interface
20	38	189	28	209	169	2	Metal ribbon
25	38	19	--	---	---	1	--
	24	232	50	268	196	2	Metal ribbon
30	38	149	117	331	0	8	Metal ribbon and Si pull-outs
	24	216	11	223	209	2	Metal ribbon
Average (All Bonds)		139	109	331	0	18	

Specimen #1 (100X)

Copper Ribbon

Substrate

Failed @ 69 grams

Specimen #2 (100X)

Hole pulled out of center of copper ribbon
Failed at 223 grams

Figure 8 Photomicrographs of failed bond areas for two different copper ribbon to plated silver test specimens.

Substrate Bond Area (100X)

Failed at 181 Grams
(Note Piece of Ribbon Attached to Substrate)

Figure 9 Photomicrograph of the bond area on the substrate for a high strength bond (Nickel Ribbon).

Substrate Bond Area (100X)

Failed at 23 Grams
(Note Mirror Surface and Crater Pull-Out)

Figure 10 Photomicrograph of the bond area on the substrate for a low strength bond (Nickel Ribbon).

These studies of bonding Cu and Ni ribbon to plated Ag metal suggest that the main failure made is at the Ti/Pd/Ag-Si interface. The difference in the data in Table 21 and 22 as compared to Table 20 is probably due to variability in the metal adherence.

Copper ribbon bonds were strong only as high energy levels and no bonds were formed at lower levels of energy. The higher energy with greater frictional heating would tend to initiate some metallization sintering increasing the contact metal adherence. However, with the Ni ribbon bonds were formed at low levels of energy and no sintering would occur and the bond strengths (i.e. metal adherence) was more variable.

The bond strengths given in this section show considerable variation. At this point we cannot define the minimum bond strength required.

The average pull strength for 52 bonds in the 0.1 second matrix was 59 grams with a standard deviation of 33. Somewhat higher strengths were measured in the 0.25 second matrix for 42 bonds (average 79 grams, standard deviation 34).

3.5.2.3 Bonds to Aluminum and Copper

Cells metallized with Ti-Pd electroplated copper front contacts and aluminum back surface fields have been selected for module assembly. The next series of ultrasonic bond tests were designed to determine if good quality bonds could be made to these metallization systems at high yield.

- Aluminum to Electroplated Copper

Earlier work has shown that aluminum ribbon forms more reliable bonds to either plated copper on the front of the cell or aluminum on the back surface of the cell. Thus a study was made of the bonding parameters of Aℓ to electroplated Cu. These tests were performed to verify that good quality bonds could be made with this metal system for demonstration modules. A clamping force-power matrix was examined for two different weld times. The results are shown in

Table 22. The number in parenthesis is the average pull strength of 3 to 5 bonds. A total of 66 bonds were measured giving an overall average pull strength of 74 grams with a standard deviation of 60. Good bonds were made at all clamping force-power settings in both of the test matrixes. The strongest bonds (150 to 250 grams) were developed in the matrix with the longest weld time (1.2 seconds). In general these results are equivalent to or better than those measured previously between aluminum ribbon and plated silver. The electrical parameters for these bonds were similar.

- Ultrasonic Bonding to Aluminum Metallization

Several different types of aluminum back surface field processes have been evaluated. In general, it is possible to produce strong bonds to sputtered and reacted aluminum although the reproducibility is not as good as with silver or copper metallizations.

Pull strength data have been obtained for copper, nickel, and aluminum ribbon leads bonded to sputtered and alloyed aluminum. The data is shown in Table 23.

TABLE 23

ULTRASONIC BONDING TO METALLIZATION

Interconnect Strap	# of Bonds	Av. Strength (grams)	Std. Derivation
Copper	8	88	54
Nickel	8	30	10
Aluminum	9	100	85

Since the demonstration modules will be fabricated using Al back surface fields, contacting to Al is a necessity and the reproducibility problems make module fabrication difficult.

TABLE 22

90° PULL TEST DATA

POWER (WATTS)	CLAMPING FORCE (OZ)	90° PULL STRENGTH AV (GMS)	# BONDS TESTED
	1.5 MIL AL TO 4 μm THICK PLATED CU - WELD TIME 1 SEC		
20	18	32	3-5
20	24	30	3-5
20	32	38	3-5
25	18	54	3-5
25	24	74	3-5
25	32	61	3-5
30	18	94	3-5
30	24	92	3-5
30	32	98	3-5
	1.5 MIL AL TO 4 μm PLATED CU - WELD TIME 1.25 SEC		
20	18	117	3-5
20	24	59	3-5
20	32	46	3-5
25	18	114	3-5
25	24	34	3-5
25	32	49	3-5
30	18	82	3-5
30	24	93	3-5
30	32	153	3-5

3.5.2.4 Ultrasonic Bonding in Module Fabrication

As described in the preceeding sections, the technical feasibility of ultrasonic bonding of solar cell interconnections has been demonstrated. In this section we will discuss tests concerned with using ultrasonic bonding in actual module fabrication.

The module fabrication procedure (discussed in detail in Section 3.7.2 involves making interconnections to the front of the cell, then mounting the cell on a glass superstrate with adhesive, and after curing, completing the back interconnects.

Several features of this fabrication process were evaluated to establish feasibility.

An ultrasonic bond test was performed to determine if leads could be bonded to dendritic web silicon solar cells embedded in a silicon rubber (RTV) material. The test was designed to simulate the method used to interconnect a solar cell array as described in our process sequence. When the cells are embedded in an adhesive there is some concern that they would vibrate during ultrasonic bonding. This could result in lower bond strength or even prevent bond formation.

In this test, cells were embedded in GE RTV 615. The resin was spread evenly over a glass substrate to a thickness of 2-3 mils. Solar cells were laid on top of the glass surface with a circular motion (sun side down). The array was cured at 70°C. Ni ribbon leads were then ultrasonically bonded to the Ti/Pd/plated Ag back surface. (This contact system was used for the test due to the reproducibility problem with the Al system.

These data show bond strengths equivalent to or better than those previously reported for cells not embedded in RTV. The next test was similar, except that ribbon leads were first bonded to the sun side of the cells before embedding in RTV. This test was designed to provide a more complte simulation of an actual interconnected module. The concern here was that the ribbon lead thickness might aggravate the

tendency for the cells to crack under the high-point loading required during ultrasonic bonding of the leads to the back side of adjacent cells in the array. The first attempt was not successful because of excessive thickness of the RTV under the embedded cells with the result that many cells were cracked. A second assembly was prepared and extra care was taken to ensure that only the minimum thickness of RTV was present between the cell and glass for proper adhesion (~ 2 mils). The results of this test were significantly better. It was possible to produce strong bonds to plated Ag using three different metal ribbon leads (Al, Cu, and Ni) without cracking the cells. The bonds cannot be pull tested because of the short lengths of ribbon extending from the welds. However, a qualitative evaluation of bond strengths indicates that the pull strengths are comparable to those previously tested.

In order to interconnect a working cell array on larger plates, additional clearance is needed between the weld tip and the base of the ultrasonic shank. An extended shank (6.587 inches) has been obtained together with a longer weld tip. This assembly will permit the interconnection of cell arrays mounted on plates up to 30 x 30 cm to ensure the best possible bonding conditions, the modified welder was taken to the Sonobond factory for set-up. The spot welder was adjusted by Sonobond and a number of good bonds were made using the extended shank. Bonds were made between aluminum ribbon and metallized silicon web (sputtered aluminum back surface metal and electroplated copper.)

During the various tests discussed above, a large number of failures occurred. On interconnections to the back (Al) side the failure mode was cell breakage, generally in an irregular manner initiating at the bond point. On the front of the cell the failure mode was similar in that a number of small cracks would propagate from the contact point, and in extreme cases the cell would shatter. The failure rate during this process was greater than 50%.

Subsequent tests showed the following:

1. This problem did not arise, or was much less noticeable, with boron back surface field cells, even when the cells were <125 μm thick.

2. The problem was less significant when the Aℓ back surface field cells were thicker than 200 μm.

It would then seem that the low yield is due to two, probably interrelated, conditions of thin cells and the inherent brittleness of Aℓ BSF cells.

At this point we conclude that although parameters have been developed for ultrasonically bonding metal interconnects to the cell, the yield of the process is so low that the process is not usable to fabricate the demonstration modules.

3.5.2.5 Ultrasonic Bonding to Screen Printed Samples

Silk screening of grid lines is the selected top contact process by several contractors. To determine the suitability of ultrasonic bonding to this type of contact, samples were obtained and a series of bonding tests carried out.

A group of 3 inch silicon wafers were obtained from RCA[10] with a screened on grid pattern. Attempts were made to ultrasonically bond copper, nickel, and aluminum ribbon leads. Adequate bonds could not be obtained with copper or nickel straps but good results were obtained with aluminum ribbon. In fact, it was possible to make strong bonds with pull strengths of 50-100 GMS over the complete force-power matrix described in the preceding section for weld times of 0.1 seconds and 0.25 seconds.

3.5.2.6 Ultrasonic Seam Bonding

A Sonobond seam welder (Model MS-5010) designed for welding large sheets of aluminum foil was modified to determine the feasibility for seam wleding interconnections to the silicon web cells. Several successful seam welds were made between 6-8cm lengths of metallized silicon (aluminum BSF) and aluminum foil. The aluminum foil was bonded

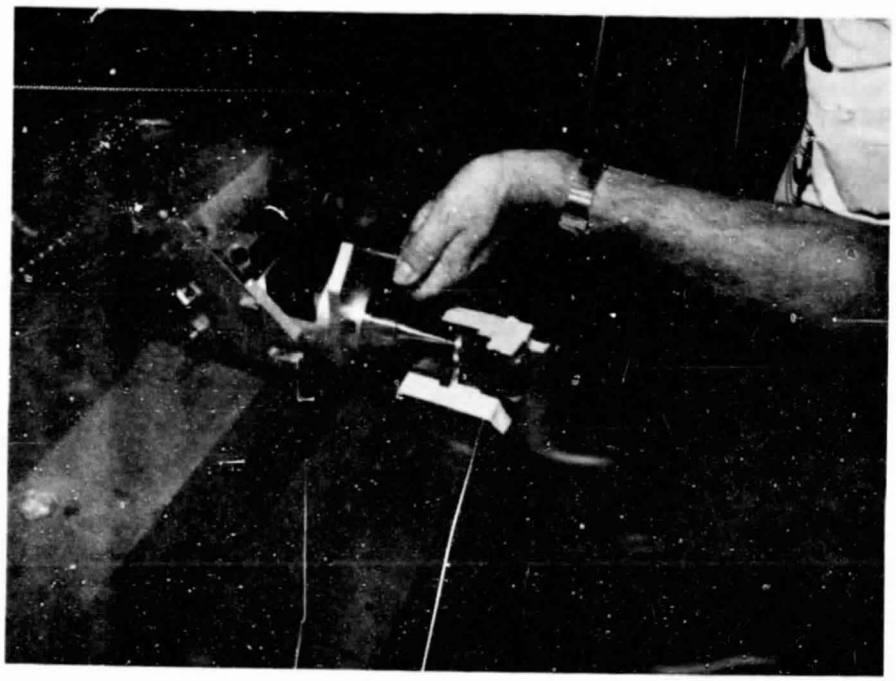

Figure 11 Ultrasonic seam welding an aluminum interconnect foil to a dendritic web solar cell.

continuously over the entire length of the silicon strip in less than 3 seconds.

The photograph in Figure 11 shows the set-up with the silicon web and aluminum foil taped to an underlaying sheet of copper foil. The circular weld head was rolled over this assembly at a rate of 1cm/sec using a pressure of 25 grams (approximately 35 watts power). The aluminum foil bonded tightly to the silicon along its entire length. No indication of cracking or cell damage was visible. Several additional pieces of silicon were bonded with equally good results. It is evident that further evaluation with specialized fixturing and interconnect materials is needed to establish a viable process. However, these preliminary results are very encouraging particularly in comparison to the difficulties experienced with cell cracking using a spot bonder.

3.5.2.7 Summary and Conclusions

An experimental evaluation of ultrasonic bonding parameters and materials has demonstrated the feasibility of attaching interconnecting leads to a wide variety of deposited metals on dendritic web solar cells. Considerable practical information has been obtained on candidate material systems, process parameters and bond characteristics as well as the requirements for the design of improved jigs and fixturing. Proper fixturing and processing techniques were found to be the key to producing good quality bonds without damaging or cracking thin dendritic web cells.

The yield has been low when tests were made on 7.cm long cells due to the AIBSF process induced brittleness of thin (4-6 mils) dendritic web material. It is essential that nearly 100% yield is achieved during module assembly. Therefore, it was decided to use solder bonds for the demonstration modules to be delivered under this contract.

Preliminary experiments with an ultrasonic seam welder produced very promising results indicating that a high throughput, automatable process can be developed for solar cell interconnection.

3.6 Mask Design

3.6.1 Design

One of the program objectives was to design a more efficient metallization grid pattern. That is, a grid pattern which collects the largest amount of energy from the cell.

To derive the best grid configuration, the various loss mechanisms in the cell must be considered and their sum minimized. The grid pattern considered in these calculations is a series of straight lines emanating from a central pad at a specific angles of a 1 cm long by "h" cm wide cells. The angles were chosen to give equal area sectors between the grid lines and the minimization discussed below was carried out only on this geometry.

The ohmic losses and the active area losses considered were:

1. sheet resisitivity of the diffused surface layer,
2. resistivity of the grid fingers (assumed 10 μm high),
3. current loss due to active area of cell being covered by the grid finger,
4. the interface resistance between the silicon and the metal contact, and
5. the bulk resistance of the silicon.

To determine the minimum loss, effects of these parameters were determined by a field theory method over the sectors between the grid fingers, summed, and then minimized with respect to the geometric parameters.

The first calculation determined the optimum number of grid fingers for a given finger width and for 1.6 cm and 2.5 cm wide cells. In this calculation, it is assumed that the grid pattern repeats every one cm; therefore, the results are valid for cells of any length.

Table 24 shows the results of this calculation for 25 μm and 50 μm finger widths. The term η/η_o is the ratio of the efficiency of the given grid configuration to a no loss configuration.

TABLE 24

OPTIMUM NUMBER OF GRID FINGERS AT GIVEN FINTER WIDTH FOR 1.6 cm and 2.0 cm WIDE CELLS

Cell Width = 1.6 cm			Cell Width = 2.0 cm		
η/η_o	# Fingers	Width of Fingers (μm)	η/η_o	# Fingers	Width of Fingers (μm)
.970	4	25	.959	3	25
.970	5	25	.964	4	25
.969	6	25	.964	5	25
.958	4	50	.964	6	25
.965	5	50	.963	7	25
.948	6	50	.961	8	25
			.954	3	50
			.954	4	50
			.950	5	50
			.945	6	50
			.940	7	50

These indicate that for either the 1 mil or 2 mil finger width, four to five fingers are required per half cell.

It is instructive to determine the effect of the cell width on the normalized efficiency, η/η_o.* The calculation was carried for cells from 1 cm to 10 cm wide and for finger widths from 5 μm to 200 μm. These data are shown in Fig. 10. One factor to be noted is that there is a distinct penalty in efficiency incurred when wider cells are used, especially with narrow grid fingers. For the wider grid fingers (100-200 μm) which impose their own penalty, the effect is minimal up to a 4 cm wide cell. However, for the thinner grid fingers (25-50 μm), the difference between a 1 cm wide cell and a 4 cm wide cell is significant.

An implicit result of the data in Fig. 12 is that for higher efficiency cells, the grid finger width must be as small as possible, and no more than 50 μm wide. Such widths are attainable only by photolithographic techniques. The additional cost of this method (if any) must be considered in a trade-off with decreased cell efficiency when using wider grid fingers.

A new mask, incorporating the new pattern has been prepared. 1.6 and 2.5 cm wide masks with grid fingers of 25 μm and 50 μm have been fabricated. This mask is shown in Fig. 13. The figure is a 10-times enlargement of a 1.6 cm x 4.0 cm mask.

3.6.2 Results

To determine the effectiveness of the mode discussed in the last section, a test was made where cells having the new design mask patterns were alternated down the length of the web with the standard mask pattern. The standard mask pattern is shown in Figure 14. This consists of a series of collecting grids, with a nominal 0.2 cm spacing and vertical bus bars perpendicular to these grids with a nominal 1.0 cm spacing. The total grid area coverage is 8.9% .

---

* η_o is defined as the efficiency of the cell when all ohmic and active area losses are zero.

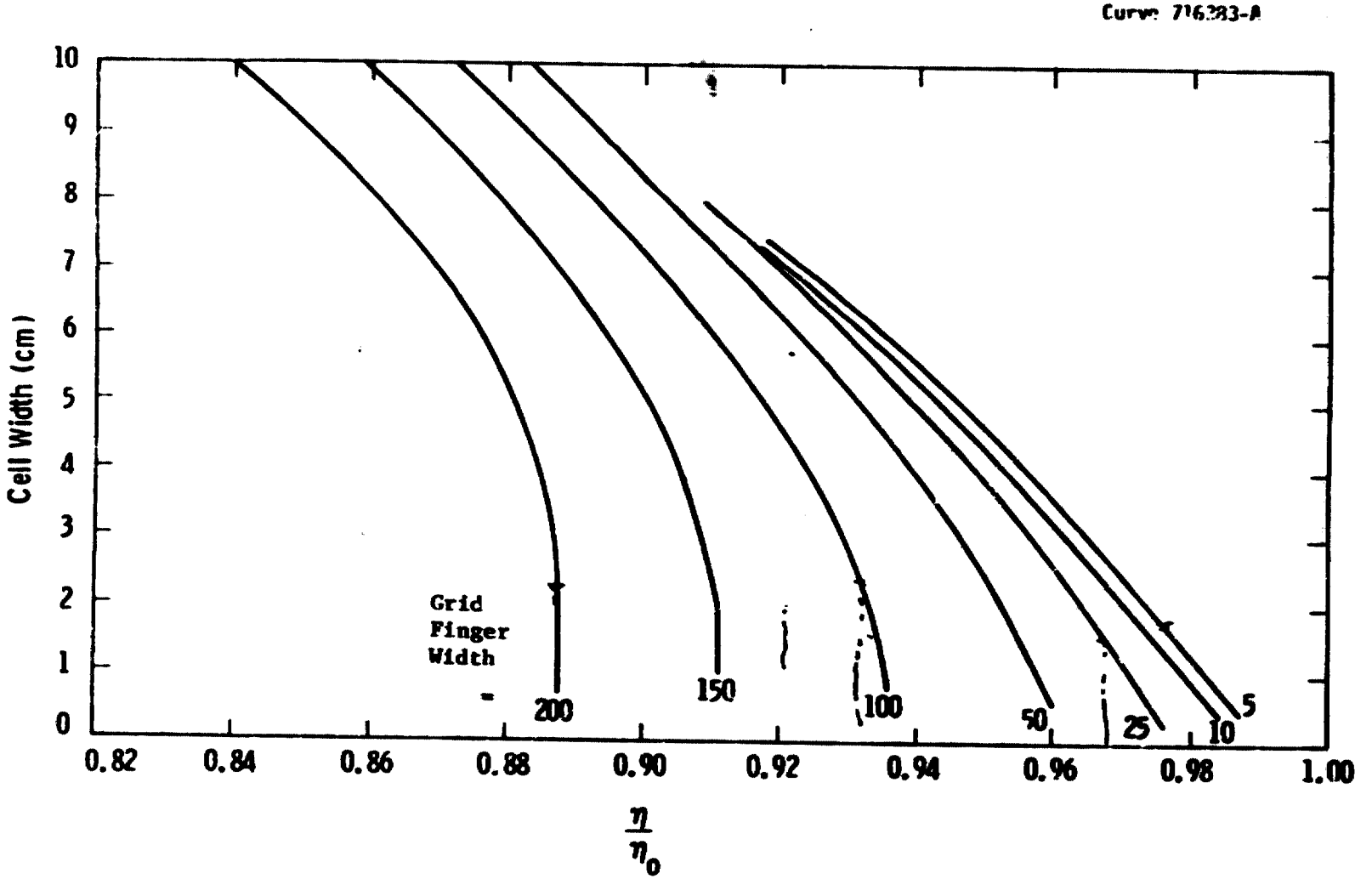

Figure 12 Effect of cell width on efficiency at several grid finger widths.

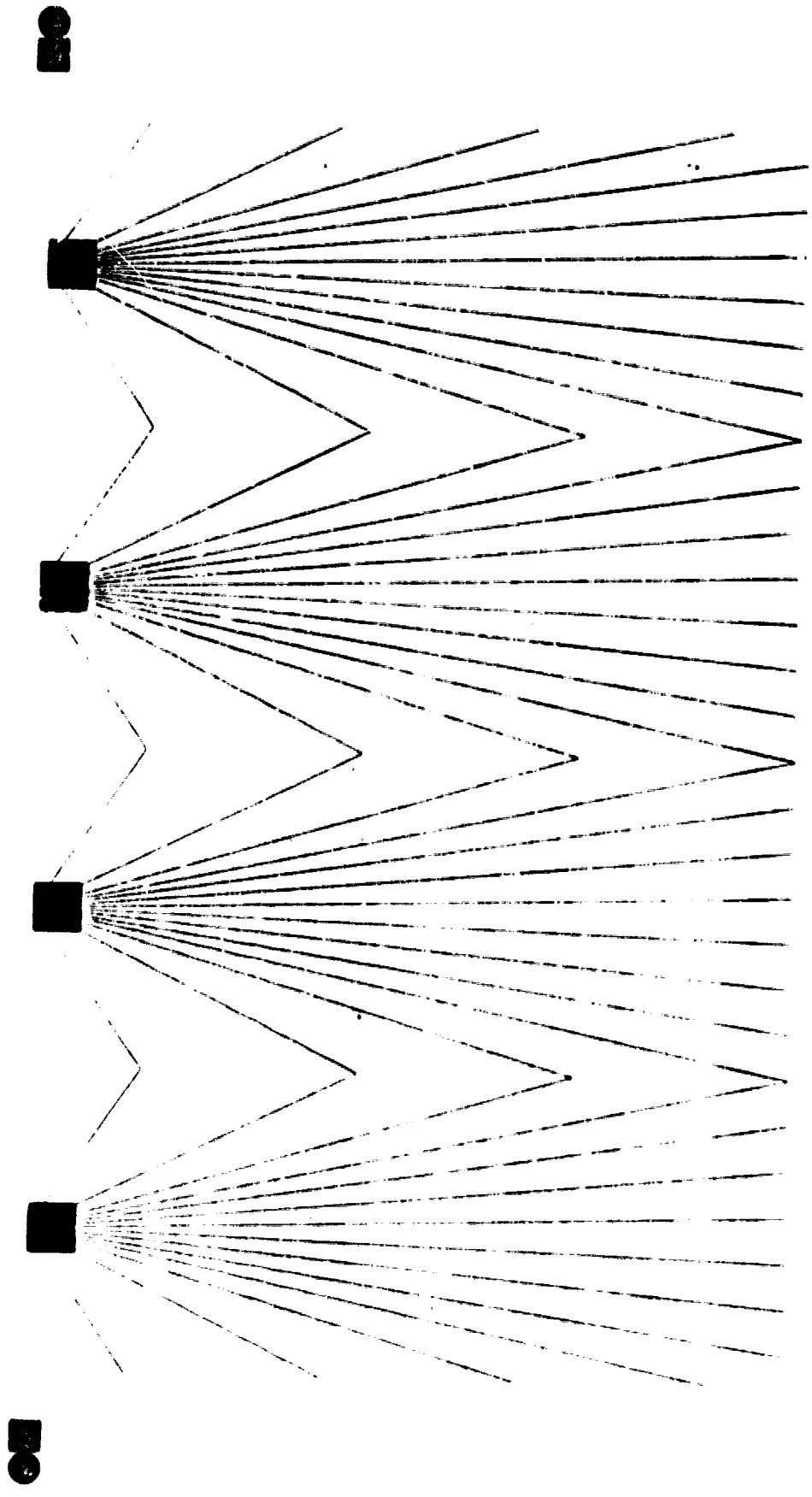

Figure 13 New Mask Design

Figure 14 Standard Mask Pattern on 1.6 cm x 7.0 cm Solar Cells

This web strip was processed in the normal manner. The short circuit current density and efficiency of cells having the new mask design were about 5.1% higher than the standard mask cells. This is what would be expected on a strictly optical area coverage factor of the two mask designs. Similar OCD lifetimes indicate the I_{SC} increase is not due to a change in bulk characteristics. The measured shunt resistance was above $10^6\Omega$ with the series resistance less than 0.5Ω. These values would not affect the data.

These results indicate that a significant improvements is obtained using this grid design.

3.7 Demonstration Module Fabrication

3.7.1 Cell Fabrication Process

The cells used in the demonstration modules were fabricated from dendritic web silicon. The web, as received, had the material characteristics as given in Table 25.

The cell fabrication process was as follows

- Material cleaned using standard pre-diffusion cleaning - Material in strip form, 26 cm long.
- n+ surface produced on both sides by $POCl_3$ diffusion.
- Phosphorus glass source removed from one side of the web.
- Aℓ deposited on cleaned n+ surface, and alloyed in at 850°C.
- Phosphorus glass removed from non-BSF side and coated with anti-reflection coating by dipping.

- A photoresist coat applied by dipping.
- Grid structure opened in PR and AR coatings.
- Ti + Pd evaporated over entire surface.
- dipped in electroless Cu plating for 10 seconds to produce a Cu flash coating.
- PR rejected to form grid structure on strip.
- Cu electroplated on grid to a thickness of 6-7 μm.
- Cells separated from dendrite-web matrix by laser scribing and breaking. Cell size is 1.6 cm x 7.0 cm.
- Cells tested at AM-1 and 91.6 mw/cm^2.

The efficiency, open circuit voltage and short circuit current distributions on cells fabricated in this way are shown in Figures 15 to 17. The demonstration modules were fabricated using cells selected from this group.

TABLE 25

Material Characteristics of Dendritic Web Silicon

1. Single crystal - (111) orientation.
2. The etch pit density, as determined after a 5-minute Sirtl etch, to be equal to or less than 3 x 10^4/cm^2. The etch pits should be of the small, shallow variety with a minimum of the large, deep pits.
3. For mechanical stability, the web should have a residual stress of less than 1.5 x 10^8 dynes/cm^2.
4. The web should be flat with no twist or bow.
5. The surface striations across the web shall be no more than 0.5 μm in height.
6. The width, excluding dendrites, should be 22 mm or greater for a 1.6 x 7.0 cm cell.

TABLE 25 (Cont'd.)

7. The thickness of the web at the center should be 120 μm ± 20 μm.
8. The web should be p-type.
9. The resistivity should be 4-12 Ω-cm.
10. The lifetime (ocd after cell fabrication) should be greater than 10 μsec.
11. The material should be supplied as grown.

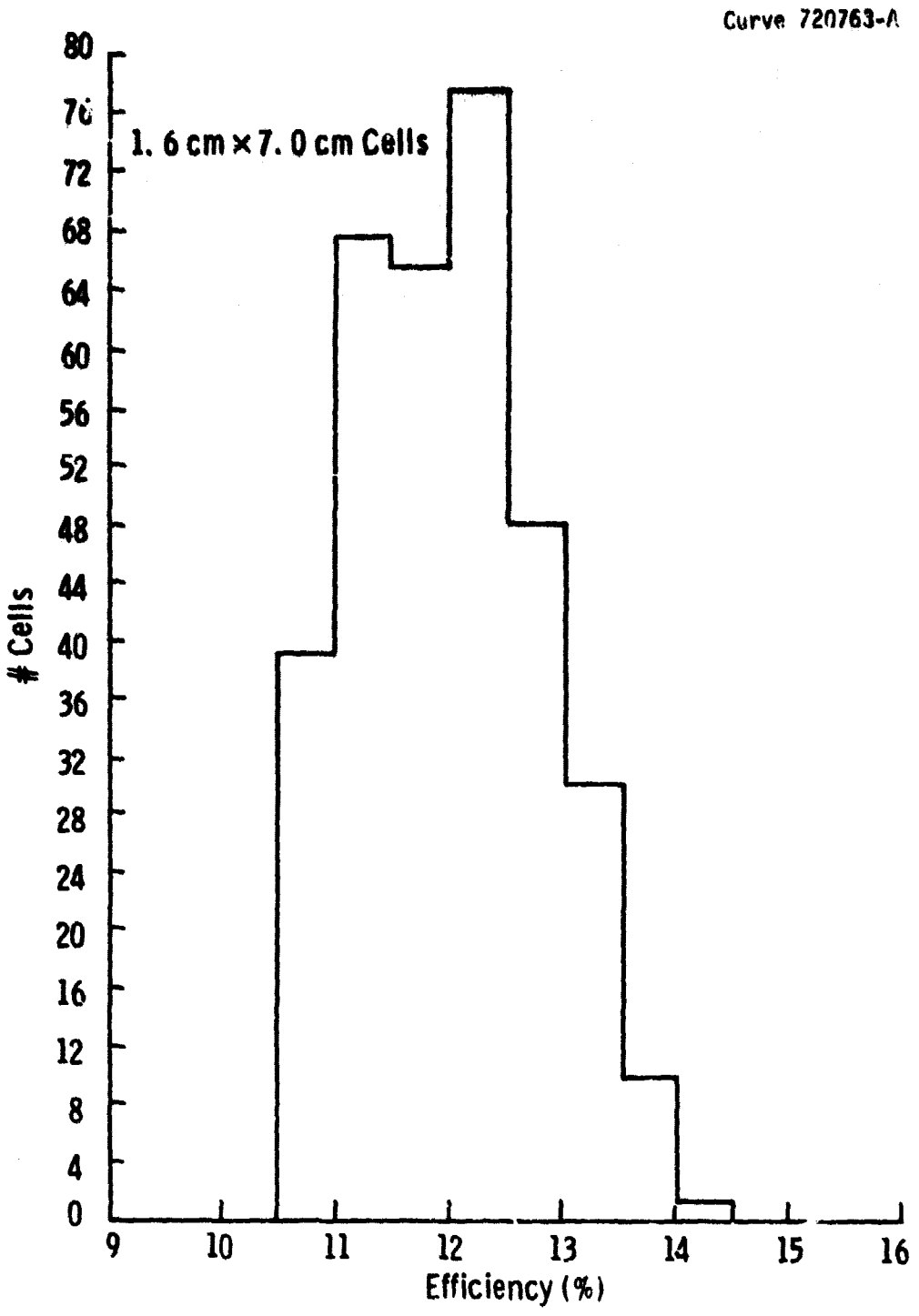

Fig. 15 — Efficiency distribution of cells used in demonstration modules

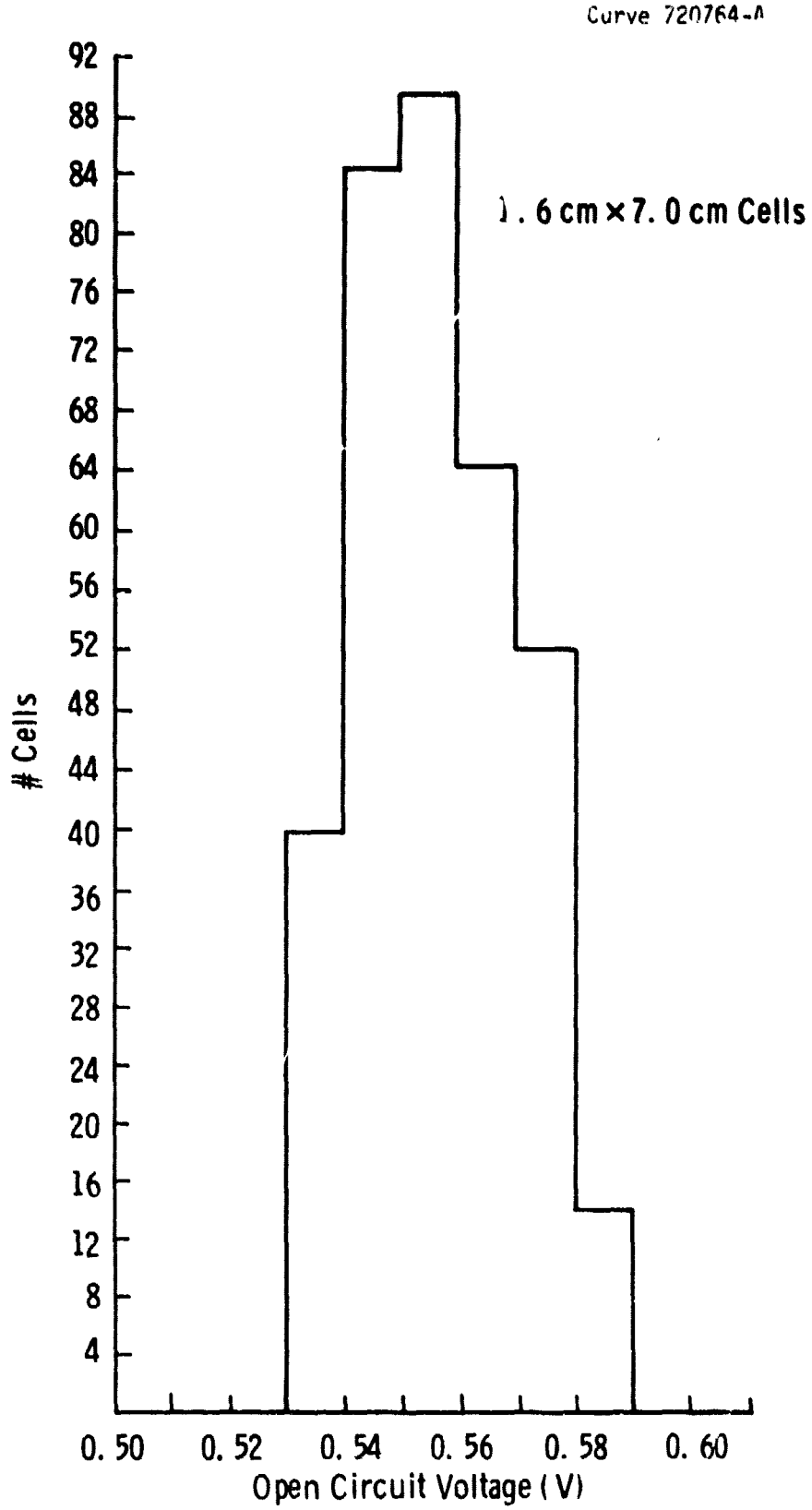

Fig. 16 – Open circuit voltage distribution of cells used in demonstration modules

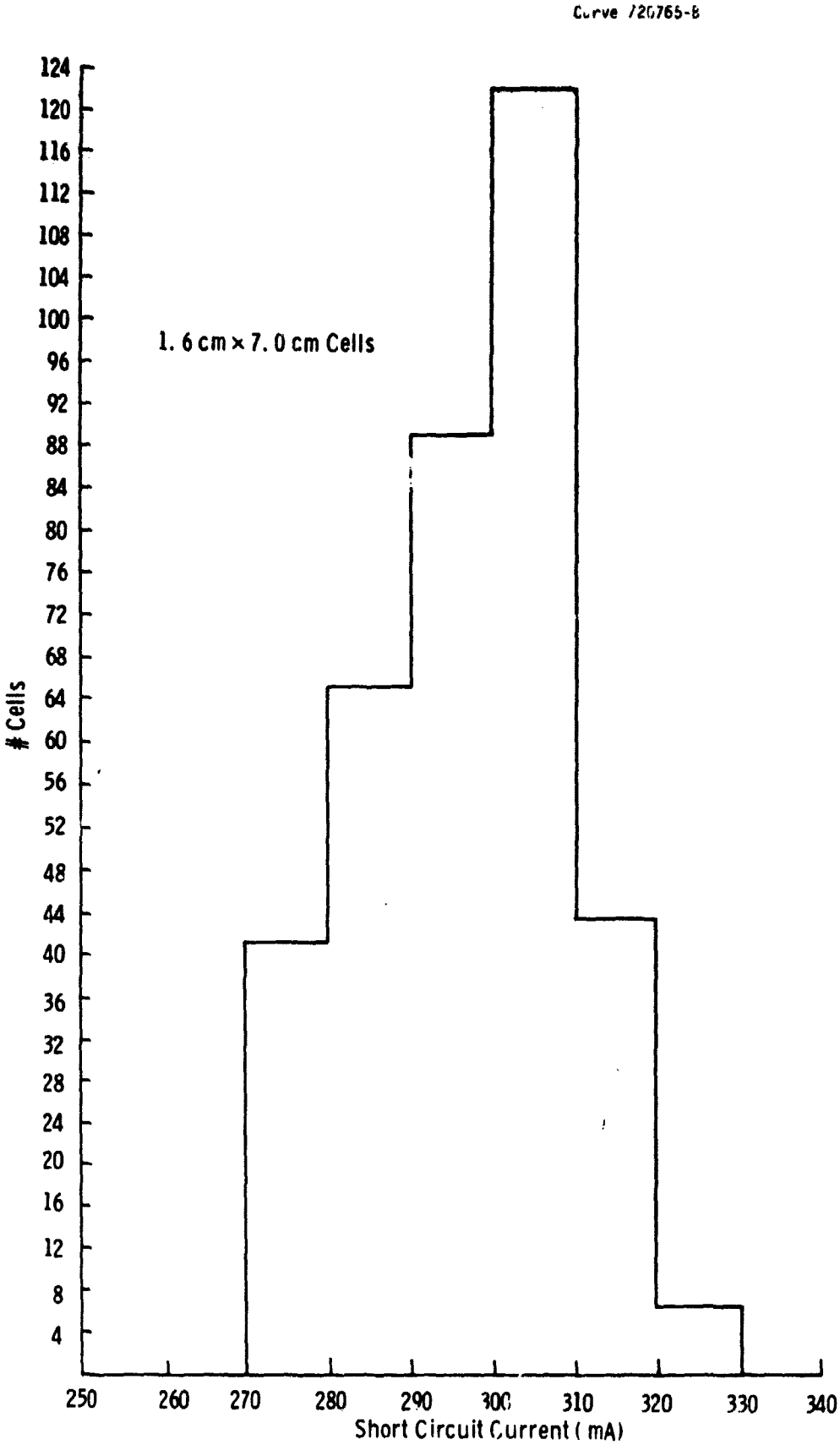

Fig. 17 – Short circuit current distribution of cells used in demonstration modules

In previous sections, we specified sputtering as the preferred technique for applying aluminum to the back of the solar cell as the initial step in forming an aluminum back surface field. In a parallel Westinghouse sponsored program we have recently developed another method for applying the aluminum which is as effective as sputtering but is simpler and less costly. In this second technique, plasma spraying, an Aℓ powder is fed into a plasma stream where it is melted and sprayed onto the silicon. The plasma is generated by flowing an inert gas through an electric arc.

One advantage of this process is that the Aℓ is still hot when it contacts the Si and thus forms an adherent layer. This adherance is important in the subsequent drive in process.

Cells fabricated using this process have shown properties equal to or better than cells fabricated using sputtered Aℓ.

Due to equipment availability and the time required to sputter 10 μm layers of Aℓ in non-optimum apparatus, the solar cells discussed in this section were all fabricated using this plasma spraying method.

This technique is considered Westinghouse proprietary and an invention disclosure has been filed.

There are several real and potential problems with these cells. First, when the dendrites are removed, the cells tend to bow lengthwise due to the aluminum metal remaining on the back. This bow is small; the angle with the horizontal being 1 - 2° and the cell can be made flat with a small amount of pressure. However, this bow is sufficient to cause problems during the module fabrication. For example, when the cells are placed on a layer of the adhesive, some weight must be applied to flatten the cell either against the glass or the substrate. This can lead to misalignment of the cells as they slide on the adhesive.

The Al BSF cells are also more brittle than cells with boron BSF (or no BSF). This leads to more breakage during the various processing steps, decreasing the yield.

One obvious way of removing the bowing, and probably making the cell less susceptible to breakage would be to remove the excess aluminum by etching after the initial drive-in. This has been done in several cases, and after the Al is etched off the cell flattens out; however, its brittleness has not improved. However, if this process was used for all cells the extra steps of etching and recontacting would be required. The cost and cost effectiveness of adding these steps to the process sequence would have to be determined.

In earlier sections we noted that the OCD lifetimes of the Al back surface cells were generally lower than comparable boron back surface field cells. This has a direct bearing on the short circuit current.

In view of these considerations and also in view of the only minimal improvement in cell parameters (i.e. Al BSF vs. B BSF) consideration may be given to revising the process sequence to include a boron diffused BSF. Techniques to cost reduce the B BSF formation should then be studied.

3.7.2 Module Fabrication Process

During the latter part of the program we fabricated four demonstration modules; each approximately 30 cm x 30 cm. Each module was composed of 72 cells each 1.6 cm x 7.0 cm for a total cell area of 806.4 cm^2.

The cells as discussed in the previous section had Al back surface fields with evaporated Ti Pd and electroplated Cu top contacts.

The fabrication process we originally planned to use to build the modules was as follows:

- Aluminum leads ultrasonically bonded to the front contacts.
- Cells loaded, sun side up, on fixture discussed in Section 3.2.2.
- Sunadex* glass 0.125" thick prepared by painting with 0.001" to 0.002" thick coating of RTV 615.**
- Cells, in fixture, placed on glass and assembly is given a short cure time.
- Fixture removed and back interconnections made by ultrasonic bonding.
- Interconnected module coated on back with adhesive and 0.125" thick phenolic board attached as a substrate.
- Assembly cured.

During the initial fabrication steps, problems arose so it became obvious that changes in this process were required; at least for these four demonstration modules.

First, as noted in the section describing the work on ultrasonic bonding, we were successful in bonding Al and Cu interconnect straps to Al, Cu, and Ag contact metals. However, during the first interconnection step of attaching the aluminum foil to the electroplated copper, a large number of failures occurred. The failure mode was cracking of the cells at the point where the ultrasonic tool and the foil contacted the cell. On this part of the cell, a number of small cracks would propagate from the contact point, and in extreme cases the cell would shatter. The failure rate during this process was greater than 50%.

* Trademark - ASG Corp.
** Trademark - General Electric Corp.

As discussed earlier, this yield problem was not as significant with the boron doped BSF cells or on thick Al BSF cells (>200 μm).

It would then seem that the low yield is due to two, probably interrelated, conditions of thin cells and the inherent brittleness of Al BSF cells.

The same problem was encountered to about the same degree when the Al foil was ultrasonically connected to the Al on the back of the cell. This low yield creates an almost impossible situation in the building of the module, especially considering each module requires 14 interconnections per cell x 72 cells = 1000 interconnections per module. For this reason, it was decided to fabricate the modules by the soldering method used earlier.

The second problem was the bowing of the cells as discussed in the previous section. To avoid extensive bubbles between the cell and the glass superstrate due to bowing, the cells were initially laid down on the substrate.

A sketch of the module design is shown in Fig. 18 and a photograph of the completed module is shown in Fig. 19. Eighteen series connected cells are mounted on a 1/4" thick phenolic board, about 7.1 cm x 29.4 cm. Four of these boards are then mounted on a 1/8" phenolic board 29.4 cm x 28.4 cm. External connections are made by soldering onto a copper fitting on the large board. With this design, each of the 4 strings of 18 cells can be individually tested, and a variety of series/parallel interconnections can be made. This modular concept permits easier assembly of large panels from smaller sub-modules and also makes possible the replacement of single strings of cells in case of breakage.

The cell operating temperature of these sub-modules was determined by measuring the decrease in V_{oc} as a function of time under AM-1; 100 mw/cm^2 illumination (Ref. 8, pp. 83). The stagnation temperature of 30°C above room temperature was reached after 70 minutes. This data is in general agreement with Ref. 8 even though a phenolic backboard is used in place of the Al frame.

Dwg. 1709B35

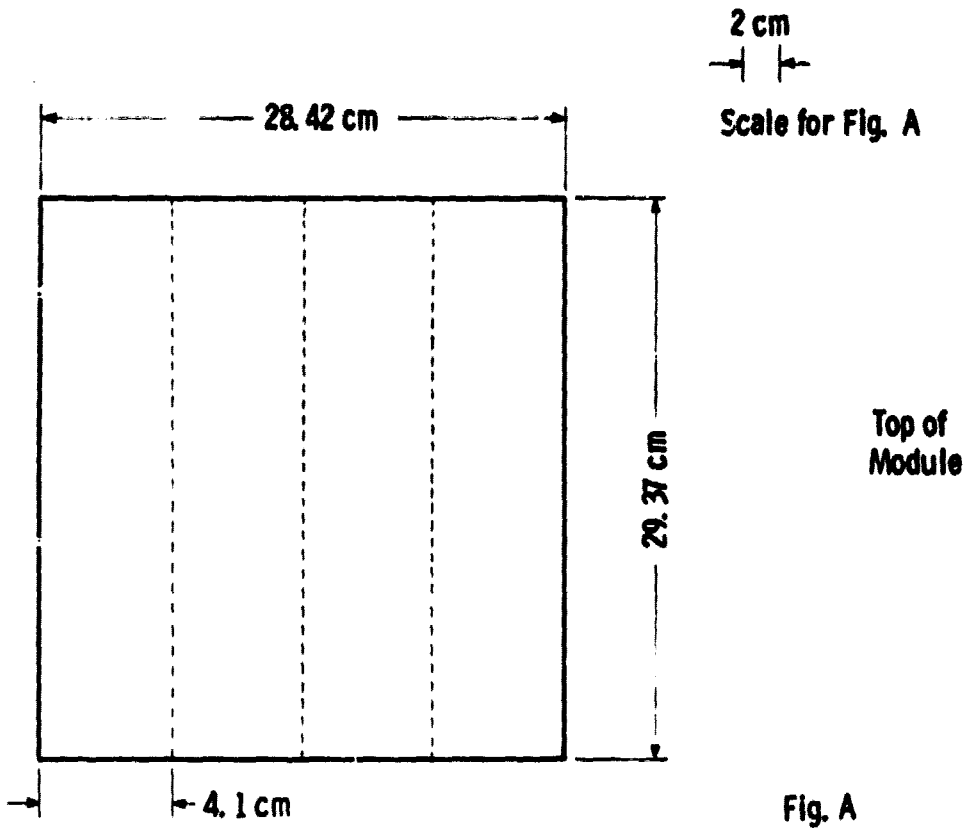

Fig. 18 Demonstration module design

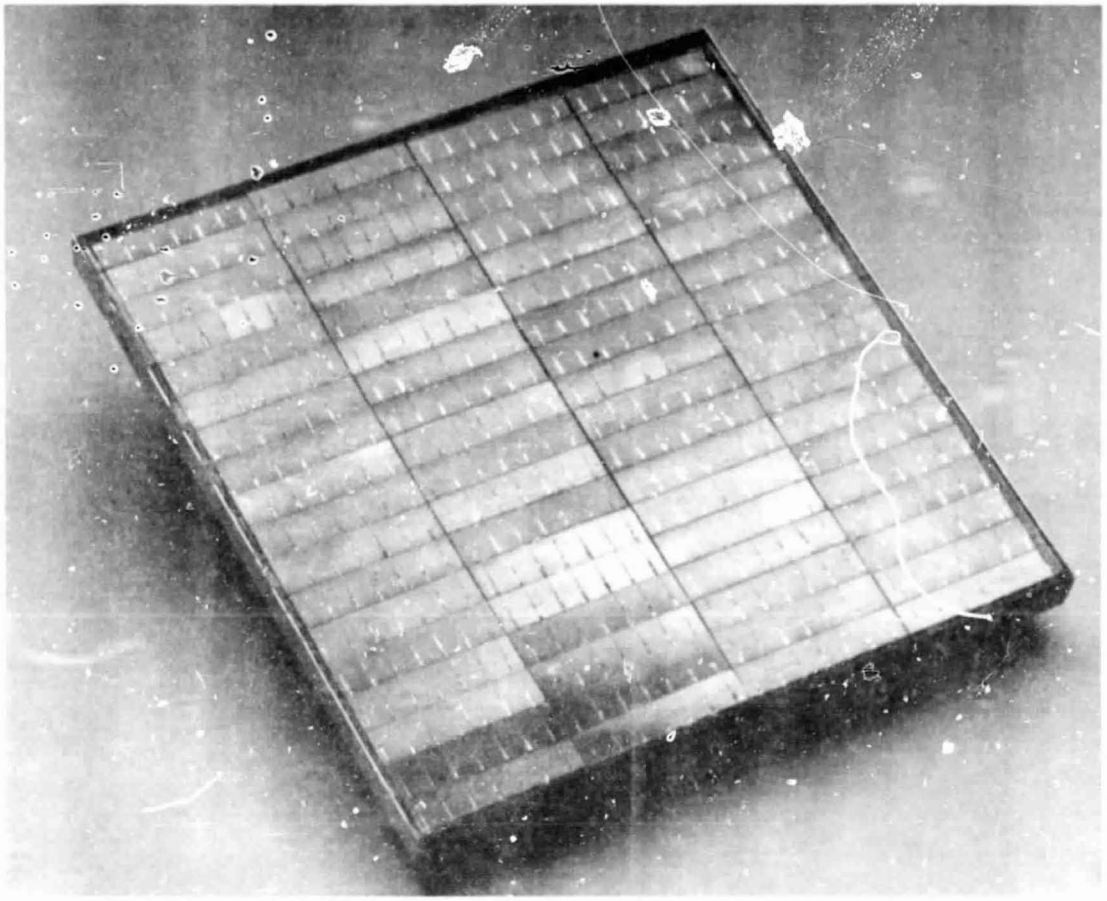

Fig. 19 Photo of Demonstration Module

3.7.3 Test Data on Demonstration Modules

Four demonstration modules were fabricated as discussed in the last section. The data for these modules is given in Table 26. The modules were first tested with all 72 cells in series.* This is the underlined data in the Table. Following these results, each of the 18 cell strings were tested individually and these data are noted as 1A, 1B, etc.

TABLE 26

Test Data on Demonstration Modules

Module No.	V_{oc} (V)	I_{sc} (MA)	η (%)
1	38.81	295	10.44
1A	9.83	295	11.10
1B	9.85	313	10.77
1C	9.73	308	10.50
1D	9.75	285	10.10
2	39.10	303	11.24
2A	10.08	315	12.20
2B	9.79	293	10.66
2C	9.97	323	12.05
2D	9.75	295	10.94
3	38.90	311	10.93
3A	10.13	323	11.78
3B	9.46	306	10.36
3C	10.08	310	10.46
3D	9.59	316	11.21
4	39.81	289	11.01
4A	10.07	309	12.01
4B	10.48	280	10.93
4C	10.66	294	11.25
4D	10.11	308	11.20

*These measurements were made at NASA-Lewis Research Center. We wish to thank Dr. Henry Brandhorst's group for their assistance.

3.8 Cost Analysis

3.8.1 Modification in Conceptual Factory

In the first annual report on this program we described a conceptual factory for the parallel processing of lengths of web. This factory consisted of eight separate lines, each producing 25 MW/yr of solar panels. To achieve this output, each line had an input of 5000 cm^2/min of dendritic web silicon in 3 meter lengths.

The various elements of this processing line were then used as inputs into the SAMICS program to obtain a selling price under volume manufacturing conditions.

During this past year, we have continued to make modifications in the processing line based on changes in the processing sequence, further inputs from vendors etc. Artists sketches of the modified line are shown in Figs. 20 - 25. (Several of these processes are unchanged but are included for completeness). Figure 20 shows a number of web growth furnaces; each producing 25 cm^2/min of web.* The web being 5 cm wide between dendrites. Therefore, 200 furnaces are required to provide the necessary input to the processing line. The as grown web is wound on reels. Fifty such reels are ganged on a mandrel as the web fed through a laser cutter. Pieces of web, each 3m long are loaded into specially designed, light weight frames and held in a buffer station before moving to junction formation steps. Each frame holds 75,000 cm^2 of web, and thus to meet the throughput requirement, each frame must be processed in 15 minutes.

Figure 21 shows the junction formation processes in the sequence. The web enters the process and is washed with an organic solvent and dried. It then moves into a diffusion furnace where an n^+ junction is diffused into each side. After diffusion the phosphorous glass is etched off one side. The web enters a sputtering appratus where about 10 μm of Al is

*This work is being carried on under Contract 954654 (Task 2) and is included here only for completeness.

C-2

3.8 Cost Analysis

3.8.1 Modification in Conceptual Factory

In the first annual report on this program we described a conceptual factory for the parallel processing of lengths of web. This factory consisted of eight separate lines, each producing 25 MW/yr of solar panels. To achieve this output, each line had an input of 5000 cm^2/min of dendritic web silicon in 3 meter lengths.

The various elements of this processing line were then used as inputs into the SAMICS program to obtain a selling price under volume manufacturing conditions.

During this past year, we have continued to make modifications in the processing line based on changes in the processing sequence, further inputs from vendors etc. Artists sketches of the modified line are shown in Figs. 20 - 25. (Several of these processes are unchanged but are included for completeness). Figure 20 shows a number of web growth furnaces; each producing 25 cm^2/min of web.* The web being 5 cm wide between dendrites. Therefore, 200 furnaces are required to provide the necessary input to the processing line. The as grown web is wound on reels. Fifty such reels are ganged on a mandrel as the web fed through a laser cutter. Pieces of web, each 3m long are loaded into specially designed, light weight frames and held in a buffer station before moving to junction formation steps. Each frame holds 75,000 cm^2 of web, and thus to meet the throughput requirement, each frame must be processed in 15 minutes.

Figure 21 shows the junction formation processes in the sequence. The web enters the process and is washed with an organic solvent and dried. It then moves into a diffusion furnace where an n^+ junction is diffused into each side. After diffusion the phosphorous glass is etched off one side. The web enters a sputtering appratus where about 10 μm of Al is

*This work is being carried on under Contract 954654 (Task 2) and is included here only for completeness.

C-2

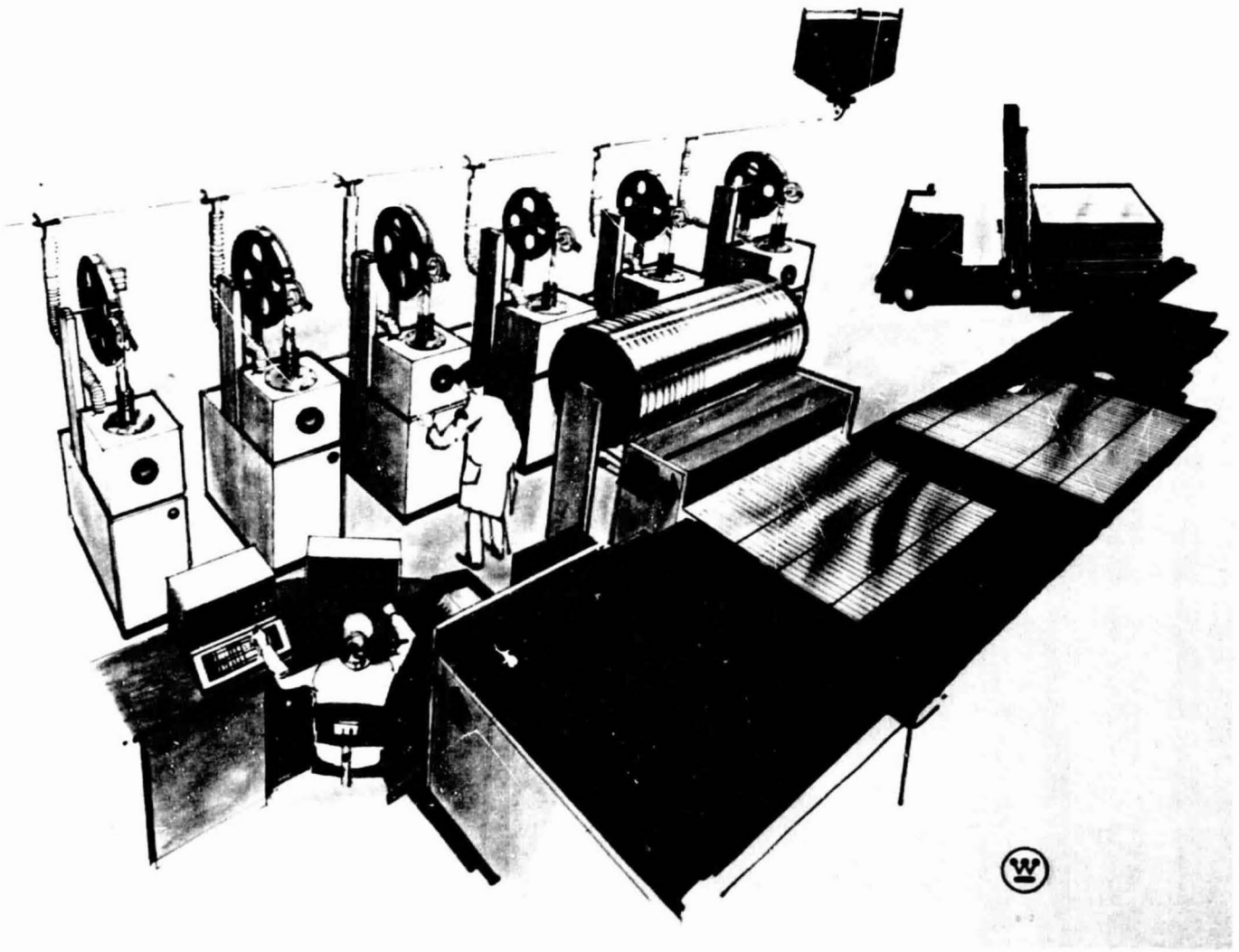

Figure 20 Web Growth

Figure 20 Web Growth

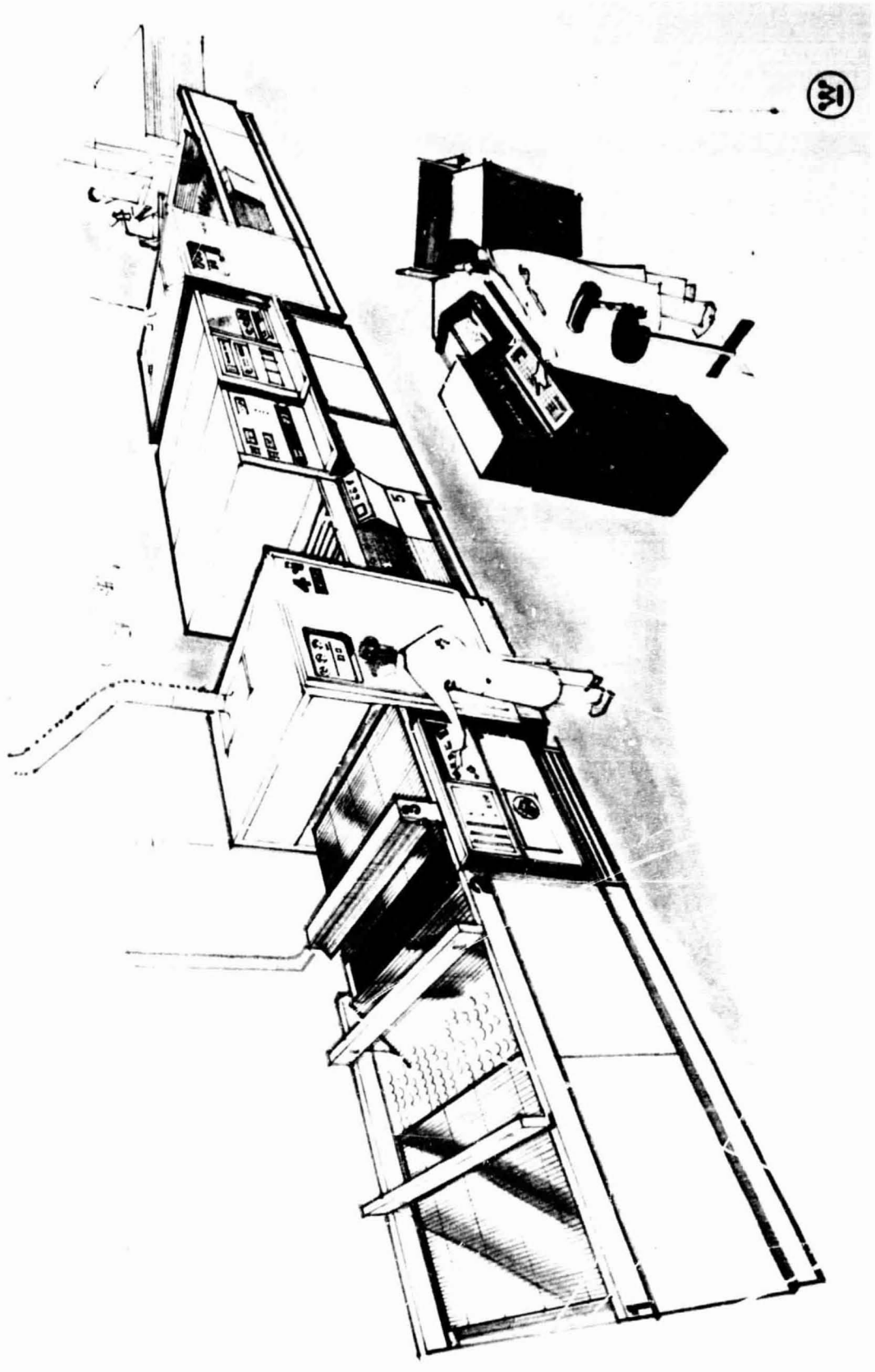

Fig. 21 Junction Formation Process

sputtered on the n^+ surface where the glass has been removed. The web is then reacted at 850°C for one minute. The entire web is then etched to remove the remaining phosphorous glass. The web at this time has an $n^+ p\ p^+$ structure.

Figure 22 shows the application of the antireflection coating and the photoresist, both by dipping. The equipment is designed to handle the 37 x 37 frames. In station 7 of this process, the web lengths are passed (one at a time) into an exposure system where a suitable grid pattern is put onto the photoresist layer. The final stages etch the grid pattern into a photoresist and antireflective coatings and the webs are again loaded into frames for metallization.

Figure 23 shows the metallization process for the web solar cells. The web strips, with the grid pattern opened pass into a metallization chamber where both front metal is applied. Our costing studies are for an evaporated metal system but sputtering is a viable alternative. After the photoresist is rejected (rejecting the excess metal) the contacts are sintered and move to a plating station where Ag* is plated to the proper thickness. Plating is used in this build-up since the only silver used is that deposited on the cells, and the step is cost effective. After a final cleaning the webs are stacked in a buffer station before moving to a scribing process.

We have found that after the aluminum drive in, there is sufficient Al remaining on the back of the cell to serve as a contact metal. Thus the metallization step does not include metallizing the back (p^+) surface. This makes the metallization step a simpler process.

Figure 24 shows the cell separation process. In this step the dendrites are scribed off and the cell is scribed to its final size. (For costing purposes this size is 5 cm x 20 cm.) The cells are unloaded from the rack, one at a time, and pass under a single laser head. This laser has sufficient power so that it can make both the transverse

*Silver has been used in the costing studies as the top contact metal. We have shown, however, the copper is an acceptable substitute.

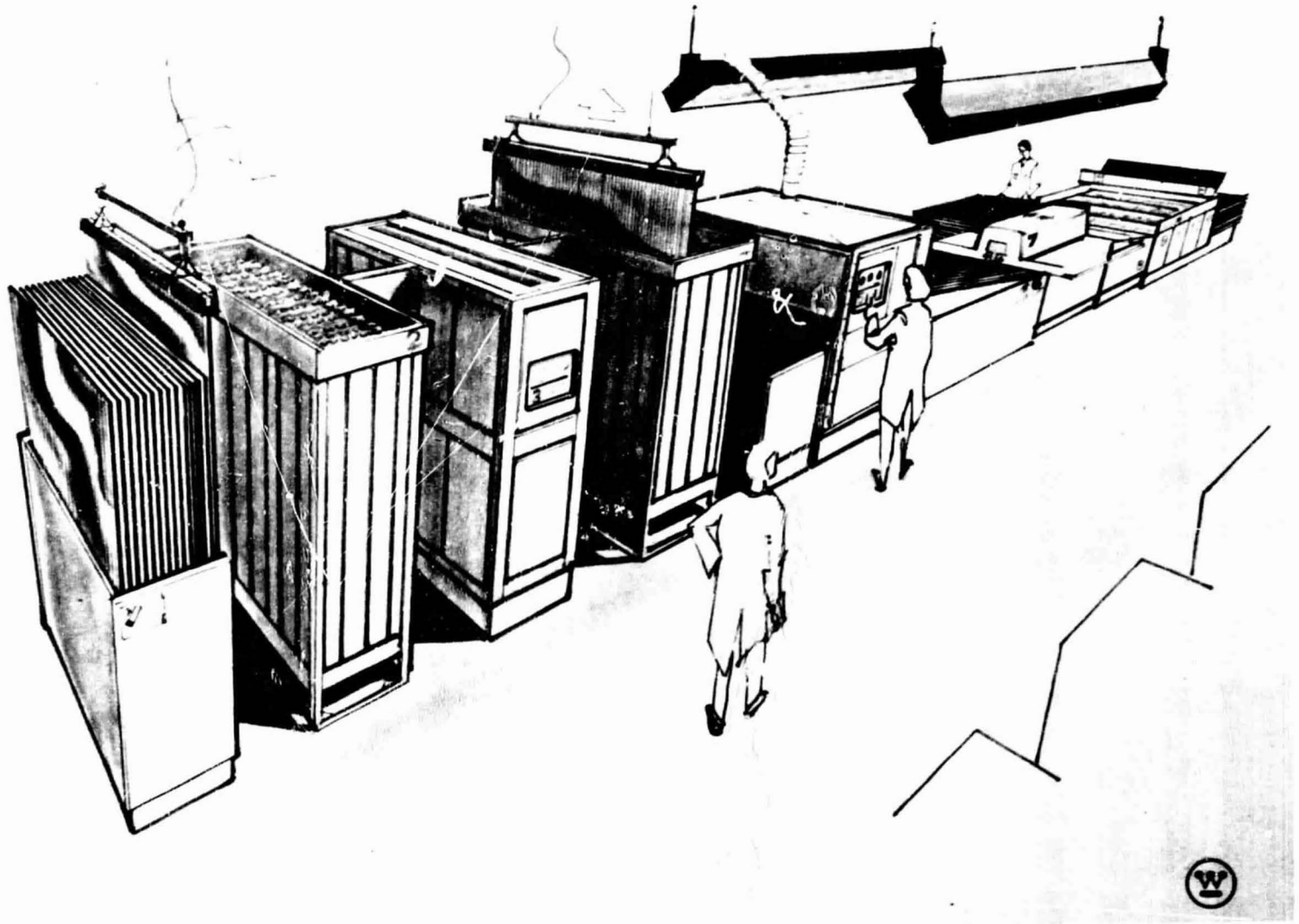

Fig. 22 Application of AR and PR and Grid Delineation

Figure 23 Metallization

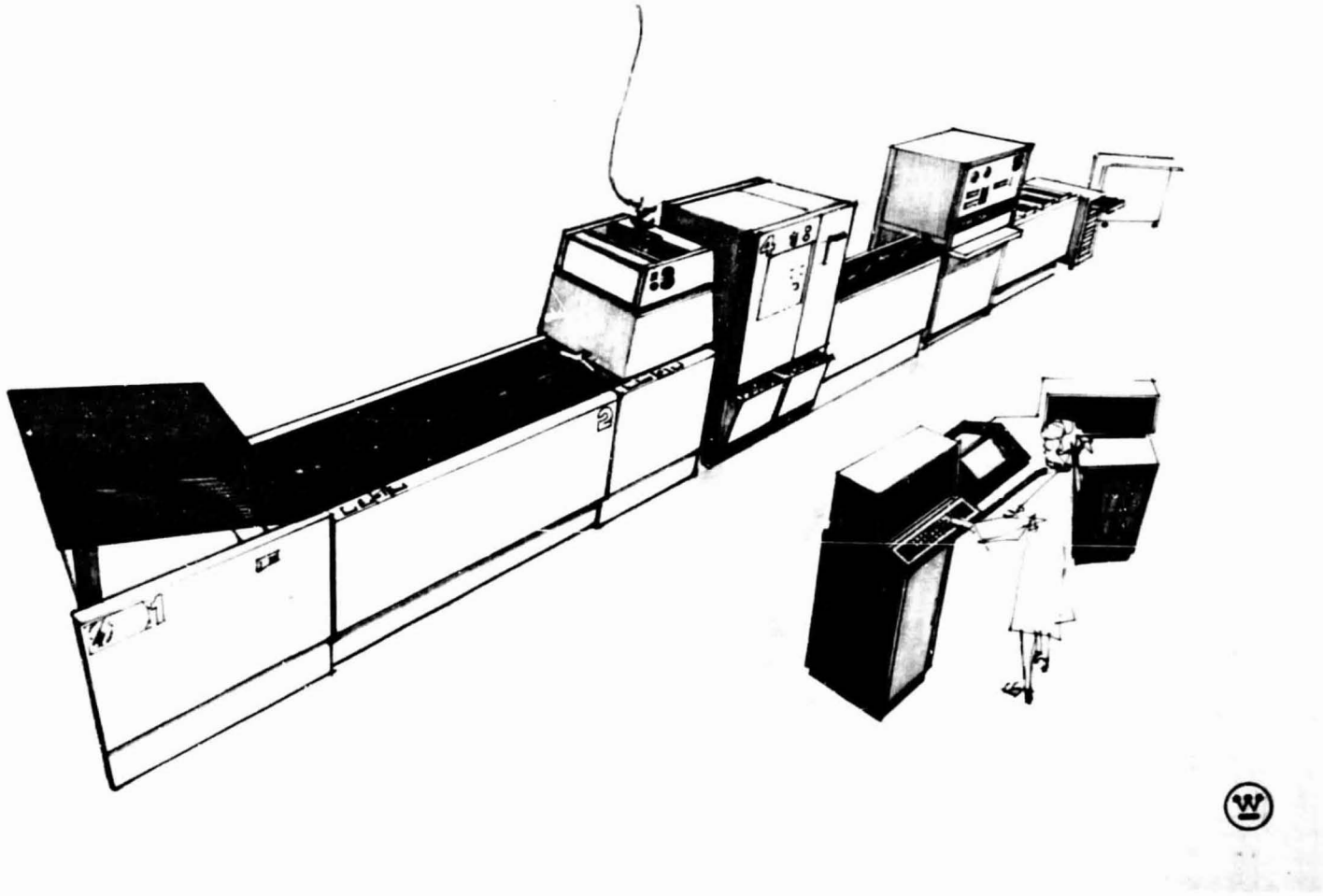

Figure 24 Cell Separation and Testing

and longitudinal cuts. The laser beam is directed by a mirror which has been programmed to scribe out the 5 cm x 20 cm cell. The final stations break the cells from the dendrite-web matrix and perform an electrical test on each cell. The cells that pass a previously determined specification are loaded into cassettes, with each cassette holding about 5000 cells. The yield of 85% is assumed at this point.

Figure 25 shows the final processing step, Interconnection and Encapsulation. The cells are unloaded from the cassette and an Al strip (interdigitated) is ultrasonically connected to the front of the cell. The cells are placed sun side down on glass which has previously been coated with a thin layer of adhesive. Automated positioning machines are capable of placing the cells to achieve a 96 - 98% packing factor. The back interconnections are made using a second ultrasonic welder, and a back board with electrodeposited connecting strips is put over top of the cells. A final test of the entire panel completes this process. A yield of 95% is assumed at this testing stage.

Crating and shipping, although included in our costing, is not shown in this line.

3.8.2 Cost Analysis of Basic Process

The manufacturing line described in the previous section was used to determine the various inputs into the Format A forms. Table 27 gives a summary of these inputs. The numbers of the processes are not generally consecutive due to changes in the original plan as well as consolidation of some steps for ease in costing. These process steps agree with the SAMICS Format A's.

Definitions for Table 27 are:

- PY = Person year - The number of operators on the floor during running time.
- All commodity and utility usage expressed in usage/min.
- Capacity of factory is 25 MW/yr.

(Text continued on page 104)

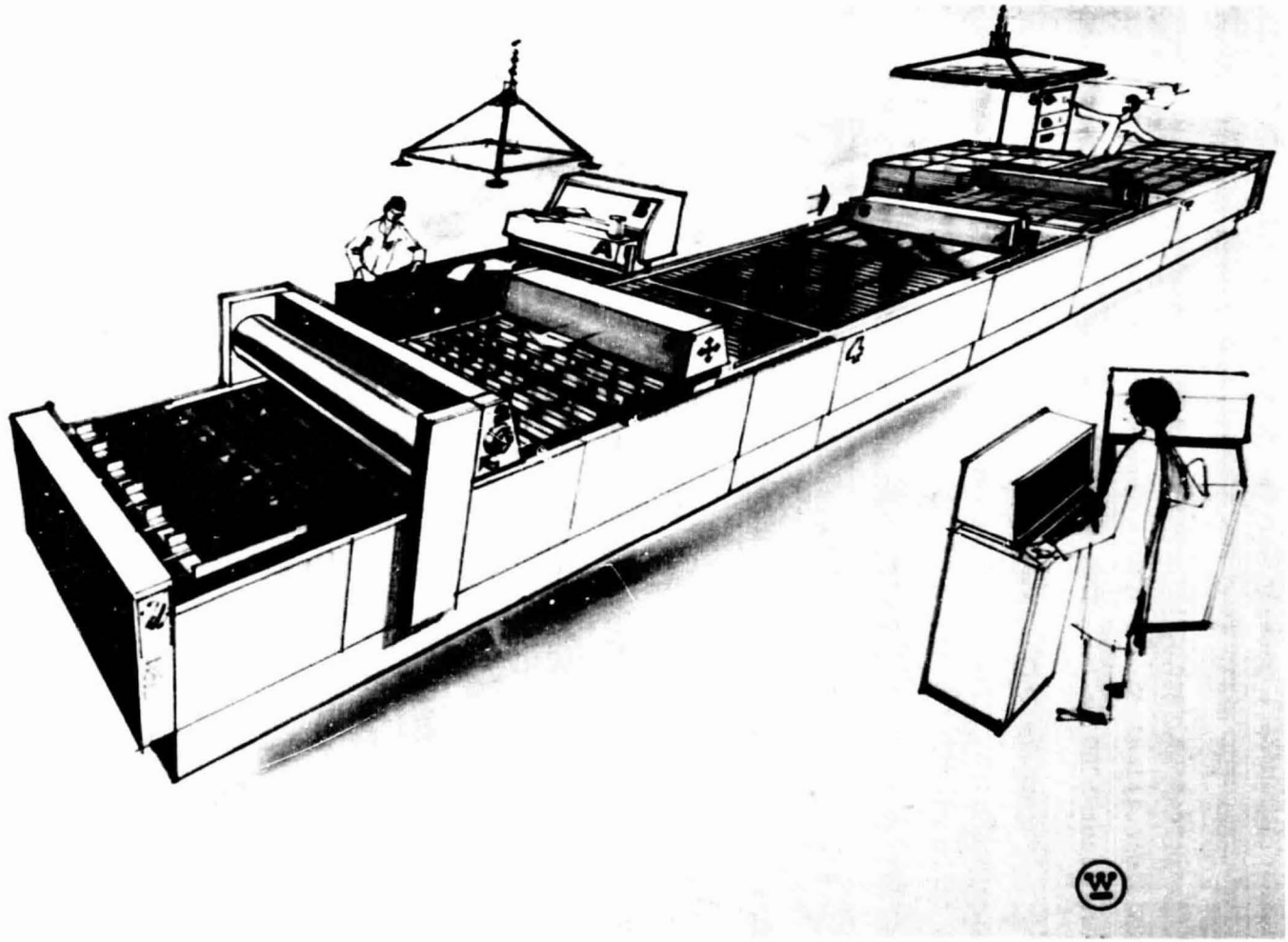

Figure 25 Interconnections and Encapsulation

TABLE 27

Cost Inputs For Factory Manufacturing Solar Panels

From Dendritic Web Silicon

(All 1980$)

1.01	Load web into frames; Clean and plasma etch.	Labor:	1.67 PY	
		Space:	405 ft^2	
		Capital:	Dip Cleaner (Eng. Estimate)	$ 90,000
			Plasma Etching (Estimate from LPE Corp.)	$840,000
		Commodities:	Si Web (Cost at $0.00274/$cm^2$)	5000 cm^2/min
			Acetone	0.002 lb/min (SCAC)*
			HF	0.06 lb/min
			Purge Gas ($134/tank per LFE)	1.2×10^{-4} tanks/min
			DI H_2O	0.04 ft^3/min (SCAC)
		Utilities:	Electric	0.05 KW/min (SCAC)

*SCAC = SAMICS Cost Accounting Catalog

1.08 n^+ Diffusion using POCl	Labor:	0.9 PY		
	Floor Space:	400 ft^2		
	Capital:	Diffusion Furnace (Eng. Estimate)	$456,000	
		Cooling Buffer (Estimate)	$ 13,400	
		Tank Etcher (Eng. Estimate)	$ 40,000	
	Commodities:	$POCl_3$	0.003 lb/min	(SCAC)
		Liq. N_2	0.0007 cu ft/min	(SCAC)
		HF	0.06 lb/min	(SCAC)
		DI H_2O	0.04 cu ft/min	(SCAC)
		Cooling H_2O	0.21 cu ft/min	(SCAC)
		Poisonous Acid Disposal	0.015 gal/min	(SCAC)
	Utilities:	Electric	0.334 KW/min	(SCAC)
1.101 Deposition of Al	Labor:	1.0 PY		
	Floor Space:	300 ft^2		
	Capital:	Sputtering Apparatus $1,700,000 (per estimate from Leybould Heraus, Vac Tec and others)		
	Commodities:	Al Sputtering Target (Cost at $14/lb per Vac Tec Corp)	0.0016 lb/min	
		Liq. N_2	0.0001 cu ft/min	(SCAC)
	Utilities:	Electric	0.25 KW/min	

1.102 Al Drive In	Labor:	1.5 PY		
	Floor Space:	300 ft^2		
	Capital:	Drive Furnace and Holding Table (Estimate from existing equipment, e.g., Radiant Technology)	$430,000	
	Commodities:	Liq. N_2	0.0002 cu ft/min	(SCAC)
		Cooling H_2O	0.15 cu ft/min	(SCAC)
	Utilities:	Electric	0.142 KW/min	(SCAC)
2.01 Antireflection Coating Application by Dipping	Labor:	0.40 PY		
	Floor Space:	160 ft^2		
	Capital:	Holding Table and Dip Tank (Estimate)	$ 94,000	
		Firing Furnace (Estimate)	$ 26,000	
	Commodities:	Isopropyl Alcohol	0.013 gal/min	(SCAC)
		AR Solution	0.0009 l/min ($2.00/l)	
		Cooling H_2O	0.06 cu ft/min	(SCAC)
	Utilities:	Electric	0.10 KW/min	(SCAC)
2.04 Photoresist Coating Application by Dipping	Labor:	0.5 PY		
	Floor Space:	65 ft^2		
	Capital:	Dip Tank	$ 80,000	
		Bake Furnace (Both Engineering Estimates)	$ 26,000	
	Commodities:	AZ-111 Photoresist ($105/gal per Shipley Co.)	0.0012 gal/min	
		AZ-111 Thinner ($2.20/gal per Shipley Co.)	0.0015 gal/min	
	Utilities:	Electric	0.025 KW/min	(SCAC)

2.06	Expose web and load into cassettes	Labor:	1.0 PY	
		Floor Space:	250 ft^2	
		Capital:	Loader and Unloader (Estimate)	$ 80,000
			Exposure Apparatus (Based on Preliminary Design)	$ 75,000
		Commodities:	Replacement Parts (lamps, masks, etc.)	$ 12,000/yr.
		Utilities:	Electric 0.05 KW/min	(SCAC)
2.09	Development of Photoresist	Labor:	0.4 PY	
		Floor Space:	120 ft^2	
		Capital:	Tanks for Dipping into Developer & Cleaner (Estimate)	$ 30,000
		Commodities:	AZ303A Developer	0.00021 gal/min ($6.30/gal per Shipley Co.)
			Acetone	0.033 lb/min (SCAC)
		Utilities:	Electric	0.025 KW/min (SCAC)
2.11	Antireflection Coating Etch and Clean-up	Labor:	0.6 PY	
		Floor Space:	185 ft^2	
		Capital:	Dipping Tank (Estimate)	$ 26,000
			Wash Tank and Holding Table (Estimate)	$ 39,000
		Commodities:	DI H_2O	0.24 cu ft/min (SCAC)
			HCl	0.001 lb/min ($1.00/lb, catalog price)
			NH_4F Etch	0.005 lb/min ($2.20/lb, catalog price)
		Utilities:	Electric	0.024 KW/min (SCAC)

3.01 Deposition of Metal on Web

Labor:	1 PY		
Floor Space:	400 ft^2		
Capital:		$900,000	
	(Budgetary estimate for evaporator of suitable size per Leybould Heraus and others)		
Commodities:	Cooling H_2O	0.007 cu ft/min	(SCAC)
	Titanium Metal	0.00013 lb/min	(SCAC
	Palladium Metal	0.0049 troy oz/min (use $64 troy oz as Catalog price)	
Utilities:	Electric	0.22 KW/min	(SCAC)

3.03 Rejection of Photoresist to form Metal Grid

Labor:	0.5 PY		
Floor Space:	150 ft^2		
Capital	Stripping Tank (per estimate)	$ 26,000	
Commodities:	AZ Stripper	0.037 gal/min ($2.70/gal, Shipley Co.)	
Utilities:	Electric	0.033 KW/min	(SCAC)

3.04 Sintering of Metal Contacts

Labor:	0.5 PY		
Floor Space:	200 ft^2		
Capital:	Sintering Furnace (Estimate from existing equipment, e.g., Radiant Technology)	$125,000	
Commodities:	Cooling H_2O	0.03 cu ft/min	(SCAC)
	Liq. N_2	0.005 cu ft/min	
Utilities:	Electric	0.033 KW/min	(SCAC

3.05	Plating of Silver and Cleaning	Capital:	Plating and Wash Tanks (Estimate)	$ 65,000	
		Commodities:	DI H_2O	0.04 cu ft/min	(SCAC)
			Silver	2.5 gm/min	(SCAC)
			Bath Components	$0.114/min (catalog price)	
			Acid Disposal	0.004 gal/min	(SCAC)
		Utilities:	Electric	0.81 KW/min	(SCAC)
4.01	Laser Scribing of Cells	Labor:	1.0 PY		
		Floor Space:	250 ft^2		
		Capital:	Laser Scribe (Estimate from Quantronics Co.)	$195,000	
			Cassette Loader (Estimate)	$ 26,000	
		Commodities:	Cooling H_2O	0.5 cu ft/min	(SCAC)
		Utilities:	Electric	0.18 KW/min	
4.03	Breakout and Testing of Cells	Labor:	1.0 PY		
		Floor Space:	330 ft^2		
		Capital:	Table & Tester (Estimate (W) ARD)	$120,000	
			Break Out Unit (Engineering Estimate)	$ 40,000	
		Commodities:	None		
		Utilities:	Electric	0.05 KW/min	(SCAC)

5.01	Foil Contacts Bonded to Top of Cells	Labor:	1.0 PY		
		Floor Space:	180 ft^2		
		Capital:	Ultrasonic Bonder and Table (Estimate based on contacts with Sonobond Corp.)	$140,000	
		Commodities:	Al Foil	0.006 lb/min	(SCAC)
		Utilities:	Electric	0.05 KW/min	(SCAC)
5.03	Cells Placed on Glass Superstrate Using Adhesive	Labor:	0.6 PY		
		Floor Space:	150 ft^2		
		Capital:	Placement Machine and Table (Based on preliminary estimates and contacts with Gardner-Denver Corp.)	$110,000	
		Commodities:	Glass	5.3 ft^2/min	(SCAC)
			Adhesive	0.029 lb/min	(SCAC)
		Utilities:	Electric	0.04 KW/min	(SCAC)
5.05	Interconnect Back Contacts to Cells	Labor:	0.5 PY		
		Floor Space:	80 ft^2		
		Capital:	Ultrasonic Bonder (Based on contacts with Sonobond Corp.)	$135,000	
		Commodities:	None		
		Utilities:	Electric	0.083 KW/min	(SCAC)

5.06	Substrate Attached and Panel Tested	Labor:	0.75 PY		
		Floor Space:	260 ft^2		
		Capital:	Coating Apparatus and Attachment of Back (Estimate)	$ 67,000	
			Transport Apparatus (Estimate)	$ 26,000	
			Tester (Estimate)	$ 85,000	
		Commodities:	Adhesive	0.56 lb/min	(SCAC)
			Back Board	5.6 ft^2/min (Charge at $.25/$ft^2$)	
		Utilities:	Electric	0.07 KW/min	(SCAC)
5.09	Yield Dummy - Modified to include Computer Control for Factory (Floor Space and Labor Allocated to Individual Processes)	Labor:	-		
		Floor Space:	-		
		Capital:	(Estimate)	$525,000	
		Commodities:	None		
		Utilities:	Electric	0.01 KW/min	(SCAC)
5.10	Crating and Shipping	Labor:	1.0 PY		
		Floor Space:	150 ft^2		
		Capital:	Overall Equipment (Estimate)	$ 12,000	
		Commodities:	Crating Material	0.033 KW/min	(SCAC)

- Floor space is space occupied by equipment plus maintenance area.
- Capital estimates are based either on the best engineering estimates at the time or on budgetary estimates from vendors.
- Cost estimates of commodities are either from the SAMICS Cost Accounting Catalog (SCAC) or based on estimates of vendors.

Using inputs given in Table 27 and the SAMICS program, the data in Table 28 is obtained. All costs in this table are in 1980$. A selling price per peak watt of $.75 is obtained.

Figure 26 shows the entire process sequence with the major inputs for the individual processes. In this case, the n^+ and p^+ junction formation steps are separated. The value added figures for each sub-process step indicate where potentially significant cost savings can be made.

3.8.3 Sensitivity Analysis of Costs

In the previous sections, we discussed a conceptual factory processing line for solar panels and using SAMICS methodology, a selling price for the panel was determined. In this section, we will discuss several iterations which were carried out to determine the sensitivity of the selling price to various input factors.

The conceptual factory line discussed was highly automated. This automation is necessary to achieve the high throughput with minimum of labor charges. This high degree of automation, however, implies large capital spending for machinery, controls, computers, etc.

The process analyzed in the previous section required a capital expenditure of slightly over $\$10 \times 10^6$ for a 25 MW line. It is thus of interest to determine the effect on the selling price of the panels if this capitalization is reduced or increased. This was accomplished by increasing the capital in various processes, and in one case by adding computerized control for all processes.

TABLE 28

PROCESS SEQUENCE FOR DENDRITIC WEB
SOLAR PANELS - TOTAL COSTS - 1980$

ASSUMPTIONS: 25 MW/yr production
12% panel
5 cm wide web
85% yield of cells
95% yield of panels
Silicon input cost - $0.234/watt peak

Capital	$10,350,000
Direct Labor	$ 1,920,000
Floor Space	4800 ft^2
Commodities	$ 3,410,000

Selling Price per Watt-Peak $0.75

FIGURE 26

PROCESS SEQUENCE COSTS (ALL 1980$)

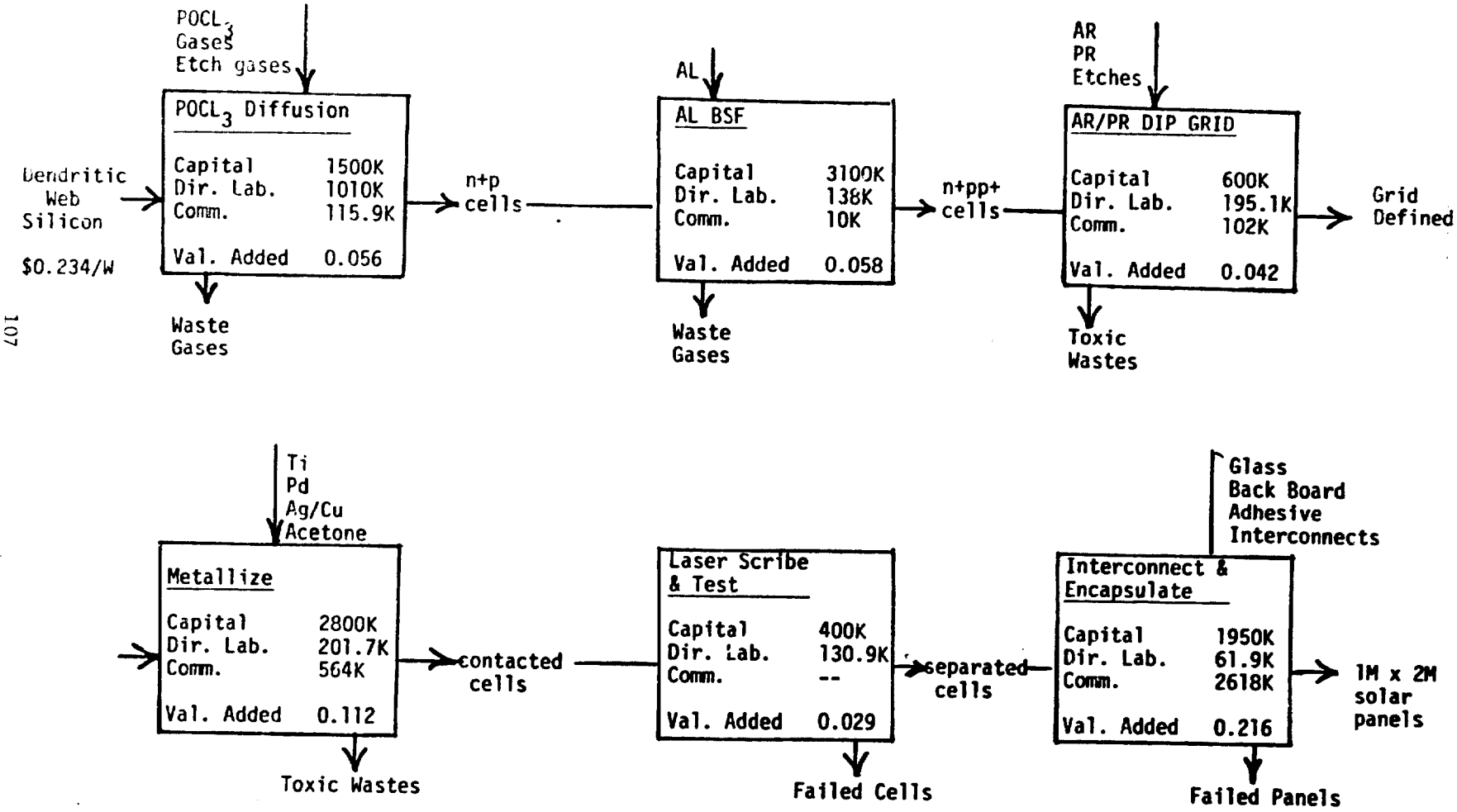

The results of these calculations are shown in Table 29. This calculation is valid over the range of ± 10% of $10 x 10^6. The "charge" of $0.03/peak watt (1980$) for each 10^6 is relatively small and would indicate that any process should be capital intensive for efficient production

We next examined the effect of the process yield on the costs. In the standard calculation, it was assumed that 85% of the cells tested met specifications and that 95% of the panels fabricated with these cells were good. This is equivalent to an overall yield of about 81%. (In the calculations, there was no credit taken for the cells or panels which did not meet specifications. In an actual manufacturing situation, these would have some value either as reprocessed material or as lower selling price-lower efficiency panels.) To determine the effect of the process yield on either side of the 81%, the yield was varied between 70% and 90% and the calculation carried out. These results are shown in Table 30 which shows that each 10% increase in yield decreases the selling price by $0.07/peak watt (1980$). Due to the complexity of the SAMICS program, this is not strictly a linear function, and this value is valid only between 70% and 90% yield. However, the yield effect is considerable and it indicates, for example, that it would be profitable to spend an extra $2 x 10^6 in capital if the yield could be increased by 10%.

The next variation involved the panel efficiency. In the basic process in the previous section this was taken to be 12% and in these sensitivity studies, the panel efficiency was varied from 10% to 16%. This variation has a very straightforward effect on the overall costs since the increased efficiency reflects back on all processes and costs, including the amount of silicon required for the 25 MW/yr output. This result is shown in Table 30. Again, it is profitable to spend money on capital or processing costs to achieve the increased efficiency.

TABLE 29

Sensitivity Analysis (1980$)

CAPITAL EXPENDITURES

For $\$10 \times 10^6 \pm 10\%$ capital expenditure, each $\$10^6$ of capital adds \$0.03/watt peak to the selling price.

YIELD

In 70 - 90% yield range, each 10% increase in yield decreases the selling price by \$0.07/watt peak.

PANEL EFFICIENCY

For 1% increase in panel efficiency, the selling price is decreased by 0.064$/watt peak.

WEB WIDTH

When the web width is decreased from 5.0 cm to 2.5 cm, the selling price is increased by 0.07$/watt peak.

The width of the dendritic web in our process sequence is taken to be 5 cm. In certain processing steps it may be advantageous to work with narrower web. Also it has been shown that for narrow grid lines ($\sim$ 25 μm) the width of the cell should not exceed 3 cm.

For these reasons, a cost analysis was carried out where the web width (i.e. cell width) was taken to be 2.5 cm. This assumption required extra capital costs, mainly in the laser scribing and encapsulation processes. There were also additional material costs involved in that more photoresist materials would be needed, twice the number of interconnect straps would be required etc. The calculation was carried out assuming the same yield (81% total) and panel efficiency (12%) as in the basic case. In point of fact, a slight increase in both these numbers might be expected due to less breakage with the narrower web and more optimum cell structure.

When the added costs were taken into account the selling price increased by \$0.07/peak watt (1980\$) over the cost for the 5 cm wide web (Table 29).

The calculations discussed in this section were made to indicate areas where the most attention should be paid to the processing. It is obvious that if either the panel efficiency or the process yield can be increased a large saving can be generated, and that it is worthwhile to increase capital spending to obtain these savings.

4. CONCLUSIONS

Based on the results of this program during the past year, we conclude:

1. Plasma etching is a suitable substitute for extensive wet chemical pre-diffusion cleaning.
2. Operational back surface fields may be produced in dendritic web silicon using either sputtered Al or silk screened Al paste. Sputtered Al is preferred due to the problem of silk screening between the dendrite.
3. The ultimate V_{oc} enhancement was not obtained with the Al BSF; possibly due to the front junction.
4. The Motorola total plated contact system (PdNi) is not compatible with our process sequence.
5. The evaporated Ti-Pd electroplated Cu system shows long term stability.
6. The ultrasonic welding of interconnects has been shown feasible, but the yield is sufficiently low as to make it unusable at this time.
7. Over 400 cells have been prepared using the modified process sequence. The sub-processes are compatible.
8. A cost analysis of the sequence results in a selling price of $0.75/peak watt (1980$ in 1986).
9. Cost analyses suggest that a capital intensive process has the best chance of achieving the cost goals.

5. RECOMMENDATIONS

We recommend that:

- An encapsulation sequence be devised that is more cost effective than our present sequence using adhesive.
- Ultrasonic welding equipment and techniques be studied to achieve a satisfactory yield factor.
- The front n^+p junction be studied to determine if it is controlling the V_{oc} enhancement, and if so, methods should be studied for its improvement.
- A continuing cost analysis be carried out to study changes in the process sequence.

6. NEW TECHNOLOGY

1. An improved mask has been designed and tested. This mask design minimizes the resistive elements in cell current collection.

2. Plasma etching has been shown suitable for pre-diffusion cleaning.

3. Evaporated TiPd-electroplated Cu has been shown stable under long term heating.

7. REFERENCES

1. A. Sinha and S. K. Chattopadhyaya; Solid State Electronics, 21, 943-951, 1978.
2. A. Sinha and S. K. Chattopadhyaya; IEEE Trans. on Electron Dev., ED-25, #12, 1978.
3. M. P. Godlewski, C. R. Baraona and H. W. Brandhorst, Jr., 10th IEEE Photovoltaic Spec. Conf., p. 40, 1973.
4. J. R. Hauser and P. M. Dunbar; IEEE Trans. on Electron Devices; ED-24, 1977.
5. Quarterly Report, Oct. 1978, Contract 954853, W. Taylor et al.
6. Quarterly Report, March 1978, Contract 954868, R. D'Aiello et al.
7. Quarterly Report #4, Contract 954873, R. Campbell et al.
8. First Annual Report, Contract 954873, R. Campbell et al.
9. "Process Procedures for Metallization," issued by Motorola Corp., 1978 (Can be obtained from B. D. Gallagher; PP&E at Jet Propulsion Laboratory.)
10. R. D'Aiello; Contract 954868. RCA.

APPENDIX A

THEORETICAL DESIGN CONSIDERATIONS FOR BACK SURFACE FIELD SOLAR CELLS

J. R. Davis and A. Rohatgi
Westinghouse R&D Center
Pittsburgh, PA 15235

ABSTRACT

A simple analytic model of a solar cell is described which provides optimum design rules for back surface field structures. The model provides useful insight into the relative impact of surface and bulk recombination on device performance.

THEORETICAL DESIGN CONSIDERATIONS FOR BACK SURFACE FIELD SOLAR CELLS

J. R. Davis and A. Rohatgi
Westinghouse R&D Center
Pittsburgh, PA 15235

The theoretical maximum efficiency of a silicon solar cell is about 25% but present day cells fall considerably short of this limiting value. This is largely a consequence of heavy doping effects, band-gap narrowing and high recombination at and near the cell surfaces. In this Appendix we describe a simple model which provides useful insight into these effects and guidelines for fabricating high efficiency solar cells. The calculations can be performed with a programmable calculator and are in good agreement with experiments. The model is based on the use of an internal recombination velocity as a characterization parameter for the minority carrier loss mechanisms in the various regions of the device which directly provides the junction saturation current. The major benefit of reducing recombination is the increase in the open circuit voltage, V_{oc}, which follows from reductions of the saturation current, J_o. Noting that V_{oc} and I_{sc} are both improved under the same conditions, we will neglect further discussion of I_{sc} and focus only on V_{oc}. Open-circuit voltage is inversely related to the saturation current (J_o).

$$V_{oc} = n V_T \ln \left[1 + \frac{J_{sc}}{J_o} \right] \tag{1}$$

where

$$J_o = q n_i^2 \frac{D_n}{L_n} \left[\frac{S_o \cosh\left(\frac{W_B}{L_n}\right) + \frac{D_n}{L_n} \sinh\left(\frac{W_B}{L_n}\right)}{\frac{D_n}{L_n} \cosh\left(\frac{W_B}{L_n}\right) + S \sinh\left(\frac{W_B}{L_n}\right)} \right] \tag{2}$$

D_n and L_n are the diffusivity and diffusion length for a p-base device, W_b is the base-width and S_o is the surface recombination velocity at the back of the base region. Equation (2) dictates that for good devices, (large L_n), J_o decreases as S_o is made smaller.

The recombination at the back surface can be reduced by introducing a back-surface-field or low-high junction.[1-4] A detailed analysis of low-high structures by Gunn[5] provides a beginning place for our model. The starting expression for the present discussion is an equation, derived from the carrier transport equations which transforms the surface recombination velocity at the back of the device (S_o) to an effective recombination velocity seen by minority carriers at the low side of the low-high interface as a function of the properties of the low and high regions. This equation for a p-p^+ structure is:

$$S_e = \frac{n_p^+}{n_p} \frac{D_n^+}{L_n^+} \left[\frac{\frac{S_o L_n^+}{D_n^+} + \tanh\left(\frac{W_p^+}{L_n^+}\right)}{1 + \frac{S_o L_n^+}{D_n^+} \tanh\left(\frac{W_p^+}{L_n^+}\right)} \right] \tag{3}$$

where n_p^+, L_n^+, D_n^+ = concentration, diffusion length and diffusivity of the minority carrier in the heavily doped p^+ region.

W_p^+ = width of the heavily doped region.

S_o = surface recombination velocity at the back of the high region.

S_e = effective recombination velocity at the low side of the low-high junction.

n_p = minority carrier concentration in the low region.

The necessary modifications are introduced in the above expression to include the effects of degeneracy and band-gap narrowing. An empirical expression was devised for the effective band-gap narrowing, (ΔV_G) based on the data of Lanyon[6] and Lindholm[7] corrected for degeneracy effects. The values thus adjusted for Fermi statistics provide an effective value for n_i^2 which can be used in the usual Boltzman expression for the np product, i.e.:

$$np = n_{ie}^2 = \exp \frac{(\Delta V_G^+ - \Delta V_G^-)}{V_T} n_i^2$$

where ΔV_G^+ and ΔV_G^- are the effective band-gap narrowing in the high and low doped regions respectively,

$$\Delta V_G = 0.231 \left[\left(\frac{10^{20}}{N} \right)^{3/4} + 1 \right]^{-2/3} \qquad (4)$$

and

$$n_i^2 = N_c N_v \exp\left(- \frac{E_G}{V_T} \right)$$

where N_c and N_v are the effective densities of states in the conduction and valence band respectively

Equation (3) can now be written as:

$$S_e = \frac{N_A}{N_A^+} \frac{D_n^+}{L_n^+} \exp\left(\frac{\Delta V_G^+ - \Delta V_G^-}{V_T} \right) \left[\frac{\frac{S_o L_n^+}{D_n^+} + \tanh\left(\frac{W_p^+}{L_n^+}\right)}{1 + \frac{S_o L_n^+}{D_n^+} \tanh\left(\frac{W_p^+}{L_n^+}\right)} \right] \qquad (5)$$

Empirical expressions were derived to relate the diffusion length and diffusivity to the impurity concentrations (N).

The expression for diffusivity D was obtained from the data of Conwell as given in Grove[8].

$$D = \frac{D_o}{1 + \left(\frac{N}{10^{17}} \right)^{0.6}} + A_o \qquad (6)$$

where for p-type

$$D_o = D_{no} = 35$$

$$A_o = 1.8$$

and for n-type

$$D_o = D_{po} = 12.5$$

$$A_o = 1$$

The diffusion length is obtained using an expression like Kendall's[9] for the lifetime in bulk silicon (τ_K) combined with Beck and Conradt's[10] data for Auger recombination τ_A.

$$\tau_n = \left(\frac{1}{\tau_A} + \frac{1}{\tau_K}\right)^{-1} \tag{7}$$

where

$$\tau_K = \frac{\tau_o}{1 + \frac{N}{7 \times 10^{15}}} \tag{8}$$

Note the value chosen for τ_o is related to the quality of silicon. Except for the data in Table III, we have used a value of 17×10^{-6} corresponding a moderate grade of material. We have found a value of 200 to 400 μs more appropriate for modeling high performance devices.

The Auger lifetime is given by:

$$\tau_A = \frac{1}{(K_A \cdot 10^{-31}) N^2} \tag{9}$$

where constant $K_A = 1.2$ for p-type

$K_A = 2.8$ for n-type

Then the diffusion length is obtained from:

$$L = \sqrt{D\tau} \tag{10}$$

It should be noted that the derivation of Eq(5) is completely general in that it may be applied to the calculation of an effective recombination velocity across an arbitrarily chosen plane anywhere in the device, as for example, within the base region where the doping is constant, we set $N_A = N_A^+ = N_A$ (base). The effective velocity at this plane then characterizes the total recombination beyond this plane. The calculation can be done iteratively from the back surface, across the base to the edge of the depletion region and thus account for all the recombination processes in the base and back. Restating Eq. 2 in terms of Se as given in Eq. 5 permits expressing the base component of the saturation current density as:

$$J_{op} = (qn_i^2/N_A)S_{ej} \tag{11}$$

where S_{ej} is the recombination velocity at the edge of the depletion region in the base. A similar calculation for the n-region above the junction will give J_{on} providing N_D is chosen at the edge of the depletion region. Then neglecting current contributions from the depletion region,

$$V_{oc} = V_T \ln \left(\frac{J_L}{J_{on} + J_{op}}\right) \tag{12}$$

Now examine the application of this analysis to the design of the heavily doped back-surface-field region of a solar cell. A base doping of 4×10^{15} cm^{-3} is chosen to avoid high-level injection conditions which have not been acounted for in this model. A value of 10^6 cm/s is

assumed for S_o, which is reasonable for a metal backed device. Calculations were made using equation 5 which showed that for any given N_A^+ there is a minimum value of the interface velocity (S_{e-min}) which can be realized if W_p^+ is sufficiently large. An example of these results is shown in Figure (1) for $N_A^+ = 3x10^{18}$ cm^{-2}. The width at which S_e reached S_{e-min} value is a function of the diffusion length in the p^+ region and increases as N_A^+ is reduced. For metal backed devices, S_e at the low side of the interface decreases as W_p^+ increases reflecting the decoupling of the high recombination at the surface (Figure 1). S_e reaches S_{e-min} and remains at this value as W_p^+ equals or exceeds about $3L_n^+$, this being the maximum distance over which minority carriers can communicate. Figure 2 shows that for metal backed devices with abrupt profiles S_{e-min} reaches its lowest value with $N_A^+ \approx 3x10^{18}$ cm^{-3}. This minimum occurs because of the intrusion of band-gap narrowing at higher doping and Auger recombination.

If S_o is reduced, e.g. by oxide passivation, the velocity transform equation shows that S_e can be reduced considerably as seen in the lower curve of Figure 1. For S_o = the diffusion velocity = D_n^+/L_n^+, S_e will be independent of the p^+ width. The diffusion velocity for $N_A^+ = 3x10^{18}$ cm^{-3} is 1.24 10^4 cm/s and the corresponding value of S_e is 68 cm/s, the large drop across the interface being due entirely to the high field at the p-p^+ junction. If the surface recombination velocity is smaller than the diffusion velocity, S_e can be made even smaller than S_{e-min} by reducing the width of the p^+ region (Figure 1). This occurs because bulk recombination is dominant and diminishes as W_p^+ is reduced.

Now we examine the effect of a graded doping impurity profile in the back-field region. An exponential profile is assumed and is approximated by a series of discrete steps of uniform doping. The value of S_e calculated for each step becomes the S_o for the next step. The results shown in Table I indicate that for an ohmic back device (S_o = 10^6 cm/s) any modification of a single abrupt structure produces inferior interface velocities provided the doping in the p^+ region is kept around $3x10^{18}$ cm^{-3}. Table I also shows that if one has to contend with heavy doping ($N_A^+ >> 3x10^{18}$) then a graded profile is preferred although the result remains inferior to the stepped profile with lower concentration.

In Table II, a low surface recombination velocity is assumed and the best result is obtained with an abrupt profile and a p^+ region with zero width. This obvious impossibility is a consequence of neglecting the width of the low-high junction field region. With more realistic p^+ widths the graded profile shows an advantage.

Table III shows a comparison of measured and calculated data for two devices made on high quality silicon. The calculated data is in good agreement with the measured characteristics using a value of τ_o = 200 μsecs in Equation 8.

A simple recombination model which agrees with experiment has provided useful design rules for back surface field solar cells. The analysis indicates that an optimum structure consists of a passive surface and a thin p^+ region with constant doping in the mid 10^{18} range. The junction side of the device can be analyzed in the same way and similar results are obtained.

ACKNOWLEDGEMENTS

The authors wish to acknowledge helpful discussions with M. Wolf and F. A. Lindholm.

REFERENCES

1. M. P. Godlewski, C. R. Baraona and H. W. Brandhorst, Jr., 10th IEEE Photovoltaic Specialists Conf., p. 40 (1973).
2. J. G. Fossom, IEEE Trans. Electron Dev., ED-24, 322 (1977).
3. J. G. Fossom and E. L. Burgess, Appl. Phys. Lett. 33(3), p. 238 (1978).
4. A. Sinha and S. K. Chattopadhyaya, J. Solid-State Electronics, 21. p. 943 (1978).
5. J. B. Gunn, J. Electron. Contr. 4, 17 (1958).
6. M. P. D. Lanyon and R. A. Tuft, Proc. of International Electron Device Meeting, Washington D.C., p. 316 (1978).
7. F. A. Lindholm, private communication.
8. A. S. Grove, Physics and Technology of Semiconductor Devices, John Wiley, New York (1967).
9. D. Kendall, Conf. on the Physics and Application of Lithium Diffused Silicon, NASA-Goddard Space Flight Center, 1969.
10. J. D. Beck and Conradt, Solid State Communications 13, p. 93 (1973).

Table I - Effect of Profile and Surface Doping Concentration in the p+ Region. ($N_A = 4 \times 10^{15}$ cm^{-3}, $W_{p+} = 20$ μm, $S_o = 10^6$ cm/s)

No. of steps (n)	Effective Recombination Velocity (S_e, cm/s)	
	$N_{p+} = 3 \times 10^{18}$ cm^{-3}	$N_{p+} = 1 \times 10^{20}$ cm^{-3}
1 (abrupt)	68	705
2	106	131
100 (graded)	176	120

Table II - Effect of Profile and Width of p+ Region on S_e.
(S_o = 500 cm/s, $N_A^+ = 3 \times 10^{18}$ cm^{-3},
$N_A = 4 \times 10^{15}$ cm^{-3})

No. of steps (n)	Effective Recombination Velocity (S_e, cm/s)			
	W_p+ = 20 μm	1 μm	0.1 μm	0.0 μm
1 (abrupt)	68	16.8	4.17	2.74
100 (graded)	117	9.2	3.38	--

Table III - Comparison of Measured and Calculated Data

MEASURED DATA

Sample	PERFORMANCE[1]			EMITTER[2]				JUNCTION[3]	BASE[3]		BSF[3]		
	η	I_{sc}	V_{oc}	N_s	X_{dn}	X_{dp}	$N_{X_{dn}}$	X_j	W_B	N_A	W_p^+	N_A^+	Profile
	%	A	V	cm^{-3}	μm	μm	cm^{-3}	μm	μm	cm^{-3}	μm	cm^{-3}	—
1S-3	16.1	.032	.600	$\sim 2\times10^{20}$	.056	.71	8.8×10^{16}	$\sim$.25	100	1.5×10^{15}	10	3×10^{18}	ABRUPT
117B1 (No AR coating)	10.0	.0225	.556	$\sim 10^{20}$	.050	.48	1.3×10^{17}	$\sim$.25	260	4×10^{15}	- N O N E -		

CALCULATED DATA

	V_{oc}[5]	J_o	J_{on}	J_{op}	S_{ejn}[4]	S_{ejp}	S_{epp^+}	S_{on^+}[6]	S_{op^+}[7]
1S-3	.601	2.9×10^{-12}	1.1×10^{-12}	1.8×10^{-12}	2700	75	14.4	4000	10^6
.17B1	.555	1.18×10^{-11}	4.55×10^{-13}	1.29×10^{-11}	1640	1310	—	4000	10^6

(1) 91.6 mW AM2 (ELH)

(2) Depletion data calculated from zero bias capacitance measurements assuming an erfc profile. N_s deduced from sheet resistance measurements.

(3) Spreading resistance data

(4) erfc approximated by an exponential profile

(5) Calculated using measured I_{sc}

(6) Measured on a similarly prepared surface

(7) Estimated

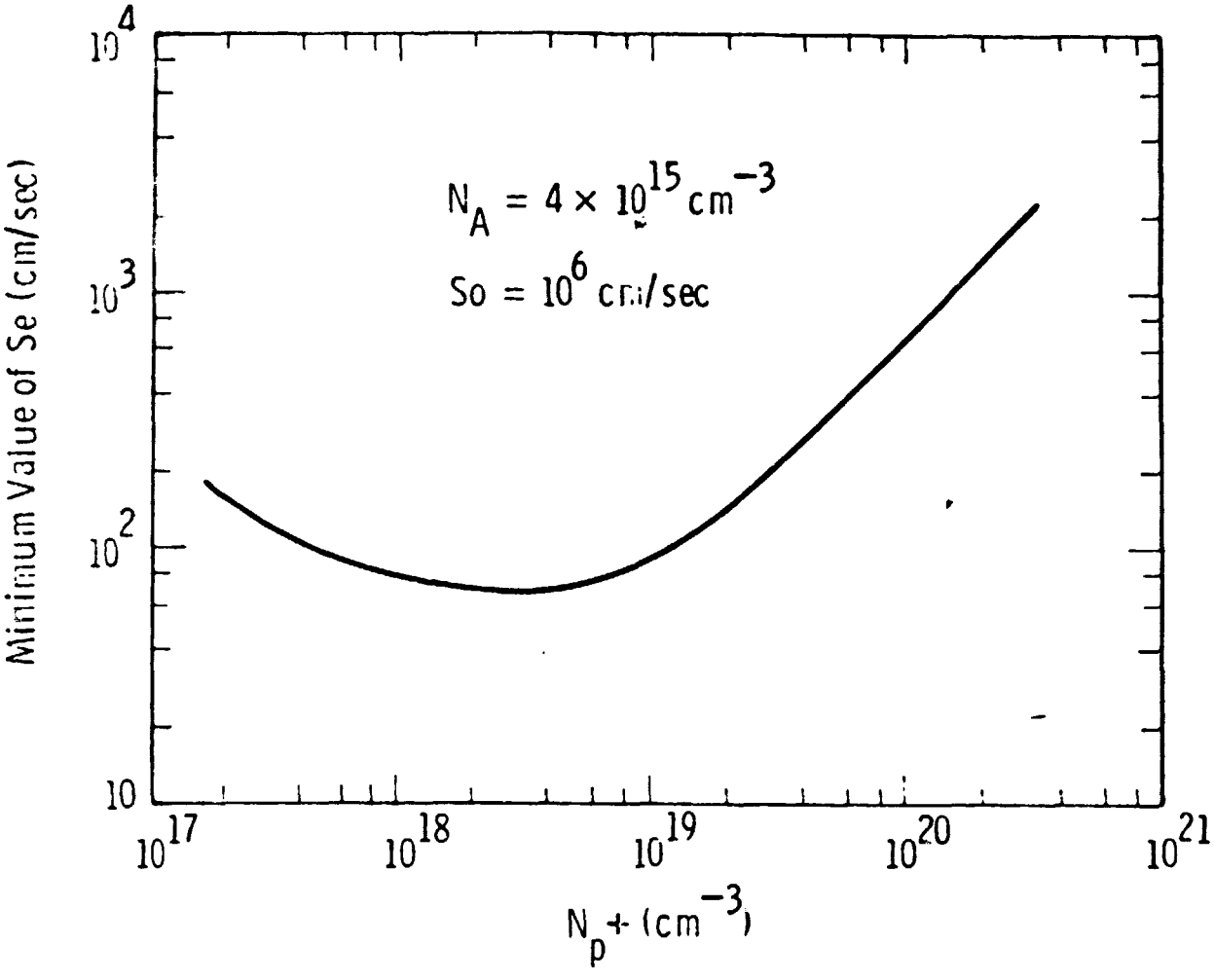

Fig. 2 – Effect of abrupt doping concentration in the p+ region on the minimum effective recombination velocity at the p– p+ interface. W_{p+} was optimized at each concentration

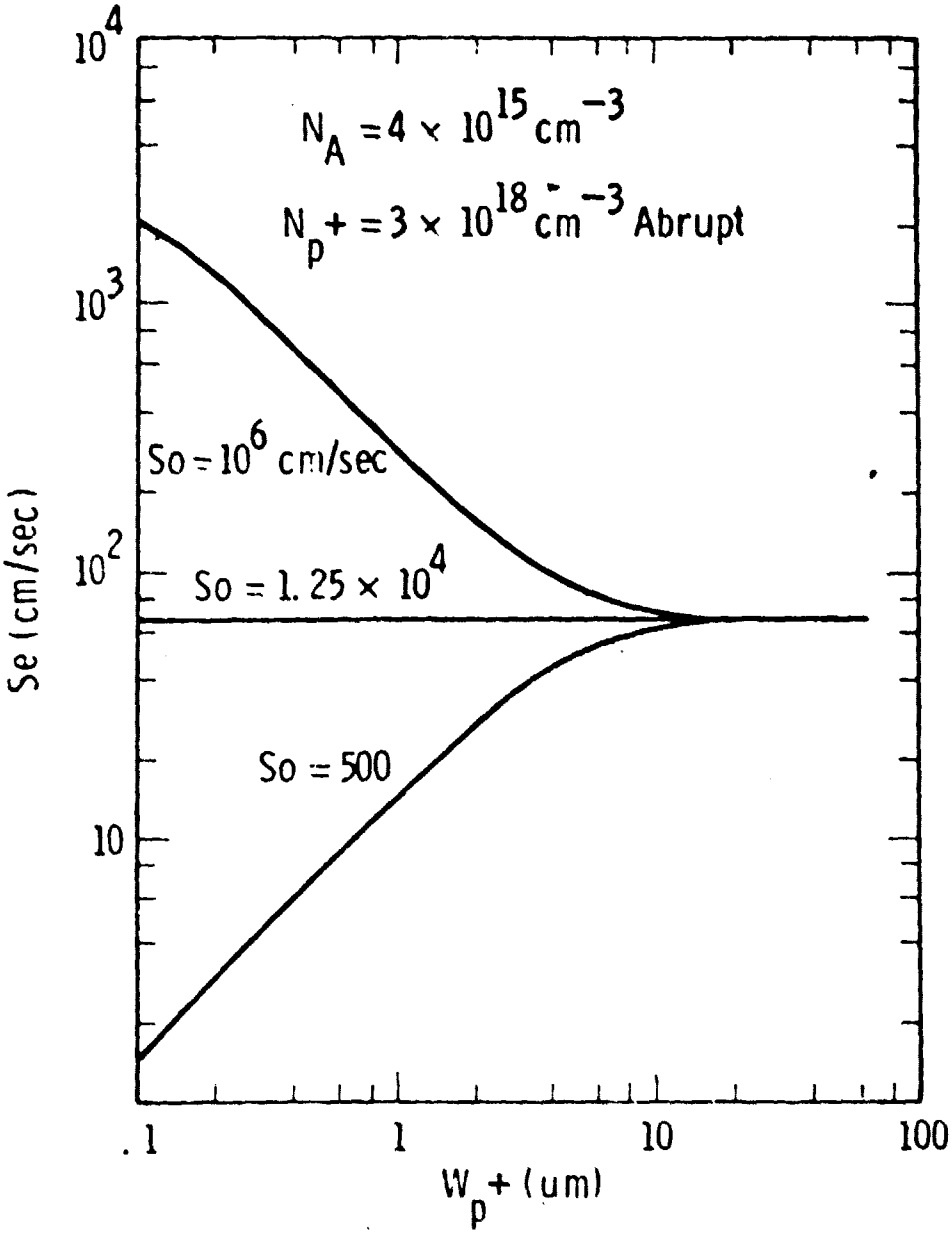

Fig. 1 – Effect of surface recombination velocity. So, and width of p+ region (W_{p+}) on the effective recombination velocity at p – p+ interface

LIST OF TABLES

APPENDIX B

PROCESS SPECIFICATIONS FOR PROCESS SEQUENCE - DENDRITIC WEB SOLAR MODULES

The process sequence we have defined for the fabrication of solar modules from dendritic web silicon consists of six main processes which have been further divided into 15 sub-processes relating to specific treatment of the web.

The specifications of control parameters for these sub-processes are given in this appendix.

1. Plasma Etching

This is a pre-diffusion cleaning step for the as-grown web. If the web has a lightly adhering, particulate oxide on the surface, plasma etching must be preceeded by an HF/H_2O cleaning.

Process Specification:

Insert web in plasma etch apparatus under following conditions:

- Purge system with O_2.
- Apply 200 watts $\pm$ 10 watts rf power.
- Flow 300 cc/min. $\pm$ 10 cc/min of PDE-100 gas. or equivalent (PDE-100 is a proprietary mix of CF_4 and O_2 supplied by LFE Corp.).
- Hold for 3 min. $\pm$ 0.5 min. and remove web.
- Temperature not to exceed 120°C.

Process Control:

No test at this point, but web surface should be shiny and reflective.

2. n^+ Diffusion

In this sub-process an n^+p junction is formed in the p-type web by diffusing in $POCl_3$.

Process Specification:

- Use reagent grade $POCl_3$ (e.g., per Fisher Co. standards) at 0°C.
- Gases used - 200 cc/min. N_2 through $POCl_3$
  1560 cc/min N_2 carrier
  62.5 cc/min O_2 carrier

  Rates are for a 4" dia. diffusion tube and the flows are $\pm$ 10%.
- Temperature - 850°C $\begin{cases} + & 5°C \\ - & 10°C \end{cases}$
- Time - 35 min. $\pm$ 10 min.
- Cooling rate - approx. 5°C/min. from 850°C → 700°C.
- Remove phosphorus glass from one side of web.

Process Control:

Sheet resistivity to be 50 Ω/□ $\pm$ 10 Ω/□.

3. Deposition of Aluminum

To form a pp^+ back junction, Al must be deposited on one side of the web. We have found that the best results are obtained when the Al is deposited on an n^+ surface. This means that after the diffusion process (which converts both surfaces to n^+) neither of the n^+p junctions are removed.

This process specification details the deposition of Al by sputtering. We have achieved essentially similar results by applying the Al either by silk screening an Al paste or plasma spraying an Al powder.

Process Specification:

- Insert web into sputtering apparatus.
- Pump system to 10^{-6} Torr.
- Sputter clean for 10 minutes.
- Sputter Al on cleaned n^+ surface. Al to be 99.99% pure. A total of 10 μm ± 3 μm to be sputtered at a rate of about 1 μm/min.

Process Control:

After removal from apparatus, web should not show excessive bow or curvature.

4. Aluminum Alloying

In this process the deposited Al is driven into the web to form a pp^+ junction.

Process Specification:

Heat web in furnace (Al coated side up to 850°C ± 3°C for 1 min. ± 0.25 min.

Heating to be done in N_2 atmosphere with a flow rate of 200 cc/min. ± 25%.

Cooling rate 50°C/min. ± 25°C/min.

Web etched in 1:1 H_2O:HF for 30 sec. to remove oxide from n^+ side.

Process Control:

Depth of p^+ layer to be 10 μm ± 3 μm.

5. Deposition of Anti Reflection Coating

The process defined requires an anti reflection (AR) coating to be applied to the web before metallization. This AR coating acts as a mask in the subsequent plating operation.

Process Specification:

AR Solution: 3.5% mixed oxide solution in ethyl alcohol.
The mixed oxide ratio is 88% TiO_2 and 12% SiO_2.
Application: The AR solution is applied by withdrawing the web from the AR solution at a controlled rate. The withdrawal rate to be 30 cm/min $\pm$ 3 cm/min.
Drying: The web is heated in air to 400°C and held at 400°C for 15 minutes. After firing, the color of the strip should be blue-black.

Process Control:

- Color of antireflection coating on n^+ side of web should be dark blue-black.
- Film thickness 700 Å $\pm$ 30 Å.

6. Deposition of Photoresist

A photoresist layer must be applied to the web (over the AR coating) so that photolithographic techniques may be used to define the conductive grid pattern.

Process Specification:

- Prepare a 50/50 solution of AZJ-111 photoresist and AZ111 thinner (produced by Shipley Co.).
- Immerse web, lengthwise in above solution and withdraw at 25 cm/min. $\pm$ 5 cm/min. to obtain a 1 to 2 μm coating of photoresist.
- Bake web at 90°C $\pm$ 3°C for 25 min. $\pm$ 3 min.

Process Control:

Photoresist coating should be free of obvious pinholes.

7. Exposure and Development of Grid Pattern

Standard photolithographic techniques are used to define a grid pattern through the PR and AR and thus form a metallization pattern.

Process Specification:

- Use negative mask fabricated on a plastic base; mask to fit between dendrites and lay on web.
- Expose photoresist with 55 millijoule/cm^2.
- Develop grid in photoresist using AZ311 developer, at 21°C $\pm$ 1°C for 60 sec. with mild agitation (AZ311 produced by Shipley Co.).
- Rinse in DI H_2O; 8 megohm minimum.
- Develop grid in antireflection coating using etch composed of: 150 parts DI H_2O, 60 parts HCl, and 30 parts NH_4F.
- Wash in DI H_2O; dry with forced, filtered air.

Process Control:

Width of grid lines to be 25 µm $\begin{cases} + 5 \text{ µm} \\ - 0 \text{ µm} \end{cases}$

8. Metallization

Thin layers of metal are evaporated over the entire surface of the cell. These metals serve as plating base for the electroplated conductive layer. The Ti serves as a barrier metal to prevent diffusion of conductive metals into the silicon.

Process Specification:

- Place web in evaporation system.
- Evaporate 300 Å ± 50 Å of Ti, at 2-5 Å/sec.
- Evaporate 300 Å ± 50 Å of Pd, at 2-5 Å/sec.
- Evaporation takes place over entire front surface of web.

Process Control:

Metal layer thickness can be checked using glass control slide and "Talystep" apparatus.

9. Rejection of Excess Evaporated Metal

Since the thin metal has been evaporated over the entire cell, those parts of the metal layers, overlaying the photoresist are rejected by dissolving the photoresist.

Process Specification:

- Immerse web in acetone for 5 minutes with mild agitation, e.g. ultrasonic.
- If any metal remains on silicon after this time, swab with cotton and acetone.
- Rinse with methanol.
- Dry in forced clean air.

Process Control:

No metal on cells other than in grid areas.

10. Preparation of Conductive Grid by Electroplating

The thin metal layers in the grid pattern cannot carry the current produced in the solar cell without excessive series resistance. Therefore, a thick conductive layer is electroplated on top of these layers.

Process Specification:

- Web in holder immersed in plating solution (see below) and plated at 10 to 20 mA/cm^2 for about 10 minutes (Area is area of grid).
- Web washed in DI H_2O for 5 min. and dried in forced, clean air.

Process Control:

Plated Ag to be 7 μm ± 2 μm.

Ag Plating Solution:

3.8 liters DI H_2O

195 gm Sol-u-Salt*

141 gm potassium cyanide (CP grade)

56.6 gm potassium cyanide (CP grade)

Anode - 99.99 Ag with a 2:1 anode/cathode area ratio

Use at pH of 12.5 and at 23°C ± 2°C with vigorous agitation.

11. Laser Scribing

Up to this point in the process, the cells have been fabricated on long lengths of web with the dendrites in place. The individual cells are separated from the web by laser scribing from the back and breaking out the cell.

*Sel-Rex Industrial Silver Process: Sel Rex Silver Sol-u-Salt produced by Sel-Rex Corp.

Process Specification:

- Align cell on holder* with back of cell facing laser beam.
- Scribe cell periphery with Nd-Yag laser. (Nominal power 3-5 watts repetition rate - 1000/sec).

Process Controls:

Cell area = $A_o \pm 0.5\%$.

No cracks or chips on cell.

Laser penetration from back 60 μm $\begin{cases} + & 0 \\ - & 10 \end{cases}$ μm.

12. Cell Testing

Our process sequence envisions that cells will be 100% tested. After testing, they are categorized as to final parameters.

Process Specification:

Tester should be automated and give hard copy printout of cell parameters.

- Parameters to be measured:

  V_{oc}

  I_{sc}

  V at I = 0.9 I_{sc}

  V at I = 0.8 I_{sc}

  V at I = 0.7 I_{sc}

- From these parameters determine: (1) efficiency, (2) fill factor, (3) I and V at peak power.

*A holder has been developed for this process which permits the cell to be aligned with the laser beam by observing the front of the cell in a 45° mirror. A patent application describing this holder has been filed.

Process Control:

Cells meet specifications or can be properly classified.

13. Interconnection Strap to Cell Front

The interconnect and encapsulation processes are carried out in sequence. The first task is to make the front interconnect to the cell.

Process Specification:

- Prepare Al interconnect straps - 1 mm wide by 15 mm long by 35 μm thick (all dimensions ± 10%).
- Using ultrasonic welding, bond an interconnect strap to each contact pad on front of cell.

Process Control:

Pull strength of bond - > 50 gmf

Resistance of bond < 10^{-5} Ω.

14. Cell Laydown and Back Interconnect

After the front interconnect the cells are placed sun-side down on the glass superstrate and held in place with an adhesive.

Process Specification:

- Prepare sheet of Sunadex glass - (1/8" thick by X ft. long by Y ft. wide)* by coating with adhesive.** (Sunadex produced by ASG Corp.).
- Lay top contacted cells, sun down side on adhesive, maintaining 0.3 mm spacing on all sides.

* Size of glass not defined.

** Adhesive is GE RTV 615 or similar.

- Cure adhesive - 120°C - three hours.
- Connect straps to back using ultrasonic bonding.

Process Control:

- Minimum amount of bubbles in glass/cell interface. Panel packing factor > 96%.

15. Attachment of Substrate, Curing and Final Test

To protect the back of the glass-cell panel, a substrate is attached to the back of the panel. After curing, the panel is again tested to assure that it meets specifications.

Process Specification:

- Prepare backboard by applying adhesive.
- Place backboard over cells, assuring conductors pads contact proper cell interconnects.
- Cure adhesive 120°C, three hours.
- Final test panel to determine if it meets specifications or to classify as to parameters.

Process Controls:

- Panel meets specifications.